VOL. 107 NO. ST3. MARCH 1981

JOURNAL OF THE STRUCTURAL DIVISION

PROCEEDINGS OF
THE AMERICAN SOCIETY
OF CIVIL ENGINEERS

VOL.107 NO.ST3. MARCH 1981

JOURNAL OF THE STRUCTURAL DIVISION

PROCEEDINGS OF
THE AMERICAN SOCIETY
OF CIVIL ENGINEERS

ISSN 0044-8001

AMERICAN SOCIETY OF CIVIL ENGINEERS

CONTENTS

This Journal is published monthly by the American Society of Civil Engineers. Publications office is at 345 East 47th Street, New York, N.Y. 10017. Address all ASCE correspondence to the Editorial and General Offices at 345 East 47th Street, New York, N.Y. 10017. Allow six weeks for change of address to become effective. Subscription price to members is $22.50. Nonmember subscriptions available; prices obtainable on request. Second-class postage paid at New York, N.Y. and at additional mailing offices. ST.

TECHNICAL NOTES

Proc. Paper 16075

DISCUSSION

Proc. Paper 16069

[a]Discussion period closed for this paper. Any other discussion received during this discussion period will be published in subsequent Journals.

INFORMATION RETRIEVAL

The key words, abstract, and reference "cards" for each article in this Journal represent part of the ASCE participation in the EJC information retrieval plan. The retrieval data are placed herein so that each can be cut out, placed on a 3 × 5 card and given an accession number for the user's file. The accession number is then entered on key word cards so that the user can subsequently match key words to choose the articles he wishes. Details of this program were given in an August, 1962 article in CIVIL ENGINEERING, reprints of which are available on request to ASCE headquarters.

[a]Discussion period closed for this paper. Any other discussion received during this discussion period will be published in subsequent Journals.

16090 THIN SECTIONS IN COMPRESSION

KEY WORDS: **Bulking; Compression;** Compression tests; **Nonlinear programming; Plates (structural members); Struts;** Thin plates

ABSTRACT: The finite strip method developed by Cheung is extended to include the nonlinear response of imperfect plate strips under axial compression. Local buckling and postbuckling phenomena are included in the formulation. The convergence and accuracy of the method is tested against accepted solutions for uniformly compressed plates with different boundary conditions. Studies are made of the nonlinear response of box and I-section columns. The application of the method to the interaction of local and Euler buckling of straight columns with imperfect plates is presented.

REFERENCE: Hancock, Gregory J., "Nonlinear Analysis of Thin Sections in Compression," *Journal of the Structural Division,* ASCE, Vol. 107, No. ST3, **Proc. Paper 16090**, March, 1981, pp. 455-471

16117 BRIDGE DESIGN AND REGIONAL ESTHETICS

KEY WORDS: **Bridges; Design;** Design practices; **Esthetic properties; Esthetics;** History; Regional geography; Structural design

ABSTRACT: Leading bridge designers have developed individual styles within limited locales, and those styles demonstrate similarities in personal esthetic ideas. An examination of the works of six major bridge designers characterizes these ideas and illustrates the striking fact that in each case these designers have done nearly all their major work in one well-defined region of a remarkably small area. The six bridge designers are: Thomas Telford (1757-1834), John Roebling (1806-1869), Gustave Eiffel (1832-1923), Robert Maillart (1872-1940), Othmar Amman (1879-1965), and Christian Menn (born in 1927). Their bridges are at least as good as, and probably better than, any of their time; there is a definite connection between the high quality of their work and its restriction to a samll well-defined geographic region. Their works illustrate a series of individual styles that spring from local conditions rather than an international style.

REFERENCE: Billington, David P., "Bridge Design and Regional Esthetics," *Journal of the Structural Division,* ASCE, Vol. 107, No. ST3, **Proc. Paper 16117**, March, 1981, pp. 473-486

16127 TEST OF WELDED TUBULAR JOINTS

KEY WORDS: Bayes theorem; Cycles; Fatigue (materials); **Fatigue tests; Residual stress; Statistical analysis;** Strength (mechanics); **Tube joints; Welded joints**

ABSTRACT: Low-cycle fatigue tests were performed for various sizes of X-type welded tubular joint specimens. The relationship between the repeated load and the number of cycles to failure is estimated by modifying the test data based on the Bayesean theorem. The size effect and the influence of residual stress, which is called the annealing effect, are also considered. The statistical approach that is described can be applied to the fatigue test data which are stongly influenced by the scatter of welding defects. In case of low-cycle fatigue of welded tubular joint specimens, the S-N curve can be assumed as a straight line on the regular scales. Concerning the size effect in low-cycle fatigue, the relative strength of welded tubular joint specimens shows a downward trend with an increase in the size of the specimen.

REFERENCE: Baba, Shunsuke, Arizumi, Yasunori, and Naruoka, Masao, "Low-Cycle Fatigue Test of Welded Tubular Joints," *Journal of the Structural Division,* ASCE, Vol. 107, No. ST3, **Proc. Paper 16127**, March, 1981, pp. 487-505

16128 BUCKLING OF WEB POSTS IN PERFORATED BEAMS

KEY WORDS: Analysis; **Beams (supports); Buckling;** Elastic properties; Girders; Models; **Openings;** Perforating; Plastic properties; Stability; Statistical analysis; **Steel beams; Structural analysis; Webs (supports)**

ABSTRACT: The buckling of the web post is investigated for steel I-beams containing adjacent rectangular web openings, and a method is presented for determining the buckling moment. An expression is derived for the effective buckling length of a web post, and its validity is demonstrated by means of tests on scale models. The elastic buckling moment of the post could then be found from elastic buckling theory, and it is used to obtain the actual buckling moment from an inelastic buckling analysis due to Nethercot and Trahair. Analysis of practial beams shows that web post buckling can affect the ultimate flexural strength of perforated plate girders, but it is not significant for rolled sections.

REFERENCE: Dougherty, Brian K., "Buckling of Web Posts in Perforated Beams," *Journal of the Structural Division,* ASCE, Vol. 107, No. ST3, **Proc. Paper 16128,** March, 1981, pp. 507-519

16121 BUCKLING OF COOLING-TOWER SHELLS

KEY WORDS: Boundary conditions; **Buckling; Cooling towers; Shells (structural forms); Stability; Structural analysis; Structural engineering;** Tests; Walls

ABSTRACT: The equations of the linear buckling theory are given in tensor notation, and the method of their solution is explained for the case of shells of revolution under axisymmetric loading. Partial differential equations are reduced to a system of ordinary differential equations introducing trigonometrical functions for the 14 unknowns of the problem. For integration, the differential equations are transformed into finite difference equations using the Hermitian (multilocal) method. Available test results are calculated and a good agreement is achieved. Parametric studies with different boundary conditions demonstrate the sensitivity of the buckling loads to the statement made for the buckling shape as a regular trigonometric configuration. The so-called classical boundary conditions prove to be very sensitive in this respect.

REFERENCE: Almannai, Ali, Basar, Yavuz, and Mungan, Ihsan, "Aspects of Buckling of Cooling-Tower Shells," *Journal of the Structural Division,* ASCE, Vol. 107, No. ST3, **Proc. Paper 16121,** March, 1981, pp. 521-534

16142 EDGE STIFFENED CANTILEVER SLABS

KEY WORDS: **Bending; Box girders; Cantilevers; Concentrated loads;** Design criteria; **Elastic analysis;** Isotropy; **Slabs; Structural analysis**

ABSTRACT: A realistic analysis of edge stiffened cantilever slabs having linearly varying thickness in one direction (and subjected to concentrated loads) is usually done by rigorous methods that are either computer based or are too complex for everyday design office use. Semigraphical manual methods are presented which provide solutions comparable to those given by rigorous methods. The methods provide longitudinal moments in the slab and also the maximum hogging and sagging moments in the edge beams. The charts are based on grillage analogy analyses of slabs and therefore are subjected to the same limitations as the grillage analogy method, which is demonstrated to conform closely to the classical plate solution for plates of varying thickness.

REFERENCE: Bakht, Baidar, "Simplified Analysis of Edge Stiffened Cantilever Slabs," *Journal of the Structural Division,* ASCE, Vol. 107, No. ST3, **Proc. Paper 16142,** March, 1981, pp. 535-550

16140 EXPERIMENTAL EVALUATION OF COMPOSITE ACTION

KEY WORDS: **Beams;** Comparative studies; **Composite structures; Deflection; Diaphragms (mechanics);** Experimental design; Fasteners; Joists; Layers; Loads (forces); Lumber; **Shear strain; Shear stress;** Stress (mechanics); Theoretical analysis

ABSTRACT: Experimental results for a layered lumber diaphragm are presented and compared with theoretical analysis. The influences of joists, boundary members, and layer discontinuities on deflections and strains are evaluated. The theoretical analysis overestimates deflections and strains. Layer discontinuities and boundary members have insignificant effects while gluing joists to decking results in an 18% reduction in deflection. Further tests are recommended to reach more conclusive results.

REFERENCE: Itani, Rafik Y., Morshed, Hossain M., and Hoyle, Robert J., "Experimental Evaluation of Composite Action," *Journal of the Structural Division,* ASCE, Vol. 107, No. ST3, **Proc. Paper 16140**, March, 1981, pp. 551-565

U.S. Customary-SI Conversion Factors

In accordance with the October, 1970 action of the ASCE Board of Direction, which stated that all publications of the Society should list all measurements in both U.S. Customary and SI (International System) units, the following list contains conversion factors to enable readers to compute the SI unit values of measurements. A complete guide to the SI system and its use has been published by the American Society for Testing and Materials. Copies of this publication (ASTM E-380) can be purchased from ASCE at a price of $3.00 each; orders must be prepaid.

All authors of *Journal* papers are being asked to prepare their papers in this dual-unit format. To provide preliminary assistance to authors, the following list of conversion factors and guides are recommended by the ASCE Committee on Metrication.

To convert	To	Multiply by
inches (in.)	millimeters (mm)	25.4
feet (ft)	meters (m)	0.305
yards (yd)	meters (m)	0.914
miles (miles)	kilometers (km)	1.61
square inches (sq in.)	square millimeters (mm^2)	645
square feet (sq ft)	square meters (m^2)	0.093
square yards (sq yd)	square meters (m^2)	0.836
square miles (sq miles)	square kilometers (km^2)	2.59
acres (acre)	hectares (ha)	0.405
cubic inches (cu in.)	cubic millimeters (mm^3)	16,400
cubic feet (cu ft)	cubic meters (m^3)	0.028
cubic yards (cu yd)	cubic meters (m^3)	0.765
pounds (lb) mass	kilograms (kg)	0.453
tons (ton) mass	kilograms (kg)	907
pound force (lbf)	newtons (N)	4.45
kilogram force (kgf)	newtons (N)	9.81
pounds per square foot (psf)	pascals (Pa)	47.9
pounds per square inch (psi)	kilopascals (kPa)	6.89
U.S. gallons (gal)	liters (L)	3.79
acre-feet (acre-ft)	cubic meters (m^3)	1,233

JOURNAL OF THE STRUCTURAL DIVISION

NONLINEAR ANALYSIS OF THIN SECTIONS IN COMPRESSION

By Gregory J. Hancock[1]

INTRODUCTION

The interaction between local and Euler buckling in a thin-walled compression member can produce an adverse effect on its strength. The effect is most pronounced when the local and Euler buckling loads are approximately equal. Its magnitude depends upon the plate imperfections and lack of straightness of the column. Van der Neut (20) and Graves-Smith (5) first demonstrated this mode of behavior for box columns by using mathematical models which included the nonlinear membrane stiffness of the plates forming the columns. The nonlinear stiffness results from the interaction of the plate imperfections with the local buckling and postbuckling phenomena.

The determination of the interaction between local and Euler buckling of a thin-walled compression member requires a knowledge of the nonlinear membrane stiffness of the member. Consequently an efficient method is required for determining the nonlinear stiffness of a thin-walled section. The finite element method has been used successfully by Gallagher (7) to simulate the nonlinear and postbuckling behavior of plates. However, the finite strip method developed by Cheung (3) has the advantage of considerably reducing the computation involved for uniform prismatic members. The buckling loads and modes of prismatic members have been investigated by the writer (8) using the finite strip buckling analysis developed by Plank and Wittrick (13). Recently Graves-Smith and Sridharan (6) have produced a finite strip method for the post-local buckling analysis of perfect plates and sections.

In this paper the finite strip method is extended to include the nonlinear response of imperfect plate strips under longitudinal compression. The displacement functions used in the analysis differ slightly from those of Graves-Smith and Sridharan. The accuracy of the method is tested against accepted solutions for plates with different boundary conditions.

[1]Senior Lecturer in Civ. Engrg., Univ. of Sydney, New South Wales, Australia.

Note.—Discussion open until August 1, 1981. To extend the closing date one month, a written request must be filed with the Manager of Technical and Professional Publications, ASCE. Manuscript was submitted for review for possible publication on February 26, 1980. This paper is part of the Journal of the Structural Division, Proceedings of the American Society of Civil Engineers, ©ASCE, Vol. 107, No. ST3, March, 1981. ISSN 0044-8001/81/0003-0455/$01.00.

Studies of the nonlinear response of box and I-sections under axial compression are presented. The effective flexural resistances of the box and I-sections under axial load are evaluated in these studies by applying a small curvature to the sections and then calculating the resistance from the resultant moment. The flexural resistances so determined are compared with those of Bijlaard and Fisher (1), Graves-Smith (5), and the effective section method based on the Winter effective width formula (4). The flexural resistances can be used to determine the bifurcation load for over-all buckling of perfectly straight columns with plate imperfections.

Nonlinear Analysis of Imperfect Plate Strips

The finite strip buckling analysis of a folded plate structure has been represented (8) by

$$([K] - \lambda [G(\sigma)]) \cdot \{\delta\} = \{0\} \quad \ldots \ldots \ldots \ldots \ldots \ldots \ldots \ldots \ldots \ldots \ldots \ldots (1)$$

in which $[K]$ = linear component of the stiffness matrix of the folded plate assembly; $[G(\sigma)]$ = stability matrix which is a function of the longitudinal membrane stresses (σ); $\{\delta\}$ = vector of nodal line displacements; and λ = load factor. Eq. 1 represents an eigenvalue problem which can be solved to give the buckling load factor λ and the corresponding buckling mode $\{\delta\}$ once the membrane stress distribution is specified.

Graves-Smith and Sridharan extended Eq. 1 to the postbuckling range. They assumed that the plate assembly was compressed between rigid frictionless platens and included nonlinear terms in the stiffness matrix. The resulting set of nonlinear equations is represented by

$$([K] + [G(\epsilon_H)] + [K_1(\delta)] + [K_2(\delta^2)]) \cdot \{\delta\} = \{W(\epsilon_H)\} \quad \ldots \ldots \ldots \ldots (2)$$

in which $[K_1(\delta)]$ = nonlinear component of the stiffness matrix which is a linear function of the nodal line displacements; $[K_2(\delta^2)]$ = nonlinear component of the stiffness matrix which is a quadratic function of the nodal line displacements; $\{\epsilon_H\}$ = strain vector caused by the longitudinal compression of the plate assembly between rigid platens; and $\{W(\epsilon_H)\}$ = load vector resulting from the longitudinal compressive strains. For the postbuckling analysis, the stability matrix is formulated as a function of the longitudinal compressive strains (ϵ_H) rather than stresses (σ), since the stress distribution changes from an initial uniform distribution in the postbuckling range.

Eq. 2 has been extended herein to include geometric imperfections in the plate. If $\{\delta_0\}$ is the initial value of $\{\delta\}$, then Eq. 2 becomes

$$([K] + [G(\epsilon_H) + [K_1(\delta)] + [K_2(\delta^2)] - [K_2(\delta_0^2)]) \cdot \{\delta\}$$

$$= \{W(\epsilon_H)\} + [K] \cdot \{\delta_0\} + [K_1(\delta_0)] \cdot \{\delta_0\} \quad \ldots \ldots \ldots \ldots \ldots \ldots (3)$$

which represents a set of nonlinear equations that can be solved for $\{\delta\}$ at any value of the strain vector $\{\epsilon_H\}$. The vector $\{\delta_0\}$ must be nonzero if there is to be a solution at values of longitudinal strain less than the compressive strain for local buckling. As a consequence of the plate imperfections, the equations will produce a finite solution equal to $\{\delta_0\}$ when the plate is unstrained. The numerical methods used to solve Eq. 3 for displacements are summarized in a later section.

Displacement Fields.—In this paper, only one term of the Fourier series describing the displacement fields along the length of a strip is considered. This will produce an accurate solution for loads up to approximately 1.5 times the local buckling load when the wavelength of this single term is the wavelength of the local buckle of the prismatic folded plate assembly. The buckle wavelength can be determined along with the buckling coefficient by solving Eq. 1 as set out by Hancock (8) and Plank and Wittrick (13), or by charts such as those produced by Bulson (2).

The rectangular strip shown in Fig. 1 is assumed to be compressed and bent in its plane by rigid frictionless platens located at its ends. The longitudinal compressive strains are assumed to be ϵ_1, ϵ_2 on nodal lines A_1B_1, A_2B_2

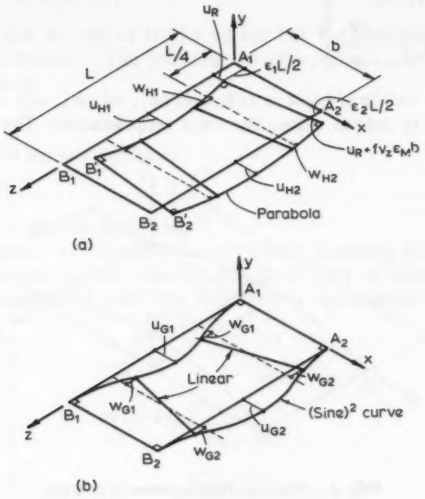

FIG. 1.—Membrane Displacements of Strip: (*a*) Hookean Displacements; (*b*) Geometric Nonlinear Displacements

respectively, and to vary linearly between these two lines. The resulting displacement field in the plane of the strip (membrane displacements) is defined by the displacements u, w in the x, z directions respectively, as shown in Fig. 1. These membrane displacements consist of two components. They are those resulting from Hookean shortening [u_H, w_H in Fig. 1(*a*)] and those geometric nonlinear components resulting from plate flexure [u_G, w_G in Fig. 1(*b*)]. The total membrane displacements are simply the sum of the two components, that is

$$u = u_H + u_G; \quad w = w_H + w_G \quad \ldots \quad (4)$$

The membrane displacements corresponding to the Hookean deformations are given by

$$u_H = u_R + f\nu_z\epsilon_M x + \frac{\rho z(L-z)}{2}; \quad w_H = (\rho x - \epsilon_1)\left(z - \frac{L}{2}\right) \quad \ldots\ldots\ldots (5)$$

in which $\epsilon_M = (\epsilon_1 + \epsilon_2)/2$; $\rho = (\epsilon_1 - \epsilon_2)/b$; u_R = a rigid body displacement of the strip; $f\nu_z\epsilon_M x$ = Poisson's ratio expansion of the strip; and the coefficient $f = 1$ initially. As proposed by Timoshenko and Gere (17) [sections 9.13, equation (n)], the term f can be used to allow for the change in Poisson's ratio expansion which results from the change in membrane stress distribution in the nonlinear range of structural response.

The geometric nonlinear components of membrane displacements which occur as a result of the flexural displacements of the strip are given by

$$\left.\begin{aligned} u_G &= (\alpha_1' + \bar{x}\alpha_2')\cdot Z_2 \\ w_G &= (\alpha_3' + \bar{x}\alpha_4')\frac{L}{\pi}\frac{dZ_2}{dz} \end{aligned}\right\} \quad \ldots\ldots\ldots\ldots\ldots\ldots\ldots\ldots (6)$$

in which $Z_2 = \sin^2(\pi z/L)$; $\bar{x} = x/b$; and $(\alpha_1', \alpha_2', \alpha_3', \alpha_4')$ = the polynomial coefficients to be solved within the finite strip analysis. The function Z_2 has

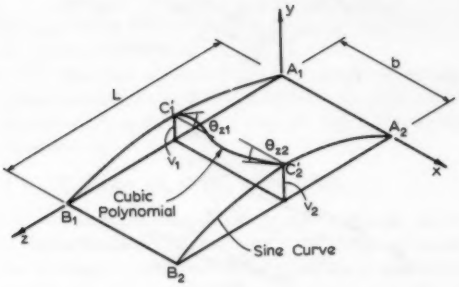

FIG. 2.—Flexural Displacements of Strip

been chosen as a sine squared function to eliminate shear straining at the ends of the strip.

The displacement field normal to the strip (flexural displacements) consists of the v-component in the y-direction as shown in Fig. 2. The mathematical formulation of this displacement is given by

$$\left.\begin{aligned} v &= (\alpha_1 + \alpha_2\cdot\bar{x} + \alpha_3\cdot\bar{x}^2 + \alpha_4\cdot\bar{x}^3)\cdot Z_1 \\ v_0 &= \alpha_{10} + \alpha_{20}\cdot\bar{x} + \alpha_{30}\cdot\bar{x}^2 + \alpha_{40}\cdot\bar{x}^3)\cdot Z_1 \end{aligned}\right\} \quad \ldots\ldots\ldots\ldots\ldots\ldots (7)$$

in which $Z_1 = \sin(\pi z/L)$. This function is identical with that used by Cheung (3). The terms $(\alpha_1, \alpha_2, \alpha_3, \alpha_4)$ are the polynomial coefficients to be solved within the finite strip analysis. The v_0 component is the initial out-of-plane imperfection of the plate. It takes the same form as v. The coefficients $(\alpha_{10}, \alpha_{20}, \alpha_{30}, \alpha_{40})$ define the geometrical imperfections of the strip and are determined prior to the analysis.

The vector of nodal line displacements has been chosen to exclude the Hookean displacements resulting from the longitudinal compression. Its components are given by

$$\{\delta\} = [u_{G1}, v_1, w_{G1}, \theta_{z1}, u_{G2}, v_2, w_{G2}, \theta_{z2}]^T \quad \ldots\ldots\ldots\ldots\ldots\ldots (8)$$

The displacements u_{G1}, v_1, θ_{z1}, u_{G2}, v_2, θ_{z2} are those at the central section of the strip as shown in Fig. 1(*b*) and Fig. 2. However, the displacements w_{G1}, w_{G2} are those at the quarter point section of the strip as shown in Fig. 1(*b*).

The eight unknown coefficients in Eqs. 6 and 7 can be represented by the vector $\{\alpha\}$ in

$$\{\alpha\} = [\alpha_1 \alpha_2 \alpha_3 \alpha_4 \alpha_1' \alpha_2' \alpha_3' \alpha_4']^T \quad \ldots\ldots\ldots\ldots\ldots\ldots\ldots\ldots (9)$$

The vector $\{\delta\}$ can be related to the vector $\{\alpha\}$ by appropriate substitution for (x, z) in Eqs. 6 and 7. The resulting set of equations can be represented in matrix notation by

$$\{\delta\} = [C] \cdot \{\alpha\} \quad \ldots\ldots\ldots\ldots\ldots\ldots\ldots\ldots\ldots\ldots\ldots\ldots (10)$$

Solution of Eq. 10 for $\{\alpha\}$ produces

$$\{\alpha\} = [C]^{-1} \cdot \{\delta\} \quad \ldots\ldots\ldots\ldots\ldots\ldots\ldots\ldots\ldots\ldots\ldots\ldots (11)$$

The matrix $[C]$ is given in Reference 9.

Nonlinear Strains.—The nonlinear strain vector, including initial plate imperfections, is the same as that used by Hu, et al. (10). It includes only those nonlinear terms associated with plate flexure. It is represented by

$$\{\epsilon\} = \begin{bmatrix} \rho_x \\ \rho_z \\ \rho_{xz} \\ \epsilon_x \\ \epsilon_z \\ \gamma_{xz} \end{bmatrix} = \begin{bmatrix} -\dfrac{\partial^2 (v - v_0)}{\partial x^2} \\ -\dfrac{\partial^2 (v - v_0)}{\partial z^2} \\ 2\dfrac{\partial^2 (v - v_0)}{\partial x \partial z} \\ \dfrac{\partial u}{\partial x} + \dfrac{1}{2}\left(\dfrac{\partial v}{\partial x}\right)^2 - \dfrac{1}{2}\left(\dfrac{\partial v_0}{\partial x}\right)^2 \\ \dfrac{\partial w}{\partial z} + \dfrac{1}{2}\left(\dfrac{\partial v}{\partial z}\right)^2 - \dfrac{1}{2}\left(\dfrac{\partial v_0}{\partial z}\right)^2 \\ \dfrac{\partial u}{\partial z} + \dfrac{\partial w}{\partial x} + \left(\dfrac{\partial v}{\partial x}\right)\left(\dfrac{\partial v}{\partial z}\right) - \left(\dfrac{\partial v_0}{\partial x}\right)\left(\dfrac{\partial v_0}{\partial z}\right) \end{bmatrix} \quad \ldots\ldots (12)$$

The linear and nonlinear components of the strain vector $\{\epsilon\}$ can be derived as a function of the nodal line displacements $\{\delta\}$ by substitution for u, v, w from Eqs. 4, 5, 6, 7, and 11 into Eq. 12. The resulting linear and nonlinear components of the strain matrix are given in Reference 9.

Plate Theory.—The plate theory used herein is the same as that presented by Cheung (3). This is the orthotropic theory derived by Timoshenko and

Woinowsky-Krieger (18). The stress vector $\{\sigma\}$ derived using this theory is

$$\{\sigma\} = \begin{bmatrix} M_x \\ M_z \\ M_{xz} \\ \sigma_x \\ \sigma_z \\ \tau_{xz} \end{bmatrix} = \begin{bmatrix} E_x t^3 \cdot (\rho_z + \nu_z \rho_x)/12\,(1 - \nu_x \nu_z) \\ E_z \cdot t^3 (\rho_z + \nu_x \rho_x)/12\,(1 - \nu_x \nu_z) \\ G t^3 \rho_{xz}/12 \\ E_x(\epsilon_x + \nu_z \epsilon_z)/(1 - \nu_x \nu_z) \\ E_z(\epsilon_z + \nu_x \epsilon_x)/(1 - \nu_x \nu_z) \\ G \cdot \gamma_{xz} \end{bmatrix} \quad \ldots\ldots\ldots\ldots (13)$$

such that $\nu_z \cdot E_x = \nu_x \cdot E_z$. The formulation of Eq. 13 into a property matrix is given in Reference 9.

Development of Stiffness Matrix.—The nonlinear stiffness matrix was developed using the theory proposed by Powell (14). This theory is based upon the virtual work principle applied to infinitesimal deformations from an equilibrium deformed position of a loaded structure. The nonlinear strain terms (Eq. 12) are included in the calculation of the stress and strain when evaluating the internal work. The original fixed frame of reference has been used for the nodal line displacements of a strip when calculating the nonlinear stiffness matrix. The resulting set of stiffness equations including the geometric imperfections and longitudinal compressive strains is given by Eq. 3. The complete derivation as well as the individual matrices in Eq. 3 are set out in Reference 9.

The flexural component of the stiffness matrix $[K]$ is identical with that developed by Cheung. The membrane component of $[K]$ differs from that used by Cheung because of the use of the sine squared function in the membrane displacement field. The $[G(\epsilon_M)]$ matrix is the same as the flexural stability matrix developed by Przemieniecki (15), except that compressive strain rather than stress has been used in the formulation.

The $[K_1(\delta)]$ matrix is a linear function of the plate flexural displacements. It produces the nonlinear coupling between membrane and flexural behavior. It can be broken into two components as

$$[K_1(\delta)] = [K_1^*(\delta)] + \frac{1}{2}\,[K_1^*(\delta)]^T \quad \ldots\ldots\ldots\ldots\ldots\ldots\ldots (14)$$

The first component relates the flexural actions to the membrane displacements. The second component $[K_1^*(\delta)]^T$ relates the membrane actions to the flexural displacements. Consequent upon the factor $1/2$ applied to the second term in Eq. 14, the resulting stiffness matrix is not symmetric. This is in accordance with the theory of Powell. The $[K_2(\delta)^2]$ component of the stiffness matrix is a quadratic function of the plate flexural displacements. It results in a modification of the flexural stiffness of the strip as the flexural displacements increase.

Solution of Nonlinear Equations.—The simultaneous equations represented by Eq. 3 are nonlinear and require an iterative solution. The Newton-Raphson method as presented by Gallagher (7) for nonlinear finite element problems has been used herein. Rearranging Eqs. 3 and 14 to an imbalance of load vector produces

$$\{F\} = \left([K] + [G(\epsilon_H)] + [K_1^*(\delta)] + \frac{1}{2}[K_1^*(\delta)]^T + [K_2(\delta^2)] \right.$$

$$\left. - [K_2(\delta_0^2)] \right) \cdot \{\delta\} - \{W(\epsilon_H)\} - [K] \cdot \{\delta_0\} - \frac{1}{2}[K_1^*(\delta_0)]^T \cdot \{\delta_0\} \quad \ldots\ldots (15)$$

An nonlinear analysis must proceed on an estimate of $\{\delta\}$ and improve upon the estimate in succeeding iterations. By expanding Eq. 15 as a Taylor series and disregarding higher order terms, then after i iterations

$$\{\delta_{i+1}\} = \{\delta_i\} - \left[\frac{\partial\{F_i\}}{\partial\delta}\right]^{-1} \cdot \{F_i\} \quad \ldots\ldots\ldots\ldots\ldots\ldots\ldots (16)$$

because we are seeking $\{F_{i+1}\} = \{0\}$.

The matrix $[\partial\{F_i\}/\partial\delta]$ is called the tangent stiffness matrix and can be derived from Eq. 15. In this paper, an approximate tangent stiffness matrix given by

$$\left[\frac{\partial\{F_i\}}{\partial\delta}\right] = [K] + [G(\epsilon_H)] + [K_1^*(\delta)] + [K_1^*(\delta)]^T + 3[K_2(\delta^2)] \quad \ldots\ldots (17)$$

has been used.

The approximate tangent stiffness matrix is symmetric. It can be derived simply from the components $[K]$, $[G(\epsilon_H)]$, $[K_1^*(\delta)]$, $[K_2(\delta^2)]$, which constitute the nonlinear stiffness matrix. It has been found to produce rapid convergence to the solution of the nonlinear Eqs. 3 for loads up to twice the local buckling load.

Stresses.—The transverse membrane stresses (σ_x) can be derived from Eqs. 4, 5, 6, 7, 12, and 13. For a plate strip which is free to expand laterally the integral of σ_x over the length of the strip is zero. The numerical value of f (in Eq. 5) can be determined by equating the integral of σ_x over the area Lt of the strip to zero. The value of f is determined for each strip after each iteration of the analysis.

The longitudinal membrane stress (σ_z) at any point in a strip can also be derived from Eqs. 4, 5, 6, 7, 12, and 13. The longitudinal stress can be integrated over the cross-sectional area bt of the strip to give the load in the strip. The values of the total load at the center and ends of a folded plate system were found to agree to at least 6 significant figures after convergence of the solution at any strain level. This confirms that the solution satisfies longitudinal equilibrium.

Analysis of Square Plates

The method described in the foregoing section has been programmed for a digital computer. The accuracy and convergence of the method has been investigated by comparing the solutions for square plates with those of Yamaki (21). His solutions are generally regarded as precise up to values of load equal to at least 3 times the local buckling load.

Two different boundary conditions have been investigated. The first considered is a simply supported square plate whose longitudinal edges are free to wave

[Yamaki I(b)]. The second condition studied is that where the longitudinal edges are built-in to prevent out-of-plane edge rotations but are free to wave in-plane [Yamaki, Case II(b)].

In both cases, the difference between the lateral deflections on successive cycles was less than 0.1% of the total deflection after 10 iterations. The same degree of convergence also applied to the longitudinal load carried in the plate.

Simply Supported Plates.—The curve of load versus compressive strain calculated for the simply supported plate is shown in Fig. 3. As a result of symmetry it was necessary to analyze only half the width of the plate by using 4 or 8 equal width strips. The solution of Van der Neut (20), which assumes that the postbuckled deflected shape is the same as the buckling mode, has also

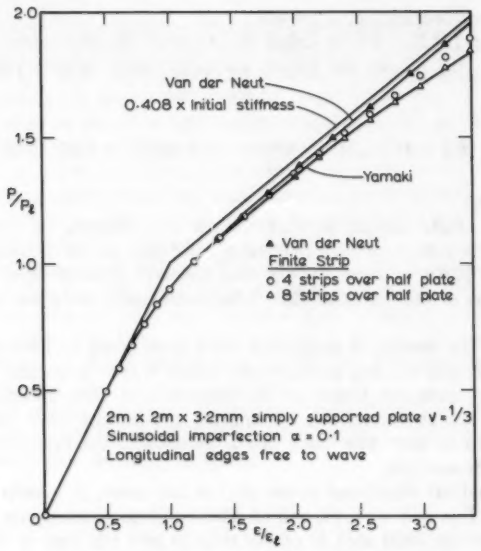

FIG. 3.—Load-Strain Curve of Simply Supported Plate

been plotted in Fig. 3. It deviates from the Yamaki solution at loads above 1.1 P_l. The straight line with slope 0.408 times the initial stiffness (21) represents the postbuckling stiffness of a perfect buckled plate assuming no change in deflected shape from the buckling mode. The Van der Neut solution asymptotes to this line. The finite strip solution for 8 strips over half the plate agrees closely with the Yamaki solution up to 1.8 P_l. The solution for 4 strips lies approximately half way between the Van der Neut and Yamaki solutions, and is sufficiently accurate for practical purposes for loads up to 1.5 P_l.

Plate with Built-In Longitudinal Edges.—The ability of the method to account for boundary conditions other than those of simple supports has been investigated for built-in longitudinal edges. In this case, the plate buckles in a complete

wavelength over the full length of the plate with a buckling coefficient of $K = 7.69$ (17) in

$$\sigma_l = \frac{K\pi^2 E}{12(1-\nu^2)}\left(\frac{t}{b}\right)^2 \quad \text{(18)}$$

The buckling mode is a sine squared function across the width of the plate. The geometric imperfection chosen has the same shape as the buckling mode.

The load-strain curve is shown in Fig. 4, in which the finite strip solutions are compared with the Yamaki solution. The accuracy of the resulting solutions

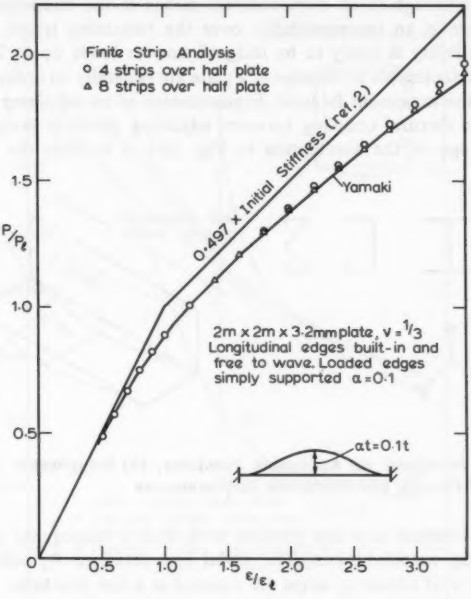

FIG. 4.—Load-Strain Curve of Plate With Built-In Longitudinal Edges

is similar to those for the simply supported plate, which demonstrates that the accuracy of the method is not significantly affected by the boundary conditions.

Analysis of Thin-Walled Columns

The extension of the analysis from a single plate to a prismatic member formed from a number of plates requires a consideration of the equilibrium of nodal line forces and the compatibility of nodal line displacements at the plate junctions. Graves-Smith and Sridharan (6) have devoted considerable attention to this problem. They found that their choice of membrane displacement

functions limited the types of plate junctions which could be analyzed. For a plate junction to be applicable, the connected plates must be free to expand as a result of the Poisson's ratio effect without inducing transverse stresses. Applicable and inapplicable junctions are shown in Fig. 5. In this paper, the over-all equilibrium condition (assumed under the heading "Stresses" in the foregoing)—that the integral of the transverse stresses over the area of the strip is zero—produces the same restrictions as were discovered by Graves-Smith and Sridharan.

A comparison of the edge flexural displacements of one strip and the edge membrane displacements of an orthogonal strip is shown in Fig. 5(*c*). It can be seen that although these displacements match at the midpoint and ends of the strip, there is an incompatibility over the remaining length of the strip. This incompatibility is likely to be insignificant for loads up to 2 P_l since the membrane displacements at the edge of a plate are generally an order of magnitude smaller than the maximum flexural displacements of an adjoining plate. Hence the membrane flexural coupling between adjoining plates is insignificant. The major advantage of the assumption in Fig. 5(*c*) is to limit the total number

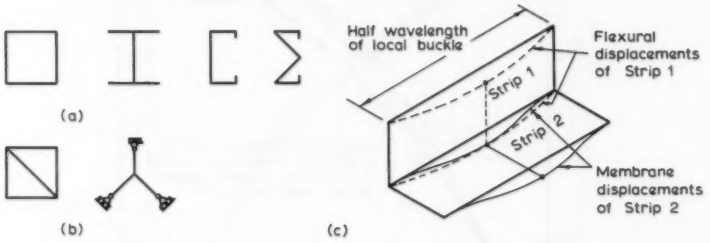

FIG. 5.—Plate Junctions: (*a*) Applicable Junctions; (*b*) Inapplicable Junctions; (*c*) Relationship of Flexural and Membrane Displacements

of degrees of freedom at a line junction to 4, with a consequent simplification in programming considerations. The nodal line rotations θ_z and longitudinal displacements w of adjoining strips are equated at a line junction.

Square Box Column.—An analysis was performed on a box column which had a uniform plate thickness and its depth equal to its width. A quarter of the column between center lines of adjacent plates was studied with each half plate divided into four equal width strips. The geometric imperfections of each plate were taken to be the same as for a simply supported plate. The directions of the imperfections were chosen so as to produce compatibility at the plate junctions.

The resulting load-strain curve was identical with that shown in Fig. 3 for a simply supported plate whose longitudinal edges are free to wave. This expected result confirms that the method can be applied to structural members.

The effective axial rigidity of the box column was computed from the central slope of a quadratic fitted through three adjacent points on the load-strain curve in Fig. 3. These rigidities are plotted against the load in Fig. 6. It can be seen that the geometrical imperfections cause a decrease from the initial rigidity

EA as the axial load increases. At high axial loads, the rigidity drops below the value of 0.408 *EA* calculated by Yamaki (21), demonstrating the increasing difference between the actual postbuckled shape and the buckling mode.

Graves-Smith (5) has proposed that the bifurcation load for over-all buckling of a thin-walled column with imperfect plate elements can be calculated from the Euler formula with the flexural rigidity *EI* replaced by the effective flexural rigidity EI_{eff}. Bijlaard and Fisher (1) also proposed this approach in the post-local buckling range of a thin-walled column composed of perfect plate elements. Consequently it is necessary to determine the effective flexural rigidity of a

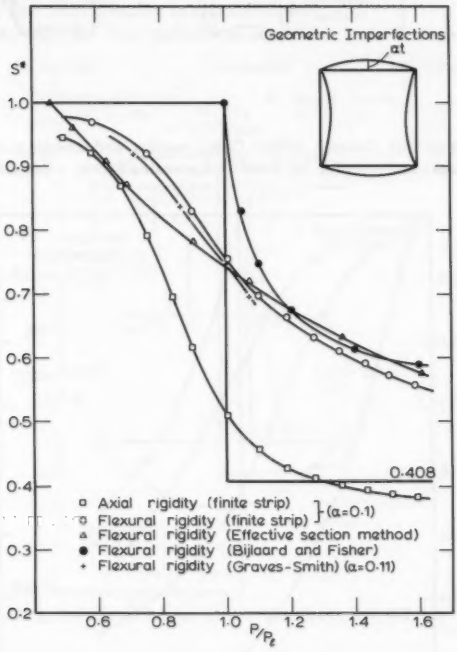

FIG. 6.—Effective Rigidities of Square Box Column

column section before the bifurcation load for over-all buckling can be calculated.

The effective flexural rigidity at a given value of the strain vector $\{\epsilon_H\}$ was determined by applying first an axial compressive strain to the box as shown in Fig. 7(*b*), and then a curvature as shown in Fig. 7(*c*). The maximum additional strain resulting from this curvature was arbitrarily chosen to be 1% of the axial strain. The resulting stress distribution was integrated to determine the bending moment corresponding to the curvature. The effective flexural rigidity was determined by dividing the moment by the curvature.

The calculations were performed with half of the box column subdivided

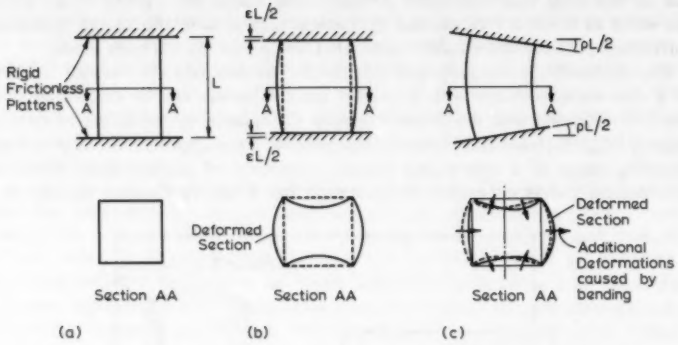

FIG. 7.—Model of Box Column Under Compression and Bending: (*a*) Unstrained; (*b*) Axial Compressive Strain (ε); (*c*) Axial Compressive Strain + Bending Curvature (ρ)

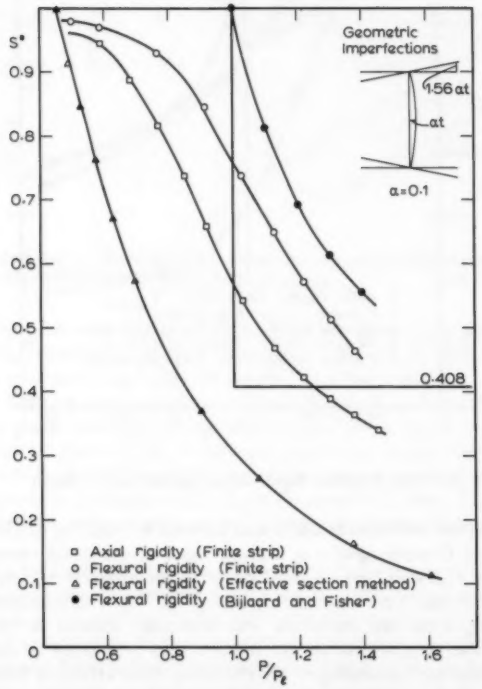

FIG. 8.—Effective Rigidities of I-Column

into 16 equal width strips. The resulting flexural rigidity values are plotted in Fig. 6, and are compared with those produced using the effective section method (4), the method of Bijlaard and Fisher (1), and the solution of Graves-Smith (5). For loads greater than 1.1 P_1, the finite strip solution and the effective width method agree closely with the solution of Bijlaard and Fisher. Fow lower load values, the flexural rigidity is sensitive to the assumed values of initial imperfections. The finite strip solution (with $\alpha = 0.1$) is in close agreement with the solution of Graves-Smith (with $\alpha = 0.11$). A recent solution by Koiter and Van der Neut with $\alpha = 0.05$ lies very close to the finite strip solution with $\alpha = 0.1$ and Graves-Smith solution ($\alpha = 0.11$). Koiter and Van der Neut have indicated that their solution is conservative.

I-Section.—An analysis was performed on an I-section for which the flange

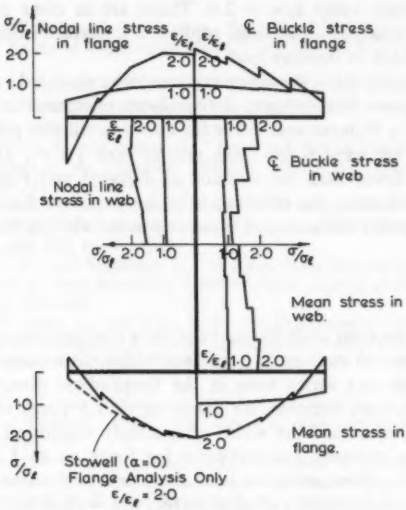

FIG. 9.—Longitudinal Stress Distribution in I-Beam

width equalled the web depth. The plate thickness was constant throughout the section. The plate buckling coefficient in Eq. 18 is 2.6 for this section where the value of (t/b) is that for the web [Bulson (2), Fig. 7.12]. The buckle half-wavelength is 1.5 times the web depth (Bulson, Fig. 1.13). The geometric imperfections chosen for the section are shown in Fig. 8. The imperfections in the web of the I-section were chosen to be the same as the buckling mode of the web alone (i.e., sinusoidal). The imperfections in the flange were chosen to be the same as the buckling mode of a flange outstand alone (i.e., straight). The imperfect web and flange were assumed to be connected at 90°. This results in an imperfection of the flange tip of 1.56 αt when αt is the imperfection of the web center line. The imperfections were assumed to have the same wavelength as the local buckling mode.

An analysis was performed for an imperfection value of 0.1. As a result of symmetry, only one flange and half the web were considered in the analysis. The flange outstands and half the web were each divided into 4 equal width strips. The axial rigidity, which was derived using the procedure previously described for square box column, is plotted in Fig. 9. Unlike the axial rigidity for the box column, its value drops well below 0.408 times the initial stiffness at loads above 1.2 P_l.

The longitudinal stress distributions in the flange and web at values of ϵ/ϵ_l equal to 1.0, 2.0 are shown in Fig. 9. The corresponding load values are 0.912 P_l and 1.371 P_l, respectively. The stress distributions at the nodal line and buckle center line are shown in the upper portion of Fig. 9, and the mean stress is shown in the lower portion. The mean longitudinal stress in the flange and the stress distribution obtained by Stowell (16) have also been compared in Fig. 9 at a strain value $\epsilon/\epsilon_l = 2.0$. These are in close agreement despite the fact that the analysis of Stowell applies to a perfect isolated flange which has no web to which to transfer load.

The flexural rigidity about the minor axis was also calculated using the procedure described for square box column. It has been compared in Fig. 8 with the values produced by Bijlaard and Fisher for a section without plate imperfections. The two curves are parallel for loads greater than 1.1 P_l, although the finite strip solution is lower than the solution of Bijlaard and Fisher. The flexural rigidity determined using the effective section method of Kalyanaraman, et al. (11) appears to be very conservative when compared with the finite strip analysis.

Conclusions

A nonlinear finite strip analysis has been shown to produce accurate solutions for the deflections and stresses in imperfect folded plate assemblies under axial compression. Only one series term in the longitudinal direction is necessary to achieve an accurate solution for loads up to 1.5 times the local buckling load. Four strips over half the width of a simply supported plate or the full width of a flange outstand are sufficient for loads up to 1.5 times the local buckling load when determining the load-strain curve of plates in compression.

The effective flexural rigidity of an imperfect thin-walled box column subjected to loads greater than the local buckling load was found to agree with those produced by Bijlaard and Fisher (1), and the effective section method of DeWolf, et al. (4). For loads less than the local buckling load, the effective flexural rigidity was found to agree closely with that of Graves-Smith (5). The effective flexural rigidity of an imperfect thin-walled I-column subjected to loads greater than the local buckling load was found to agree more closely with the solution produced by Bijlaard and Fisher (1) than that produced using the effective section method of Kalyanaraman, et al. (11). The latter solution was very conservative when compared with the finite strip analysis.

Acknowledgments

The initial investigation was carried out while the writer was an Honorary Research Fellow, University of Birmingham, England. The assistance provided

by W. H. Wittrick, Beale Professor of Civil Engineering, is gratefully acknowledged.

The paper was completed while the writer was a Visiting Research Scholar at Washington University, St. Louis, Missouri, U.S.A. The facilities provided by T. V. Galambos, H. D. Jolley Professor of Civil Engineering, are appreciated.

The calculations were performed on an ICL1906A computer in the University Computing Centre, University of Birmingham, and a DEC20 computer in the Centre for Computational Mechanics, Washington University.

The comments of N. S. Trahair at the University of Sydney, following a review of the manuscript, are greatly appreciated.

Appendix I.—References

1. Bijlaard, P. P., and Fisher, G. P., "Column Strength of H-Sections and Square Tubes in Postbuckling Range of Component Plates," *TN 2994*, NACA, Washington, D.C., Aug., 1953.
2. Bulson, P. S., *The Stability of Flat Plates*, Chatto and Windus, London, 1970.
3. Cheung, Y. K., *Finite Strip Method in Structural Analysis*, Pergamon Press, Inc., New York, N.Y., 1976.
4. DeWolf, J. T., Pekoz, T., and Winter, G., "Local and Overall Buckling of Cold-Formed Members," *Journal of the Structural Division*, ASCE, Vol. 100, No. ST10, Proc. Paper 10875, Oct., 1974, pp. 2017–2036.
5. Graves-Smith, T. R., "The Ultimate Strength of Columns of Arbitrary Length," *Symposium on Thin-Walled Steel Structures*, Swansea, 1967; Crosby-Lockwood, ed. Rockey, K. C., and Hill, H. V., 1969.
6. Graves-Smith, T. R., and Sridharan, S., "A Finite Strip Method for the Post-Locally-Buckled Analysis of Plate Structures," *International Journal of Mechanical Science*, Vol. 20, 1978, pp. 833–842.
7. Gallagher, R. H., Lien, S., and Mau, S. T., "A Procedure for Finite Element Plate and Shell Pre- and Postbuckling Analysis," *Conference on Matrix Methods of Structural Mechanics*, Wright-Patterson Air Force Base, Ohio, AFFDL-TR-71-160, 1971, pp. 857–879.
8. Hancock, G. J., "Local, Distortional and Lateral Buckling of I-Beams," *Journal of the Structural Division*, ASCE, Vol. 104, No. ST11, Proc. Paper 14155, Nov., 1978, pp. 1787–1798.
9. Hancock, G. J., "Nonlinear Analysis of Thin Sections in Compression," Research Report R355, University of Sydney, School of Civil Engineering, Australia, 1979.
10. Hu, P. C., Lundquist, E. E., and Batdorf, S. B., "Effect of Small Deviations from Flatness on Effective Width and Buckling of Plates in Compression," *TN 1124*, NACA, Washington, D.C., Sept., 1946.
11. Kalyanaraman, V., Pekoz, T., and Winter, G., "Unstiffened Compression Elements," *Journal of the Structural Division*, ASCE, Vol. 103, No. ST9, Proc. Paper 13197, Sept., 1977, pp. 1833–1848.
12. Koiter, W. T., and Van der Neut, A., "Interaction between Local and Overall Buckling of Stiffened Compression Panels," *International Conference on Thin-Walled Structures*, University of Strathclyde, Scotland, April 3–6, 1979.
13. Plank, R. J., and Wittrick, W. H., "Buckling under Combined Loading of Thin, Flat-Walled Structures by a Complex Finite Strip Method," *Journal for Numerical Methods in Engineering*, Vol. 8, No. 2, 1974, pp. 323–339.
14. Powell, G. H., "Theory of Nonlinear Elastic Structures," *Journal of the Structural Division*, ASCE, Vol. 95, No. ST12, Proc. Paper 6943, Dec., 1969, pp. 2687–2701.
15. Przemieniecki, J. S., "Finite Element Structural Analysis of Local Instability," *American Institute of Aeronautics and Astronautics Journal*, Vol. 11, No. 1, Jan., 1973.
16. Stowell, E. Z., "Compressive Strength of Flanges," *TN2020*, NACA, Washington, D.C., Jan., 1950.

17. Timoshenko, S. P., and Gere, J. M., *Theory of Elastic Stability*, McGraw-Hill Book Co., Inc., New York, N.Y., 1961.
18. Timoshenko, S. P., and Woinoiwsky-Krieger, S., *Theory of Plates and Shells*, McGraw-Hill Book Co., Inc., New York, N.Y., 1959.
19. Van der Neut, A., "The Longitudinal Stiffness of Simply Supported Imperfect Plate Strips," *Report VTH-152*, Delft University of Technology, Dept. of Aeronautical Engineering, The Netherlands, Aug., 1968.
20. Van der Neut, A., "The Interaction of Local Buckling and Column Failure of Thin-Walled Compression Members," *Proceedings*, 12th International Congress Applied Mechanics, Springerverlag, Germany, 1969.
21. Yamaki, N., "Postbuckling Behaviour of Rectangular Plates with Small Initial Curvature Loaded in Edge Compression," *Journal of Applied Mechanics*, ASME, Sept., 1959, pp. 407–414.

Appendix II.—Notation

The following symbols are used in this paper:

b = strip or plate width;
$[C]$ = square matrix defined by Eq. 10;
E_x, E_z = Young's modulus in x, z directions respectively of a strip;
EA = axial rigidity of an undeformed section;
$(EA)_{\text{eff}}$ = effective value of EA in the nonlinear range;
EI = flexural rigidity of an undeformed section;
$(EI)_{\text{eff}}$ = effective value of EI in the nonlinear range;
$\{F\}$ = imbalance of load vector;
f = variable factor which allows for the change in Poisson's ratio expansion as a result of change in membrane stress distribution in the nonlinear range of structural response ($f = 1$ initially);
$\{f\}$ = vector of displacements u, v, w;
G = shear modulus;
$[G(\epsilon_H)]$ = stability matrix;
K = buckling coefficient in Eq. 18;
$[K]$ = linear component of stiffness matrix;
$[K_1(\delta)], [K_2(\delta^2)]$ = nonlinear components of stiffness matrix;
$[K_1^*(\delta)]$ = see Eq. 14;
k = π/L;
L = length of strip;
M_x, M_z = bending moments about x, z axes, respectively;
M_{xz} = twisting moment;
P = longitudinal compressive load in plate or section;
P_l = value of P at local buckling;
S^* = $(EI)_{\text{eff}}/(EI)$ or $(EA)_{\text{eff}}/(EA)$;
t = strip or plate thickness;
u, v, w = displacement in x, y, z directions, respectively;
u_G, w_G = values of u, w resulting from plate flexure;
u_H, w_H = values of u, w resulting from Hookean shortening;
u_R = rigid body displacement in x-direction;
$\{W(\epsilon_H)\}$ = load vector resulting from initial strains;

x, y, z = Cartesian coordinate axes;
$\bar{x}$ = x/b;
Z_1, Z_2 = $\sin(kz)$ and $\sin^2(kz)$, respectively;
$\alpha_1, \alpha_2, \alpha_3, \alpha_4$
$\alpha_1', \alpha_2', \alpha_3', \alpha_4'$ = variable coefficients in displacement functions;
α = maximum amplitude of plate imperfection divided by plate thickness;
$\{\alpha\}$ = vector of coefficients;
$\{\delta\}$ = vector of nodal line displacements;
$\{\delta_0\}$ = initial value of $\{\delta\}$ caused by plate imperfections;
ϵ = longitudinal compressive strain;
ϵ_l = value of ϵ at local buckling;
ϵ_1, ϵ_2 = values of ϵ on nodal lines 1, 2, respectively;
ϵ_M = $(\epsilon_1 + \epsilon_2)/2$;
ϵ_x, ϵ_z = longitudinal tensile strains in x, z directions, respectively;
θ_z = rotation about z axis;
ν_x, ν_z = Poisson's ratio in x, z directions, respectively;
ρ = $(\epsilon_1 - \epsilon_2)/b$;
ρ_x, ρ_z = curvature about x, z axes, respectively;
ρ_{xz} = twist;
σ = longitudinal compressive stress;
σ_{av} = average value of σ;
σ_l = value of σ at local buckling;
σ_x, σ_z = longitudinal tensile stresses in x, z directions, respectively; and
τ_{xz} = shear stress in x, y plane of strip.

JOURNAL OF THE
STRUCTURAL DIVISION

BRIDGE DESIGN AND REGIONAL ESTHETICS[a]

By David P. Billington,[1] F. ASCE

INTRODUCTION

The purpose of this paper is to show how leading bridge designers have developed individual styles within limited locales and how those styles demonstrate similarities in personal esthetic ideas. An examination of the works of six major bridge designers will characterize these ideas and illustrate the striking fact that in each case, these designers have done nearly all their major work in one well-defined region of remarkably small area.

It is the thesis of this study that the bridges of these six men: Thomas Telford (1757–1834), John Roebling (1806–1869), Gustave Eiffel (1832–1923), Robert Maillart (1872–1940), Othmar Ammann (1879–1965), and Christian Menn (born in 1927) are at least as good as, and probably better than, any of their time, and that there is a definite connection between the high quality of their work and its restriction to a small well-defined geographic region. In short, their results illustrate a series of individual styles, rather than international styles, that spring from local conditions. Each of these styles shows the vision of a single designer as he strove to meet local conditions, and to express the esthetic potential of bridge forms as he saw it.

This study summarizes briefly the career of each designer, the local conditions within which he worked, and the individual style of each. What sets these six designers apart is that they all strove consciously to design bridges that met local physical conditions with as little materials as possible, that satisfied the political constraints of utility with as little public money as possible, and that improved the environment visually by expressing as clearly as possible their idea of appropriate structural form. Thus, in this study, the bridges defined as the best are those which combine, to the highest degree, efficiency in use of materials, economy in money, and handsome appearance.

The basis for choosing only six out of perhaps the 20 best-known modern

[a]Presented at the April 14–18, 1980 ASCE Convention and Exposition, held at Portland, Oreg.

[1]Prof. of Civ. Engrg., Princeton Univ., School of Engrg./Applied Sci., Princeton, N.J. 08540.

Note.—Discussion open until August 1, 1981. To extend the closing date one month, a written request must be filed with the Manager of Technical and Professional Publications, ASCE. Manuscript was submitted for review for possible publication on July 7, 1980. This paper is part of the Journal of the Structural Division, Proceedings of the American Society of Civil Engineers, ©ASCE, Vol. 107, No. ST3, March, 1981. ISSN 0044-8001/81/0003-0473/$01.00.

bridge designers is that these six show more clearly than their contemporaries, a distinct and consistent individual style of visual form. In short, the choice is basically esthetic. It is further true that each of the six has probably been studied more thoroughly than any of his contemporaries, expecially from a combined esthetic-technical point of view. It is, however, entirely possible that with more detailed study other designers will be seen as possessing style of a quality equal to that of any of these six studied here. [A fuller list of designers in the first rank would surely include I. K. Brunel (1806–1859), Eugene Freyssinet (1879–1962), David Steinman (1885–1960), and Ulrich Finsterwalder (born in 1897). There are a number of other designers still active in 1980 who might well merit detailed study, as well.]

Although these six designers, except for Menn, are well-known, a brief review of each is useful in order to draw attention to common esthetic ideas. Therefore, after briefly reviewing the career, locale, and style of each designer, I shall explore their similarities and conclude with a few tentative generalizations.

Thomas Telford

Telford was born in Glendinning, Scotland on August 9, 1757, and helped to build a bridge at Langhold, a three-span masonry arch bridge completed about 1778. The first bridge built to his own design, also a multispan stone arch bridge, was completed in 1792. His first iron bridge called Buildwas, built in 1795, 2 mile upstream from the 1779 Iron Bridge, had a span of 130 ft, which, though 30% greater than the Iron Bridge span, required only half the weight of the earlier work.

FIG. 1.—Craigellachie Bridge

His work with metal continued with the Pontcysyllte Aqueduct built between 1795 and 1805. This was the most impressive canal structure of its day and remains today a remarkable work. Metal arches, resting on hollow masonry piers over 100 ft above the valley, carry the canal over the River Dee. The original iron work is in good serviceable condition today after about 1-3/4 centuries of use.

Telford's most modern-looking metal arch bridges are those at Craigellachie in Scotland (150 ft in span, completed in 1815); at Bettwys-y-coed, called the Waterloo Bridge (finished in 1815); near Tewkesbury, called the Mythe Bridge (170 ft in span, finished in 1826); at Holt Fleet over the Severn (completed in 1827); and at Galton (150 ft in span, built in 1829). These are all characterized by flat lattice cast-iron arches connected to the nearly flat roadways above by thin diagonals. Over about the central third of the spans the arches carry the roadway directly (1).

Telford's two greatest bridges are the 327-ft span Conway Bridge and the 579-ft span Menai Straits Bridge, both in Wales, and both completed in 1826. They are eyebar chain suspension bridges with light decks and masonry towers. Menai was the longest spanning bridge in the world until the 1834 completion of the Sarine Valley Bridge at Fribourg, Switzerland. The Conway Bridge is still in service, and has stood well for over 150 yr. The Menai, on the other hand, suffered much damage from wind and has been rebuilt several times, but is also still in service today.

For our study, here it is the flat-iron lattice arches (see Fig. 1) that constitute Telford's mature style in medium-span bridges. With the exception of Craigellachie, they were built in the west of England and Wales in hilly country cut by narrow streams. It was in the region where the Industrial Revolution is said to have begun at just the time Telford began to practice (2). Telford's arches characterize that revolution in their material, i.e., cast iron, and in their form, i.e., the lattice arch, which would be the same basic form for the longest spanning steel arches of the twentieth century.

John A. Roebling

John A. Roebling was born in Muhlhausen, Saxony, Germany on June 12, 1806. He studied civil engineering at the Polytechnic Institute in Berlin, finishing in 1828, after which he worked the next 3 yr building roads for the Prussian government. In May of 1831, he left Germany with a group of others for America, where they bought land in western Pennsylvania and founded Saxonburg as a farming community of German immigrants.

In 1837, Roebling became an American citizen. Bored with farming, he took a job as an engineer for the state of Pennsylvania, building dams and locks, and surveying line for a prospective railroad route. He soon became principal assistant to the chief engineer of the state, and at Johnstown, Pa., became familiar with the newly-constructed Portage Railroad where long canal boats were hauled up mountains by hemp ropes. Roebling successfully substituted iron wire rope for the hemp and established a factory for wire rope at Saxonburg in the summer of 1841.

In 1844, he won the competition to build his first suspension bridge, carrying a canal over the Alleghany River; and by 1849, when he moved his factory

to Trenton, N.J., he was already a success, both at factory production and bridge building. Roebling's first suspension bridge for a roadway was built in Pittsburgh, over the Monogahela River in 1845, and his next major works were the 815-ft span Niagara Falls Rail and Road Bridge, completed in 1855, and the Cincinnati Bridge begun in 1856 which was interrupted by the Civil War, but afterward completed in 1866.

In March 1857, Roebling wrote a letter to Horace Greeley, published in the *Tribune,* announcing his intention to build an East River Bridge. Greeley had proposed a bridge in the *Tribune* as early as 1849. Then in April 1967, a charter was granted by the New York Legislature in Albany, and in that September, Roebling first presented his plan in Brooklyn. His written proposal had begun with perhaps his most noted statement which included

> . . . the great towers . . . will be ranked as national monuments. . . . As a great work of art, and a successful specimen of advanced bridge engineering, this structure will forever testify to the energy, enterprise, and wealth of that community which shall secure its erection.

In February 1869, Roebling presented his plans to a consulting board including William Jarvis McAlpine, president of the newly-reformed ASCE, and also presented his plans to Henry Latrobe, son and namesake of the architect chosen by Thomas Jefferson to rebuild Washington, D.C. after its burning by the British in 1812. On June 28, 1869, Roebling's foot was crushed by a ferryboat while surveying for the bridge and he died of lockjaw on July 22. His eldest son, Washington A. Roebling, became chief engineer for the bridge. Flags in Brooklyn were flown at half mast for Roebling.

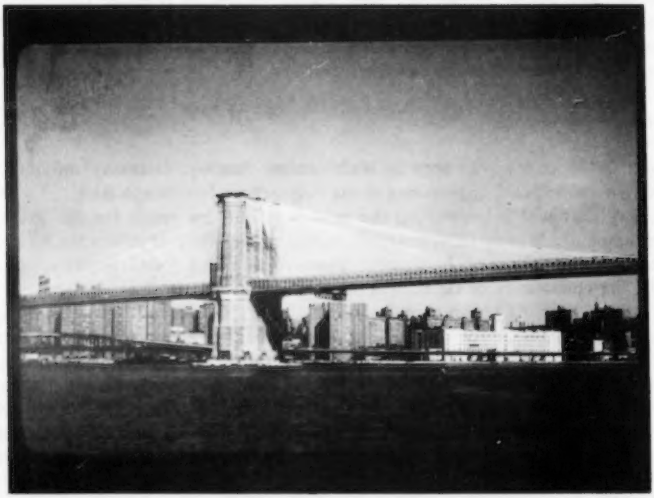

FIG. 2.—Brooklyn Bridge

The Brooklyn Bridge, under Washington Roebling's direction, began with ground breaking for the Brooklyn Tower foundation on January 3, 1870, and was officially opened on May 24, 1883. Built essentially as designed by John Roebling, it quickly became the landmark he predicted, and was officially made a National Historic Landmark in 1964 (3).

Roebling's mature style consisted of masonry towers, a thin deck supported by vertical suspenders, and cable stays radiating out from the towers (see Fig. 2). Nearly all of his bridges were built in the states of Pennsylvania, New York, and Ohio, and his three major works are all over large open waterways.

Gustave Eiffel

Eiffel was born in Dijon, France, on December 15, 1832, and after study in the local schools tried for entrance into the Ecole Polytechnique, but he failed the examination. He enrolled instead in the Paris Ecole Centrale des Arts et Manufactures from which he graduated in 1855, with a degree in chemical engineering. He had intended to enter his uncle's vinegar business, but family disputes prevented that, so he joined a construction firm, quickly rising to chief engineer of bridges (4). In the 1860s he decided to establish his own firm and by 1869 he had designed and built a series of viaducts in France's Massif Central that established his mastery of metal bridge form.

By 1878, Eiffel was regarded as the leading builder of metal structures in France, and by many, as the leader in the world. His works included major bridges in many parts of the world, the most important of which are: the 1864 viaduct over the Creuse River at Busseau, the four viaducts between Gannat

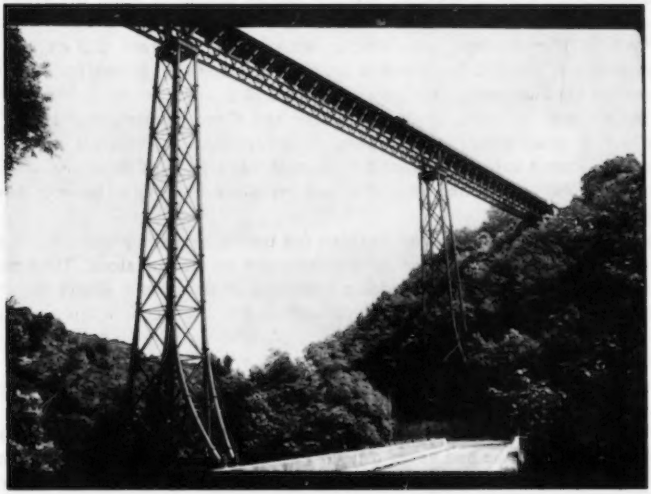

FIG. 3.—Viaduct of Rouzat

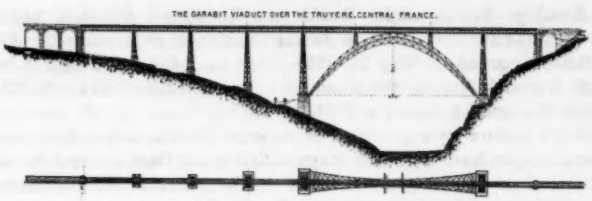

FIG. 4.—Garabit Viaduct

and Commentry of 1867–1869 (at Bouble, at Bellon, at Rouzat, and at Neuvial), the 1877 Maria Pie viaduct over the Douro in Portugal, and the Garabit Viaduct in the Massif Central, completed in 1884 as the longest spanning arch in the world, with 165 m (5).

Eiffel's designs in the Massif Central reflect the problems of heavy wind loads on very high viaducts and his style was to widen his towers and arches in the lateral direction, giving the strong visual impression of stability (see Figs. 3 and 4).

Robert Maillart

Robert Maillart was born on February 6, 1872 in Berne, Switzerland, where his father, a Belgian citizen, was a banker. He studied civil engineering at the Federal Institute of Technology in Zurich, and graduated in 1894. Ironically, one of his lowest grades was in bridge design, even though he is regarded today as one of the half-dozen greatest bridge designers since the industrial revolution.

For 8 yr following his graduation, he worked with different civil engineering organizations. In 1902, he founded his own firm for design and construction; thereafter his business grew rapidly and expanded as far as Russia and Spain. In the summer of 1914, he took his wife and three children to Russia. The World War made it difficult to return to Switzerland, so Maillart stayed and worked in Russia until 1918, when his business was liquidated by the Revolution. Forced to flee, he returned to Switzerland penniless and lonely, his wife having died in Russia.

Because of these misfortunes, Maillart felt unable to take up the construction business again, and from then on concentrated on design alone. He opened an office in Geneva in 1919, adding branches in Berne and Zurich in 1924. During the 1920s, he began to develop and modify his ideas of bridge design; until his death in 1940, he produced over 30 bridge designs of extraordinary originality. Unfortunately, no Swiss municipality would accept his designs for prominent urban locations, and most of these designs were built in rural areas, many in the mountainous countryside.

In 1936, he was elected an honorary member of the Royal Institute of British Architects although he had never officially acted as an architect on any project. The 1941 first edition of *Space, Time and Architecture* by art historian Sigfried Giedion, introduced Maillart to a wide public in the United States. Finally, Max Bill's 1949 book, *Robert Maillart*, with its photographs and commentary

FIG. 5.—Salginatobel Bridge

FIG. 6.—Schwandbach Bridge

on nearly all of Maillart's major bridges, powerfully presented him as an artist of the first rank.

Maillart developed two major new bridge forms in reinforced concrete: the hollow-box and the deck-stiffened polygonal arch. His early hollow boxes were all three-hinged arches, but he later used the form in straight spans as well. The 1930 Salginatobel Bridge (see Fig. 5) shows these three-hinged forms, while the 1933 Schwandbach Bridge (see Fig. 6) shows the deck-stiffened types. These forms were built often in narrow valleys up in the hills and mountains of Switzerland, nearly all in only two of the Swiss cantons: the Graubünden and Bern (6).

Maillart's style shows extraordinarily-thin polygonal arches or vanishingly-thin hinged points on the hollow-box forms. The concrete is fully exposed, and the forms provide strong contrast in the mountain environment. Most of his major works got built because they won cost competitions, in which he nearly always proved his designs to be less costly than alternate designs. The long tradition of Swiss design/construction competitions allowed Maillart to win designs that he probably would not have gotten had design commissions been awarded directly by public officials to consulting engineers.

Othmar Ammann

Ammann was born on March 26, 1879, in Feuerthalen, Switzerland, attended schools near and in Zurich, and entered the Federal Polytechnical Institute in 1897, graduating in 1902. He had the same professor for bridge engineering, Wilhelm Ritter (1847–1906), as did Robert Maillart (7). In 1904, Ammann came to the United States where he worked for several different firms ending up with Gustav Lindenthal from 1912–1923. There he worked on the 1915 Hellgate Bridge, and later on Lindenthal's proposals for a Hudson River suspension bridge.

Ammann left Lindenthal in 1923, submitted his own design for the Hudson River Bridge (now called the George Washington Bridge) late that same year, and in 1924 was named chief bridge engineer for the Port Authority of New York and New Jersey, where he remained until World War II. After the war he formed a partnership with Charles S. Whitney.

Ammann's major designs were: the 1931 George Washington Bridge with a span of 3,500 ft, the 1931 Bayonne Bridge with an arch span of 1,652 ft, the 1936 Triborough (suspension) Bridge with a span of 1,380 ft, the 1939 Bronx-Whitestone (suspension) Bridge of a 2,300-ft span, the 1,850-ft span Throgs-Neck (suspension) Bridge of 1961, and the 4,260-ft span Verrazano (suspension) Bridge, opened in November 1964, just 10 months before Ammann's death on September 22, 1965. The remarkable fact is that with a few exceptions (8), Ammann's long span designs are all in New York City and it is possible on a clear day to see them all from the Port Authority's World Trade Center! (He also designed the 1961 Walt Whitman Bridge in Philadelphia, as well as many smaller works.) Not any of the previous four designers had such a narrow region in which was concentrated his major works.

Ammann's style in suspension bridges consisted of strong vertical towers with a single cross member at the top (see Fig. 7) and light horizontal decks.

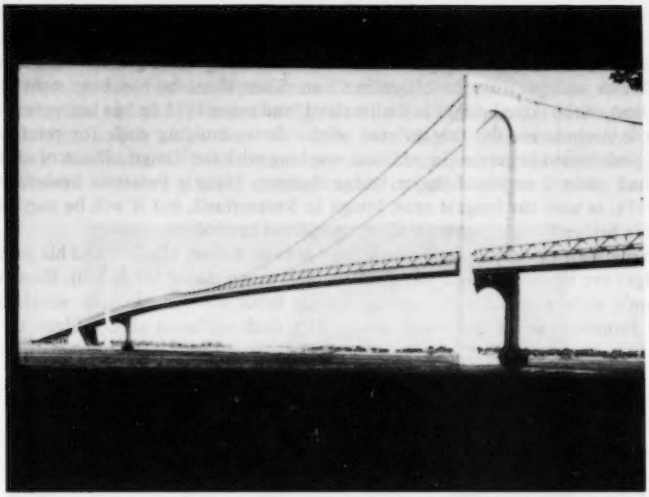

FIG. 7.—Bronx-Whitestone Bridge

The only exception to this visual pattern is in the towers of the Triborough Bridge, but there Ammann did not make the original design, but only modified, for the purpose of economy, an earlier one made by others (9).

Christian Menn

Christian Menn was born in 1927 in Meiringen, in the Berneroberland, the third of five children. Because of his father's work, he lived in various parts of Switzerland, but his family was from the Graubünden, the largest and most sparsely settled Swiss canton. When Menn was 10 yr old, he went to live with his uncle on a farm near the small Graubünden town of Sufers on the Hinterrhein, just below the San Bernardino pass. He began his studies in 1939 at the canton school in Chur, capital of the Graubünden. In 1946, he entered the Federal Technical Institute in Zurich, graduating with a degree in civil engineering in 1950, after which he entered the military service. In 1951, he contracted tuberculosis and spent 14 months in a hospital in Arosa, where he began theoretical studies and his doctoral work. After his recovery, he went back to his university and became an assistant to Professor Pierre Lardy, from whom he had first learned in detail about the work of Robert Maillart.

After receiving his doctorate in structural engineering in 1956, Menn worked in Paris on the United Nations Educational, Scientific, and Cultural Organization buildings designed by Pier Luigi Nervi. He returned to Switzerland in 1957, and in June of that year he opened his own office in Chur. In the years that followed, he designed numerous bridges and buildings, mostly in the Graubünden,

and he won first prize for several bridge competitions in other cantons of Switzerland.

In 1971, Menn was made professor of structural engineering at his old institute in Zurich and gave up the office in Chur. Since then, he has been consultant on most of the large bridges in Switzerland, and since 1977 he has been president of the commission for the revision of the Swiss building code for reinforced and prestressed concrete. In addition, working with the design offices of others, he had made a series of major bridge designs. Menn's Felsenau bridge, built in 1974, is now the longest span bridge in Switzerland, but it will be surpassed by his bridge for the Ganter Valley, completed in 1980.

Menn was strongly influenced by the works of Robert Maillart and his earliest bridges are visually almost copies of Maillart's two major forms (10). However, Menn's style evolved slowly as increasing labor costs made arch scaffolding and formwork more and more costly. His deck-stiffened arch bridges of the

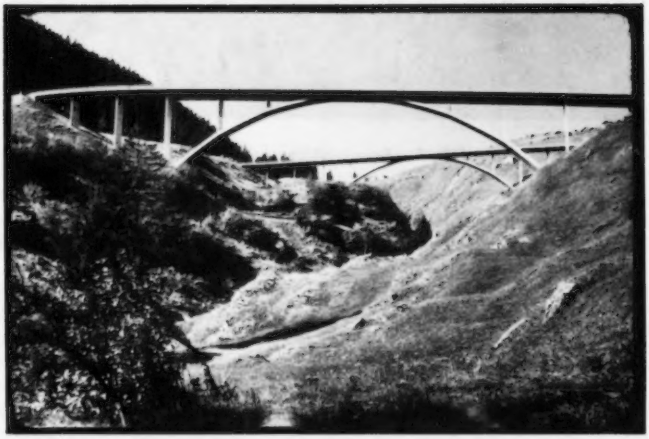

FIG. 8.—Nanin and Cascella Bridges

1960s show an extreme lightness and an increase in spacing between cross walls (see Fig. 8), both to reduce formwork and to take advantage of prestressing in the deck.

In 1970, a competition was held for a very large viaduct to be built just north of Bern over the Aare River at Felsenau. Seven groups were invited to submit designs. Menn, as head of one group, was expected to produce a fine arch design. Instead, because scaffolding for very high works was becoming increasingly costly, he submitted the plan for a fully prestressed cantilever bridge. Ulrich Finsterwalder in Germany had pioneered this type of bridge, which is built without scaffolding. The forms for small sections are moved out horizontally from already built columns, and the sections are cast and allowed to harden; they are then prestressed by tendons, which tie the newly-formed sections back

into those previously cast. The bridge is thus built out on itself, using only a small amount of forming and no scaffolding from the ground.

Menn took Finsterwalder's method and modified the design in two significant ways. First, he used two slender columns at each major support, reducing material, and giving the visual impression of lightness; second, he used, for a relatively wide bridge, only a single box with very long slabs cantilevered laterally to complete the roadway. Unlike most previous long-span cantilevered bridges, the Felsenau is curved in plan, making it more complicated (see Fig. 9).

FIG. 9.—Felsenau Bridge

Because of the economy and elegance of Menn's solution, it won first prize, and the bridge has since been completed according to his plans. The main 156-m spans, now the longest in Switzerland, together with the 60-m columns make this bridge an impressive sight as it curves out of the woods and across the river, high above the ordered suburban communities below. Thus, by the 1970s, the potentials of prestressing were being exploited more fully, and arches were no longer competitive for shorter spans.

Even more impressive than Felsenau is the design proposed by Menn in 1975 for the Ganter Bridge on the Simplon Road. Here the canton of Valais had intended to build a tunnel. Menn, however, estimated that his bridge would cost about half the amount needed for the tunnel, and bids on the Ganter Bridge proved him right. Completed in 1980, this immense work crosses a wide, deep valley with a central span 174 m long; the highest of the supporting columns is 130 m. More remarkable than the sheer size is the form, a prestressed cantilever girder in which the main prestressing tendons rise well above the girder at

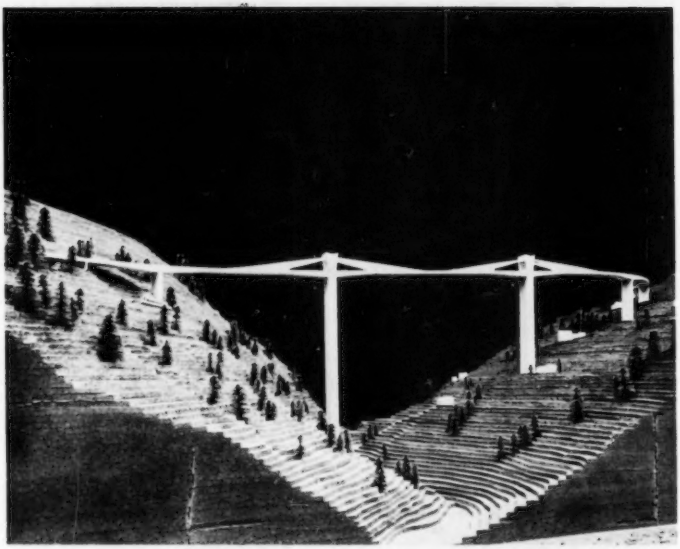

FIG. 10.—Ganter Bridge

the columns. These tendons are concreted into walls over the central part of the span to give a unique profile that fully exploits prestressing (see Fig. 10).

Similarities

Each of these six designers did evolve a personal style which sets their work apart from others. In addition, that style developed within one relatively small region which each designer knew intimately. In every case these designers have developed new forms and some at vastly increased scales. They went beyond the state-of-the-art, leading the way to a new state and a new set of art forms. In nearly all cases their designs were publicly debated in competition with designs by others. Each gained prominence by making designs which were less costly than others.

Except for Telford, whose early career predates formal technical education,

each was well trained in the best of engineering schools. Each had either direct experience as a builder (Roebling, Eiffel, and Maillart), or studied building practice firsthand so as to integrate construction ideas directly into design.

Finally, each designer wrote about esthetics, and each considered it a central design concern. Except for Ammann, none of these designers worked together with architects on their mature works; and Ammann clearly determined the form of his bridges and did not let anyone else decide major issues of appearance (11). Thus, each designer believed that the appearance was the full responsibility of the engineer and that a major goal of design was a handsome form.

Embury, the author of Ref. 11, clearly describes Ammann's control of the design, and in several other articles details his own ideas which are characterized by the following:

> It is my belief that more good engineering projects are spoiled by false deference to assumed esthetic considerations than by any economic requirements . . . the structure whose function is partly concealed and partly distorted for supposed esthetic reasons will inevitably be unsuccessful.

Bridge Esthetics

The common ideas of these six designers can be tentatively identified generally as lightness or thinness, exposed and undistorted structure, and a form that fits the local environment. Each of these general ideas needs a careful visual analysis that considers the works of each designer separately. Such analyses are beyond this present scope, so I can only conclude by a brief clarification of each idea by reference to some of the figures.

Lightness or thinness means that visually, the new materials of industrialized metal, reinforced and prestressed concrete, allow the use of very thin and open sections, and that these designers wanted to express that visually (see Figs. 1, 4, and 9). This represents a denial of the centuries-long tradition of heavy solid closed forms so typical of most masonry bridges.

Exposed and undistorted structure means that visually, the new forms were the load-carrying parts without any cladding whatsoever. Further, those exposed forms were shaped to give both a greater efficiency and a better looking result at the same time (see Figs. 7 and 10).

Finally, a form that fits the environment means one that fits the foundation conditions, the wind forces, the approaches, and the weathering. Fitting the environment does not mean making stone facades because of a rocky terrain, or any other such superficial visual expression unrelated to the structural ideas. Thus, the Rouzat towers (Fig. 3) spread to reflect visually the overturning of the wind, the Brooklyn Bridge diagonal stays show Roebling's concern with the vertical effect of wind (Fig. 2), and the curved sweep of the Felsenau (Fig. 9) and the Schwandbach (Fig. 6), fit with the turn in the highway. The Salginatobel's flat three-hinged form reflects the steep valley walls and the dangerous vertical movements in one of them (Fig. 5).

It seems that for each of these six designers the expression of bridge form came from the designers: (1) Being restricted to a well-defined region of small area and of relatively uniform topology; (2) working in a political context where

alternative designs were publicly debated, and often design competitions or design-construction competitions held for bridges; (3) slowly gaining experience through completed works so that their best works invariably came later in life; and (4) gradually evolving a personal style that is visually clear in retrospect.

All of these factors help support the conclusion that these six, along with the best of their contemporary designers, were and are artists in a new art form, Structural Art, made possible by the new materials of the industrial revolution. Thus, there are three sorts of artists in the modern world working in three-dimensional forms: engineer, architect, and sculptor. Each is an independent artist type, although each can learn from the others and although sometimes they collaborate on works. A review of bridge design reveals that structural art has developed independently from the arts of architecture and sculpture, and as such, this engineering art holds great promise for the future.

Acknowledgments

Support for the study leading to this paper came from a grant by the National Endowment for the Humanities for a program at Princeton, directed by Robert Mark and myself, and entitled "Curriculum Materials for Humanistic Studies in Modern Engineering." Also, some of the ideas presented here were developed under a grant from the National Endowment for the Arts, a Federal agency in Washington, D.D.

Appendix.—References

1. Bracegirdle, B., and Miles, P. H., *Thomas Telford,* David and Charles Publishing, Co., North Pomfret, Vt., 1973, 112 pages.
2. Ruddock, T., *Arch Bridges and Their Builders,* Cambridge University Press, Cambridge, England, 1979.
3. McCullough, D., *The Great Bridge,* Simon and Schoster, New York, N.Y., 1972.
4. Harriss, J., *The Tallest Tower,* Houghton Mifflin Co., Boston, Mass., 1975.
5. Eiffel, G., "Les Grandes Constructions Metalliques," lecture given at the French Association for the Advancement of Science, Mar., 10, 1888, p. 22.
6. Billington, D. P., *Robert Maillart's Bridges: The Art of Engineering,* Princeton University Press, Princeton, N.J., 1979.
7. Billington, D. P., "Wilhelm Ritter: Teacher of Maillart and Ammann," *Journal of the Structural Division,* ASCE, Vol. 106, ST5, Proc. Paper 15416, May, 1980, pp. 1103–1116.
8. Stussi, F., *Othmar H. Ammann: Sein Beitrag zur Entwicklung des Bruckenbaues,* Birkhauser Publishers, Basel, Switzerland, 1974.
9. "New York's Triborough Bridge," *Engineering News-Record,* Vol. 115, No. 6, Aug. 8, 1935, pp. 177–183; see also Bowden, E. W., "The Triborough Bridge Project," *Civil Engineering,* ASCE, Vol. 6, No. 8, Aug., 1936, pp. 515–519.
10. *The Bridges of Christian Menn,* Princeton University Art Museum, Princeton, N.J., 1978.
11. Embury, A., Jr., "Esthetics of Bridge Anchorages," *Civil Engineering,* ASCE, Vol. 8, No. 2, Feb., 1938, pp. 85–86; see also Embury, A. Jr., "The Architect and the Engineer," *Civil Engineering,* ASCE, Vol. 8, No. 1, Jan., 1938, p. 4.

JOURNAL OF THE STRUCTURAL DIVISION

LOW-CYCLE FATIGUE TEST OF WELDED TUBULAR JOINTS

By Shunsuke Baba,[1] Yasunori Arizumi,[2] and Masao Naruoka[3]

INTRODUCTION

Welded tubular truss structures are currently widely employed in the field of marine structures. An important problem of such structures is evaluation of the strength of welded joints under strong repeated loadings in the plastic range.

Static and high-cycle fatigue tests on welded tubular joint specimens have often been reported: for example, by Akiyama (1) for T-type, X-type, and K-type joint specimens; by Kanaya (4) and Toprac (9) for T-type joint specimens; and by Maeda (6) and Washio (10) for X-type and K-type joint specimens. However, so far as the writers know, no report has been published concerning low-cycle fatigue tests of welded tubular joint specimens.

The structure will vibrate cyclically in the plastic range under the action of strong earthquake motion or strong wave motion, which can be regarded as a kind of high-stress, low-cycle fatigue process. Experimental and theoretical studies on the low-cycle fatigue phenomenon have been reported by many researchers, in which the low-cycle fatigue is defined as a fatigue phenomenon whose number of cycles to failure N is less than 10^3 or 10^4. However, fatigue tests in which N is less than 10^2 are extremely scarce even for the simplest specimen, such as a smooth rod.

In this paper, static tensile tests and low-cycle fatigue pull-pull tests ($N < 600$) using X-type welded tubular joint specimens are described. Fifty-six specimens of the same size and the same material, whose height was 1.2 m (3 ft 10 in.), were prepared both for the static and low-cycle fatigue tests.

Since welded tubular joint specimens are complicated structures as compared

[1]Assoc. Prof., Dept. of Geotechnical Engrg., Nagoya Univ., Furo-cho, Chikusa, Nagoya, 464-Japan.

[2]Research Assoc., Dept. of Architectural Engrg., Univ. of the Ryukyus, Japan.

[3]Prof., Dept. of Civil Engrg., Nagoya Univ., Japan.

Note.—Discussion open until August 1, 1981. To extend the closing date one month, a written request must be filed with the Manager of Technical and Professional Publications, ASCE. Manuscript was submitted for review for possible publication on June 12, 1980. This paper is part of the Journal of the Structural Division, Proceedings of the American Society of Civil Engineers, ©ASCE, Vol. 107, No. ST3, March, 1981. ISSN 0044-8001/81/0003-0487/$01.00.

with a smooth rod, the numbers of cycles to failure N are likely to show a strong scatter. The scatter of N will probably result from welding defects such as lack of penetration. But in the case of X-type welded tubular joint specimens, the weld lines are long and complicated. Welding defects are therefore hard to measure along all the weld seams; and even if they could be measured, it would be impossible to evaluate the effects of welding defects on the fatigue strength. Thus, the scatter of welding defects is not a practical factor in explaining the scatter of N. The writers try to substitute the scatter of static collapse load for the scatter of welding defects.

The writers believe that the large scatter of N due to the scatter of welding defects (static collapse load) should be eliminated in considering the fatigue property of the specimens, and that the relation between the repeated load S and the number of cycles to failure N, which is called the S–N curve, should be recalculated for the particular state in which the static collapse load S_0 of all specimens is made equivalent by applying the Bayesean theorem and the concept of the weighted mean.

The effect of size of the welded tubular joint and the influence of residual stress, which is called the annealing effect, are examined by preparing four kinds of specimens of different sizes, of which half are annealed in order to eliminate the residual stress. These two effects and the relationship between them are considered herein.

Outline and Results of Test

The static tensile test and the pull-pull fatigue test were conducted using the X-type welded tubular joint specimens shown in Fig. 1.

Four kinds of specimens of different sizes—they were similar in shape—were

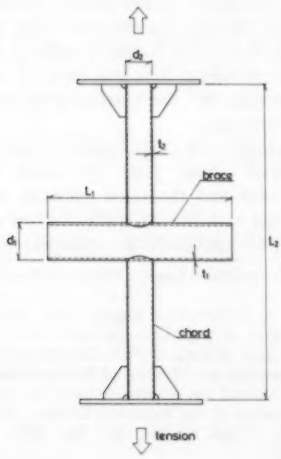

FIG. 1.—Specimen

prepared, and are described as case-1 through case-4 specimens. Let Case-3 specimen be a standard-size specimen, in which chord diameter $d_1 = 139.8$ mm, chord thickness $t_1 = 4.5$ mm, chord length $l_1 = 700$ mm, brace diameter $d_2 = 101.6$ mm, brace thickness $t_2 = 3.2$ mm, and brace length $l_2 = 1200$ mm. The dimensions of the specimens are listed in Table 1, which shows that the Case-1 specimen had a quarter as much cross-sectional chord area as the Case-3 specimen, the

TABLE 1.—Sizes of Specimens

	Chord					Brace			Similarity Among Four Specimens[a]	
Case (1)	Length l_1, in millimeters (2)	Diameter d_1, in millimeters (3)	Average of thickness $\bar{t}_1$, in millimeters (4)	Cross-sectional area $\bar{A}_1$, in square millimeters (5)	$r_a = A_1/A_3$ (6)	Length l_2, in millimeters (7)	Diameter d_2, in millimeters (8)	Thickness t_2, in millimeters (9)	d_2/d_1 (10)	d_1/t_1 (11)
1	300	60.5	2.5	421	0.215	500	42.7	2.3	0.706	24.2
2	580	114.3	3.6	1,218	0.591	900	76.3	2.8	0.668	31.8
3	700	139.8	5.0	1,913	1.000	1,200	101.6	3.2	0.727	28.0
4	950	190.7	5.2	3,087	1.431	1,650	139.8	4.5	0.733	36.7

[a]Mean of $d_2/d_1 = 0.709$; mean of $d_1/t_1 = 30.2$.

TABLE 2.—Numbers of Specimens Used in Test

	Normal		Annealed		
Case (1)	Static (2)	Fatigue (3)	Static (4)	Fatigue (5)	Σ (6)
1	1	4	1	3	9
	(1)	(5)	(1)	(4)	(11)
2	1	4	1	2	8
	(1)	(5)	(1)	(4)	(11)
3	10	37	1	2	50
	(10)	(41)	(1)	(4)	(56)
4	1	5	1	4	11
	(1)	(5)	(1)	(4)	(11)
Σ	63 (69)		15 (20)		78 (89)

Note: Numbers in parentheses refer to total number of specimens, including misses.

Case-2 specimen had half as much chord area as the Case-3 specimen, and the Case-4 specimen had one and a half times as much chord area as the Case-3 specimen. The ratios of chord areas of Case-1, Case-2, and Case-4 specimens to the Case-3 specimen were not exactly 1/4, 1/2, and 1.5, respectively, and also the ratio of chord diameter to chord thickness (d_1/t_1) was not strictly

constant for each case specimen, because commercially available standard-size tubes were employed. Case-1, Case-2, and Case-4 specimens were used to consider the size effect by comparing them with the Case-3 specimen.

Four kinds of annealed specimens, which were the same sizes as the Case-1 through Case-4 specimens, were prepared in order to consider the influence of residual stress or so-called annealing effect. The numbers of specimens of various sizes are shown in Table 2, in which the annealed and the nonannealed specimens are indicated separately.

The specimens were made of STK41 steel tube, whose tensile strength was 4.02 MPa (41 kg/mm^2), that is, whose tensile collapse load was almost 402 kN, because the cross-sectional brace area was almost 1000 mm^2. The welding operation was done by a skilled workman, and the surface of the welds was not smoothed by a grinder as can be seen in the practical structures.

The repeated load was applied by a constant-load method. It was a pull-pull test, and the minimum pull load was one-tenth of the maximum pull load or

TABLE 3.—Tensile Strengths of Case-3 Specimens

t_1, in millimeters[a] (1)	S, in kilonewtons (2)	S^m, in kilonewtons[b] (3)
4.99	249	250
4.99	255	256
5.03	267	265
5.01	275	274
4.97	275	278
4.97	292	295
4.99	301	302
5.03	314	311
4.97	314	317
4.97	320	323
4.97	324	327

[a]Mean = 5.00.
[b]Mean = 290; standard deviation = 27.2.

minimum 9.8 kN (1000 kgf). The frequency of the repeated load was 3 cycles per min, which is the shortest period for the machine to generate an exact sine-wave loading.

Details of the tests are as follows:

1. Static tensile tests for Case-3 specimens: Ten specimens were prepared for the static tensile test in order to obtain a good estimate of the mean and the variance of static tensile collapse load S_0. The results are shown in Table 3, in which the other data coming from the fatigue test are added if the specimen collapsed at $N = 1$. In cases of low-cycle fatigue test, especially if $N < 1000$, a linear relation between the static collapse load ($N = 1$) and the cyclic collapse load ($N > 1$) has been reported (3,8,11). The collapse loads are modified related to chord thickness t_1 (see next section), and the modified collapse loads are expressed as S_0^m.

2. Pull-pull fatigue tests for Case-3 specimens: Forty-one specimens were prepared and divided into five categories according to the magnitude of repeated loads, and successful data were obtained for 37 specimens. Five categories of repeated loads S were as follows (numbers of specimens are shown in parentheses): $S = 255$ kN (26,000 kgf) (9 specimens); $S = 245$ kN (25,000 kgf) (10); $S = 235$ kN (24,000 kgf) (9); $S = 216$ kN (22,000 kgf) (5); $S = 196$ kN (20,000 kgf) (4). The numbers of cycles to failure N are shown in Table 4, in which the repeated loads are also modified related to chord thickness as well as the static collapse load, and are expressed as S^m. The relationships

TABLE 4.—Applied Repeated Loads and Numbers of Cycles to Failure of Case-3 Specimens

$S = 255$ kN (26,000 kgf)										
S^m(kN)	256	255	253	256	255	253	259	253	259	
$S^m/\bar{S}_0^m$	0.882	0.878	0.872	0.882	0.878	0.872	0.892	0.872	0.892	
N	1	40	82	114	128	172	232	279	472	
N^s	185	152	162	163	169	184	177	208	214	
$S = 245$ kN (25,000 kgf)										
S^m(kN)	247	247	244	240	247	244	247	249	239	243
$S^m/\bar{S}_0^m$	0.851	0.851	0.841	0.828	0.851	0.841	0.851	0.858	0.824	0.838
N	11	95	132	227	274	293	306	329	343	385
N^s	177	182	199	241	241	250	247	249	280	283
$S = 235$ kN (24,000 kgf)										
S^m(kN)	233	230	235	233	234	237	230	232	240	
$S^m/\bar{S}_0^m$	0.804	0.791	0.811	0.804	0.807	0.818	0.791	0.797	0.828	
N	124	158	161	185	246	275	362	437	554	
N^s	215	240	233	247	271	280	332	350	360	
$S = 216$ kN (22,000 kgf)										
S^m(kN)	219	210	214	215	217					
$S^m/\bar{S}_0^m$	0.753	0.723	0.736	0.740	0.747					
N	287	289	410	448	554					
N^s	340	353	412	430	473					
$S = 196$ kN (20,000 kgf)										
S^m(kN)	196	196	196	196						
$S^m/\bar{S}_0^m$	0.676	0.676	0.676	0.676						
N	334	434	517	556						
N^s	403	473	523	544						

between the nondimensional load (S^m/S_0^m) and the numbers of cycles to failure N are shown in Fig. 2(a), in which circular symbols are employed. In Fig. 2(b), nondimensional repeated load (S^m/S_0^m) is used as an ordinate instead of the stress. Stress may be a reasonable parameter of ordinate if the specimen has the same cross section along its length; but in the case of an X-type welded tubular joint specimen, the stress is not constant except in a part of the brace distant from the joint. The axial stress, which is obtained by dividing the collapse load as a whole structure by nominal sectional area of brace, is not easily

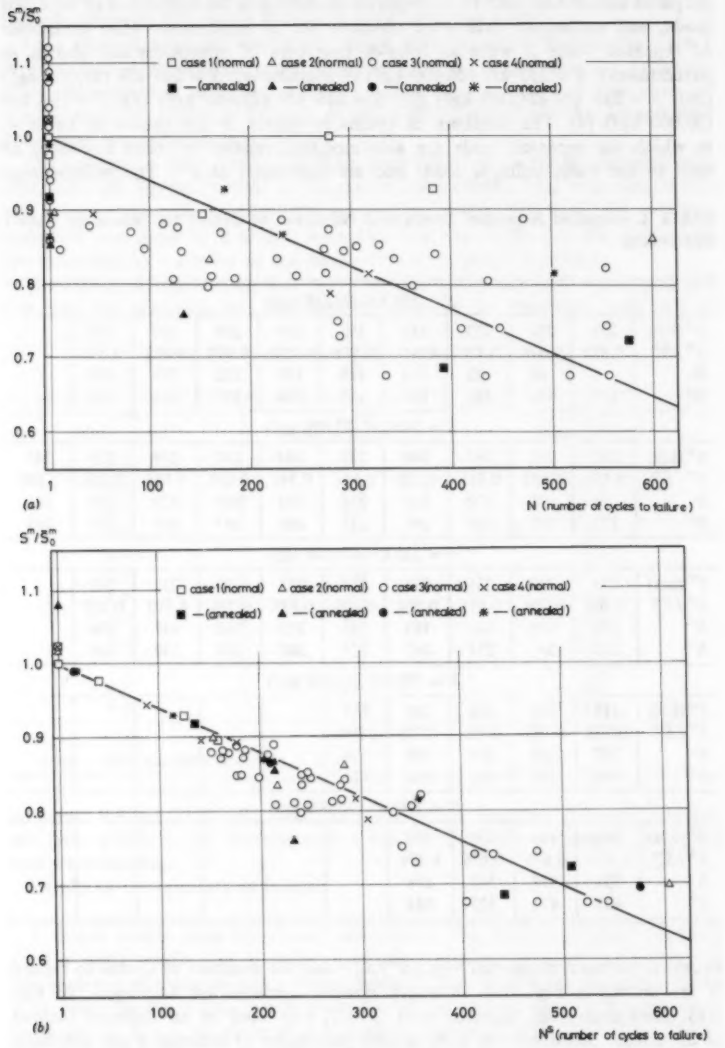

FIG. 2.—*S-N* Relationship of all Specimens: (*a*) Before Modification; (*b*) After Modification

TABLE 5.—Fatigue Test of Case-1 Specimens

Variable (1)		Data (2)	(3)	(4)	(5)	(6)
Normal:	S, in kilonewtons	98*	98	98	69	88
	S^m, in kilonewtons	77*	77	75	84	69
	$S^m/\bar{S}_0^m$	1.0	1.0	0.976	0.929	0.895
	N	1	280	1	383	153
	N^z	2	2	41	126	159
Annealed:	S, in kilonewtons	95*	84	88	83	
	S^m, in kilonewtons	116*	103	70	66	
	$S^m/\bar{S}_0^m$	1.023	0.919	0.723	0.686	
	N	1	1	577	392	
	N^z	1	136	508	441	

Note: * indicates static collapse loads.

TABLE 6.—Fatigue Test of Case-2 Specimens

Variable (1)		Data (2)	(3)	(4)	(5)	(6)
Normal:	S, in kilonewtons	180*	167	157	147	128
	S^m, in kilonewtons	189*	162	156	156	129
	$S^m/\bar{S}_0^m$	1.017	0.899	0.861	0.834	0.699
	N	1	6	601	160	735
	N^z	1	154	284	217	605
Annealed:	S, in kilonewtons	214*	167	147		
	S^m, in kilonewtons	211*	169	150		
	$S^m/\bar{S}_0^m$	1.081	0.855	0.760		
	N	1	1	133		
	N^z	1	215	234		

Note: * indicates static collapse loads.

TABLE 7.—Fatigue Test of Case-3 Specimens

Variable (1)		Data (2)	(3)	(4)
Annealed:	S, in kilonewtons	332*	292	235
	S^m, in kilonewtons	339*	294	237
	$S^m/\bar{S}_0^m$	0.990	0.865	0.696
	N	1	1	661
	N^z	16	211	576

Note: * indicates static collapse loads.

regarded as representative of the total stress state of a structure. In Fig. 2, both abscissa N and ordinate (S^m/S_0^m) are plotted on regular scales instead of log scales. There is no fixed rule of using log scales for a low-cycle fatigue problem, and regular scales are the best fitting scales for the test data.

3. Static tensile tests and pull-pull fatigue tests for Case-1, Case-2, and Case-4 specimens: One specimen was prepared for a static test, and all five specimens were prepared for every fatigue test of these specimens. The results are shown in Tables 5, 6, 7, and 8.

4. Static tensile tests and pull-pull fatigue tests for annealed specimens: One specimen, again, for a static test and all five specimens for every fatigue test

TABLE 8.—Fatigue Test of Case-4 Specimens

Variable (1)		Data (2)	(3)	(4)	(5)	(6)	(7)
Normal:	S, in kilonewtons	343*	392	294	304	275	265
	S^m, in kilonewtons	342*	277	301	295	272	264
	S^m/S_0^m	1.024	0.943	0.895	0.892	0.814	0.787
	N	1	1	45	1	318	280
	N'	1	87	141	176	295	306
Annealed:	S, in kilonewtons	334*	314	294	291	275	
	S^m, in kilonewtons	340*	321	299	298	282	
	S^m/S_0^m	0.990	0.929	0.868	0.865	0.814	
	N	1	176	234	1	503	
	N'	18	113	203	214	356	

Note: * indicates static collapse loads.

were prepared for Case-1 through Case-4 annealed specimens. The results are also shown in Tables 5, 6, 7, and 8.

Modification of Applied Load Due to Chord Thickness

The dimensions such as thicknesses, diameters, and lengths of chord and brace are not always equivalent. Among these dimensions, if there is a small variation in diameter or length or brace thickness, they have nothing to do with the collapse load of the specimen. With regard to chord thickness, however, relationships between the collapse load and the chord thickness have been provided in the form of experimental equations. In the present test, chord thicknesses were measured at eight points of each specimen, and their influence on the collapse load evaluated.

The variation of stresses at the neighborhood of "hot spot" of the Case-3 specimen under static tensile load was analyzed by finite element method where there was a 10% variation in the chord thickness.

One eighth of the specimen was divided into 15 isoparametric shell finite elements with eight nodes. The circumferential stresses of chord and the axial stresses of brace are shown in Fig. 3, in which the stresses corresponding to a 10% decrease in chord thickness are also indicated. Percentages of increase in stress caused by a 10% decrease in chord thickness are represented in Fig. 4. The average increase in stress at the joint surrounded by a dotted line in

Fig. 4 is 10.2%. According to this numerical result, it is concluded that a 10% decrease in chord thickness is equivalent to 10% increase in stress, and this relationship would be expected to hold for moderate changes in chord thickness and elastic behavior.

On the other hand, two kinds of experimental equation have been reported for X, T, and K-type tubular joint specimens (4,7), in which the static collapse load was proportional to the chord thickness to the 1/1.6 power or 1/2 power. They are interpreted as "10% decrease in chord thickness is equivalent to 16.5% or 21% increase in static collapse load." Based on both the numerical result

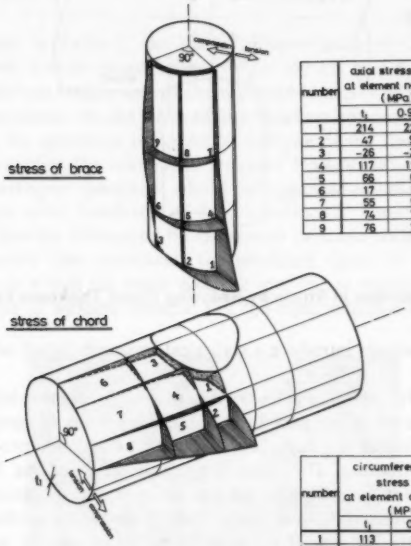

number	axial stress at element node (MPa)	
	t_1	$0.9\,t_1$
1	214	227
2	47	52
3	-26	-26
4	117	119
5	66	67
6	17	10
7	55	55
8	74	74
9	75	76

number	circumferential stress at element center (MPa)	
	t_1	$0.9\,t_1$
1	113	128
2	-221	-249
3	27	30
4	-3	-5
5	-150	-175
6	16	19
7	-2	-4
8	-49	-62

FIG. 3.—Stress Distributions of Chord and Brace: Stress Distribution

and the experimental equations, the writers use the relation that the static collapse load is proportional to the chord thickness to the 1/1.6 power, and assume the cyclic collapse load may be proportional to the chord thickness to the same power.

Modification of Number of Cycles to Failure

Strong scatter was observed in the data of number of cycles to failure N. The variation of data was so large that relationships among the data were difficult

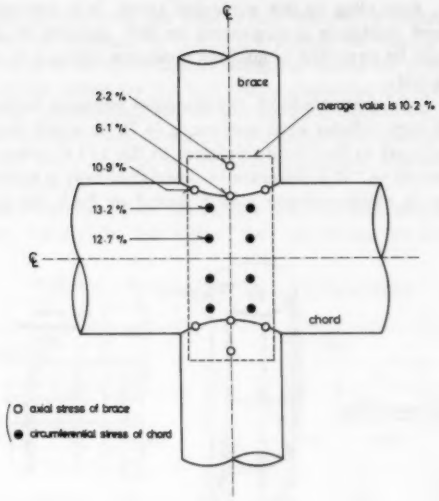

FIG. 4.—Increase in Stress by Reducing Chord Thickness by 10%

to clarify, and the writers introduce a statistical approach based on the Bayesean theorem.

Scatter of *N*.—Number of cycles to failure N is accompanied by a certain amount of scatter even in the case of the simplest specimen, such as a smooth rod, because the fatigue phenomenon is a kind of random process based on the microcrack mechanism. However, the scatter of N of the X-type welded tubular joint specimen described herein was so large that it cannot be explained adequately by an ordinary fatigue mechanism. Number of cycles to failure N seems to be strongly influenced by welding defects, and the scatter of N is increased when the scatter of welding defects is large.

The scatter of N is mainly a result of welding defects such as lack of weld penetration, condition of weld surface smoothing, insufficient weld effective length, and degeneration of material properties due to welding. But as mentioned in the foregoing, since the weld line is long and its geometrical pattern is complicated in an X-type tubular joint specimen, it is difficult to measure all factors (such as weld penetration) along all weld lines, and it is impossible to evaluate the influence of various factors on the cyclic collapse load. For example, close-up photographs of the section including weld seam at the neighborhood of "hot spot" of the specimen are shown in Fig. 5. They show that a weld penetration has been perfectly done, and the differences between them are difficult to evaluate in quantity.

As the only possible and practical resort, the following assumptions were made:

1. Scatter of welding defects can be substituted by a scatter of static collapse

load, because static collapse load is strongly influenced by the welding defects.

2. Scatter of N is mainly a result of the difference of static collapse load of each specimen; that is, numbers of cycles to failure of some specimens are extraordinarily small when the welding defects are very large (when the static collapse load is very small), and vice versa.

3. Scatter of N is partly a result of microcracking in the material, of manufacturing error, or of errors in cyclic load control, etc.

4. If there is no scatter of static collapse load, that is, if all specimens have the same static collapse load, the scatter of N is dependent only on the magnitude of the repeated load.

As can be seen in Table 3, the static collapse loads of Case-3 specimens are scattered over a wide range between $S_0 = 250$ kN and $S_0 = 326$ kN. Now let us imagine that the fatigue test of the repeated load $S = 255$ kN is performed for these 10 specimens. In the case of the weakest specimen whose collapse load is 250 kN, the specimen is bound to collapse at the first cycle ($N = 11$), even before it reaches the maximum repeated load of 255 kN. However, in the case of the strongest specimen, whose collapse load is 326 kN, the specimen may not collapse after hundreds of load repetitions. Thus the scatter of N is strongly and directly influenced by the scatter of static collapse load.

In order to avoid this confusion, the modified value of N is defined for the special case in which the static collapse load is not variable, that is, where there is no scatter of welding defects. Let the static collapse load S_0 be always

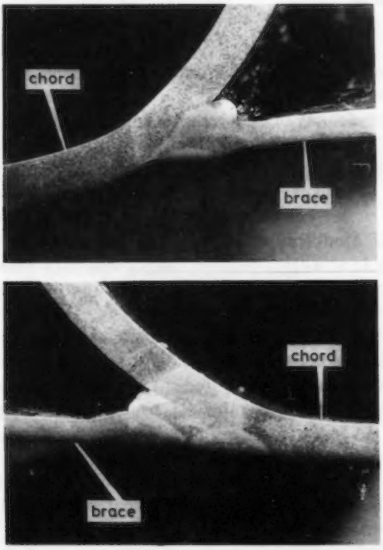

FIG. 5.—Weld Penetration near Hot Spot

equal to a certain value—an average of S_0 ($\bar{S}_0$) is used herein. In the Case-3 specimen, $\bar{S}_0$ is 290 kN as shown in Table 3. The most probable value of N in case of $S_0 = \bar{S}_0 = 290$ kN is expressed as N^e.

Assumptions in Statistical Treatments.—The following three assumptions are introduced:

1. The S-N curve is a straight line with negative gradient on regular scales. In high-cycle fatigue tests, an almost linear relation is generally obtained when the relationships of S and N are plotted on semilog or log-log scales; but in a low-cycle fatigue test whose number of cycles to failure is less than 10^3, the situation is not the same. According to our test data including the static collapse load, an approximate linear relation has been obtained when the data are plotted on regular scales as shown in Fig. 2(*a*). The S-N curve is defined as

$$S = aN + \bar{S}_0^m \quad \ldots \quad (1)$$

in which a = parameter determined from the data based on the least square estimation. Parameter a is estimated herein as $a = -0.0175$.

2. If we imagine the S-s_N curve, in which s_N is a standard deviation of N, it becomes a straight line with negative gradient. In the high stress range, the plastic deformation will occur in some parts of the specimen, the stresses at those parts are equalized, and finally the variation of N will reduce. If we consider the limited situation where the collapse loads are always equal to $\bar{S}_0^m$, standard deviation s_N is equivalent to 0 at $S = S_0$. The linear relation between S and s_N is defined as

$$S = cs_N + S_0 \quad \ldots \quad (2)$$

in which c = parameter determined from the data based on the most likelihood estimation. Parameter c is estimated as $c = -0.055$.

3. The probability density of N corresponding to an arbitrary value of repeated load S is assumed by normal distribution as is generally done in considering the probabilistic distribution of N (for instance, References 2 and 5). The probability density of collapse load S_0 is also assumed to be a normal distribution.

Basic Concept of Modification of N.—The procedure of modifying N is a statistical approach to arranging random fatigue test data based on the Bayesean theorem. The concept of the approach is explained in the following by referring to Fig. 6.

The static collapse load S_0 of the specimen, which is used in the fatigue test, is unknown. Let us consider that a fatigue test is performed for a specimen whose collapse load S_0 is unknown, under the repeated load of magnitude S^*, and that the specimen collapses after N^* cycles. The collapse load S_0 of the specimen may be S_i or S_j, for example. These two situations are shown in Fig. 6(*a*), in which the relation between S and N is linear as mentioned in the Assumption 1. In Fig. 6(*a*), the possibility of $N = N^*$ in case of $S_0 = S_i$ is very small, because the situation $N = N^*$ is located at the tail part of probability density for N, which is called $g^*_{S_i,S}(N)$. On the other hand, the possibility of $N = N^*$ is located at the central part of probability density for N, called $g^*_{S_j,S}(N)$. In other words, if the collapse load of the specimen is S_i, the specimen will

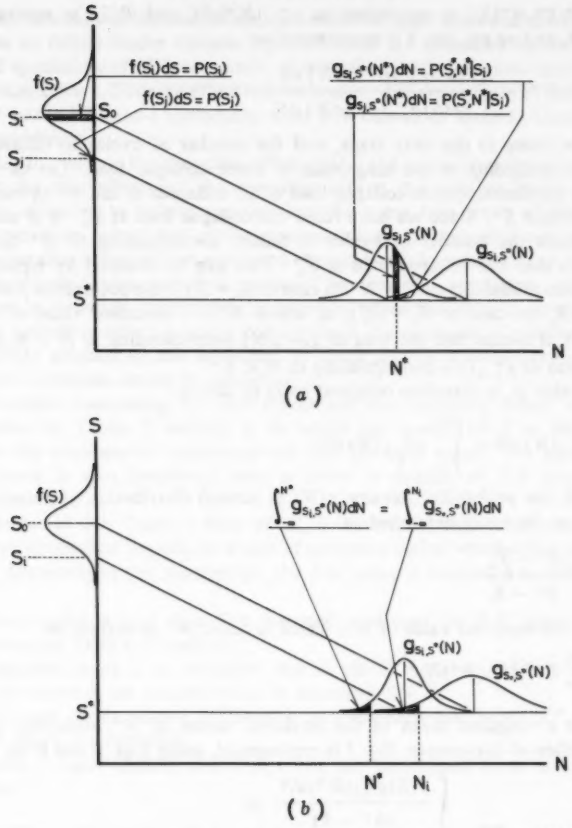

FIG. 6.—Statistical Model

seldom collapse at the N^*-th load cycle; whereas if the collapse load is S_j, the specimen will possibly collapse at the N^*-th cycle. Both possibilities are evaluated as $g^*_{S_i,S}(N^*)dN$, $g^*_{S_j,S}(N^*)dN$, respectively.

Furthermore, the static collapse load S_0 follows its own probability density, which is called $f(S_0)$. In Fig. 6(*a*), the possibility of $S_0 = S_i$, which is shown as $f(S_i)dS$, is greater than the possibility of $S_0 = S_j$, which is shown as $f(S_j)dS$.

The conditional probability $P(S_i | S^*, N^*)$ is expressed, based on the Bayesean theorem, as

$$P(S_i | S^*, N^*) = \frac{P(S^*, N^* | S_i) P(S_i)}{\sum_j P(S^*, N^* | S_j) P(S_j)} \quad \ldots \ldots \ldots \ldots \ldots \ldots \ldots \ldots \ldots \ldots \quad (3)$$

Since $P(S^*, N^*|S_i)$ is equivalent to $g^*_{S_i,S}(N^*)dN$ and $P(S_i)$ is equivalent to $F(S_i)dS$, and so on, Eq. 3 is represented as

$$P(S_i|S^*, N^*) = \frac{[f(S_i)g^*_{S_i,S}(N^*)dN]\,dS}{\int [f(S)g^*_{S,S}(N^*)dN]\,dS} \quad \ldots\ldots\ldots\ldots\ldots\ldots (4)$$

Here we come to the next stage, and the number of cycles to failure N^* is modified according to the magnitude of static collapse load. Let us imagine that the specimen, whose collapse load is S_i, collapses at the N^*-th load cycle of magnitude S^*. Since we have fixed the collapse load at $\bar{S}_0^m$, it is necessary to calculate the number of cycles to failure corresponding to N^* under the condition that the collapse load is $\bar{S}_0^m$. This can be realized by equating the occurrence probability of $N = N^*$ (in case of $S_0 = S_i$) to the occurrence probability of $N = N_i$ (in case of $S_0 = \bar{S}_0^m$), in which N_i is a modified value of N^*. In Fig. 6(*b*), it means that the area of $g^*_{\bar{S}_0^m,S}(N)$ corresponding to $N < N_i$ is taken to the area of $g^*_{S_i,S}(N)$ corresponding to $N < N^*$.

The value N_i is therefore obtained so as to satisfy

$$\int_{-\infty}^{N^*} g^*_{S_i,S}(N)dN = \int_{-\infty}^{N_i} g^*_{\bar{S}_0^m,S}(N)\,dN \quad \ldots\ldots\ldots\ldots\ldots\ldots (5)$$

in which the probability density $g(N)$ is normal distribution (Assumption 3), and N_i can be easily expressed as

$$N_i = N^* \frac{S^* - \bar{S}_0^m}{S^* - S_i} \quad \ldots\ldots\ldots\ldots\ldots\ldots\ldots\ldots\ldots\ldots (6)$$

Finally, the modified value of N^*, which is called N^s, is defined as

$$N^s = \sum_i P(S_i|S^*, N^*)N_i \quad \ldots\ldots\ldots\ldots\ldots\ldots\ldots\ldots\ldots\ldots (7)$$

which is a weighted mean of the modified values of N^* according to their probabilities of occurrence. Eq. 7 is represented, using Eqs. 4 and 6, as

$$N^s = N^*(S^* - \bar{S}_0^m) \frac{\int \dfrac{f(S)g^*_{S,S}(N^*)dN}{(S^* - S)}\,dS}{\int [f(S)g^*_{S,S}(N^*)dN]\,dS} \quad \ldots\ldots\ldots\ldots\ldots\ldots (8)$$

Test Data.—Numbers of cycles to failure N^s of Case-3 specimens are represented in Table 4. Relations between N^s and nondimensional repeated loads (S^m/S_0^m) are plotted on the *S-N* diagram as shown in Fig. 2(*b*). The condition of the data before and after modification is easily compared by referring to Fig. 2(*a*) and (*b*).

Size Effect and Influence of Residual Stress

The influence of relative size of the specimen (size effect) will be considered first, and after that the influence of residual stress due to welding, as well as the relationship between the two effects. The influence of residual stress is here called the annealing effect.

In order to evaluate the size effect, the static collapse loads and the numbers of cycles to failure under various repeated loads are examined by using four kinds of specimens of different sizes, as described in the previous section and as shown in Table 1. The size effect will be evaluated quantitatively by comparing the *S-N* curve of Case-3 specimens with *S-N* curves of Case-1, Case-2, and Case-4 specimens.

In order to evaluate the annealing effect and, at the same time, the relationship between the size effect and the annealing effect, the collapse loads and the numbers of cycles to failure are examined by using four kinds of specimens of different sizes, where half of the specimens are annealed, as shown in Table 1. The annealing effect will be evaluated quantitatively by comparing *S-N* curves of annealed specimens with *S-N* curves of nonannealed specimens, which are described as "normal" specimens. It should be noted that there is no guarantee that the annealing effect is really coming from the decrease of residual stress successfully attained by the annealing. It could also be a consequence of the change of materials caused by annealing.

Test results concerning the size effect and the annealing effect are both represented in Tables 5 through 8, in which the scatter of N is very large because the numbers of specimens are few for both cases. The concept of modification is also introduced here in order to deduce an *S-N* curve from random test data.

Estimation of *S-N* Curve.—First of all, it is assumed that parameters a and c are always constant regardless of size of specimen and of whether it is annealed or not. According to this assumption, the *S-N* curve is estimated as follows:

1. Static collapse load S_0 is first assumed, and then the *S-N* curve and the S-s_N curve are fixed automatically.
2. Repeated loads S are modified due to chord thickness, and numbers of cycles to failure N are also modified by assuming $S = \bar{S}_0$.
3. The sum of the square of distance between each data point (S^m, N^s) and the *S-N* curve is calculated.
4. Both collapse load S_0 and *S-N* curve are determined so as to minimize this sum.

Size Effect.—The ratio of the average collapse load of a Case-3 specimen ($S_{03} = 290$ kN) to the estimated collapse load of another case specimen (S_{0i}; $i = 1, 2, 4$) is called the multiplier k, that is, $k = S_{03}/S_{0i}$. The repeated loads S of Case-1, Case-2, and Case-4 specimens are transformed to the same level as the Case-3 specimen by multiplying S by k. The relation between S^m/S_0^m and N is shown in Fig. 2(*a*), and the relation between S^m/S_0^m and N^s is shown in Fig. 2(*b*). The *S-N* curve in Fig. 2(*b*) is valid for every type of specimen. Finally, let the reciprocal of k be called r_f.

The ratio of the cross-sectional chord area of Case-1, Case-2, and Case-4 specimens ($\bar{A}_i$; $i = 1, 2, 4$) to the cross-sectional chord area of the Case-3 specimen ($\bar{A}_3 = 1913$ mm^2) is called the size ratio r_a, that is, $r_a = \bar{A}_i/\bar{A}_3$. The ratio of r_f to r_a, which is called r_f/r_a, is taken as an index of size effect.

If $r_f/r_a = 1$, it implies there is no size effect. If $r_f/r_a < 1$, the specimen is weaker than the Case-3 specimen, vice versa. Parameters k, r_f, r_a, and r_f/r_a are shown in Table 9, and the relation between the size ratio r_a and the index

(r_f/r_a) is shown in Fig. 7 in which the relation obtained by the least square estimation is indicated by a thick line. In Fig. 7, r_f = ratio of fatigue strength of each specimen to Case-3 specimen, for "normal" specimen; $r_f' = r_f$ for "annealed" specimen; and r_a = ratio of cross-sectional area of each specimen

TABLE 9.—Size Effect and Annealing Effect

Case (1)	Ratio of Cross-Sectional Area: Cross sectional Area A_1, in square millimeters (2)	Ratio of Cross-Sectional Area: Ratio of A_1 for Case-3, r_a (3)	Ratio of Fatigue Property (Normal): Multiplier for Case-3, k (4)	Ratio of Fatigue Property (Normal): Ratio of fatigue property, $r_f = 1/k$ (5)	Ratio of Fatigue Property (Normal): r_f/r_a (6)	Ratio of Fatigue Property (Annealed): Multiplier for Case-3, k' (7)	Ratio of Fatigue Property (Annealed): Ratio of fatigue property, $r_f' = 0.855/k'$ (8)	Ratio of Fatigue Property (Annealed): r_f'/r_a (9)	Ratio of residual stress property, $r_f'' = k/k'$ (10)
1	421	0.215	3.438	0.291	1.353	2.776	0.308	1.433	1.238
2	1218	0.591	1.593	0.628	1.063	1.481	0.577	0.976	1.076
3	1913	1.000	1.000	1.000	1.000	0.855	1.000	1.000	1.170
4	3087	1.431	0.868	1.152	0.805	0.849	1.007	0.704	1.022

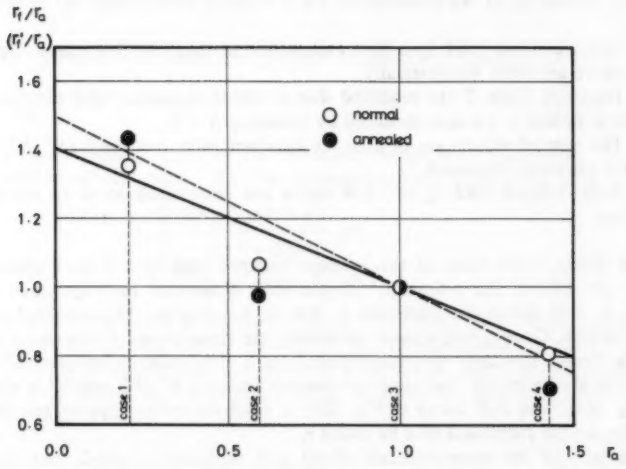

FIG. 7.—Size Effect

to Case-3 specimen. A negative correlation between r_a and r_f/r_a is observed in Fig. 7, and it is concluded that the relative strength of a welded tubular joint specimen under low-cycle fatigue test shows a downward trend when the

size of specimen increases. The reason for this could be an increase in the welding defects, such as lack of penetration with increasing wall thickness, which would cause a decrease in strength.

Annealing Effect.—The same process is applied for the evaluation of the annealing effect as for the size effect. Instead of the multiplier k, the ratio of the collapse load of the nonannealed Case-3 specimen to the collapse load of annealed Case-1, Case-2, and Case-4 specimens is employed. This is called the multiplier k'. The relations between S^m/S_0^m and N, and between S^m/S_0^m and N^s, are shown in Figs. 2(*a*) and (*b*), respectively.

The ratio of multiplier k to multiplier k', which is called $r_f'' = k/k'$, is taken as an index of annealing effect. If $r_f'' = 1$, there is no annealing effect. If r_f'' is always constant for every case, there is no relationship between the size effect and the annealing effect. Parameters k' and r_f'' are shown in Table 9, and the relation between the size ratio r_a and the index r_f'' is shown in Fig. 8.

Two kinds of straight lines can be fitted in Fig. 8. They are: (1) A dot-dash line which is parallel to the r_a-axis; and (2) a solid line which is obtained by the least square estimation (correlation coefficient is −0.74).

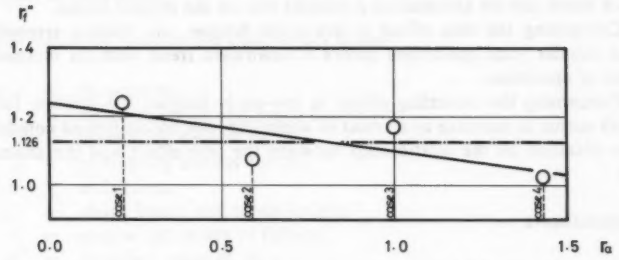

FIG. 8.—Annealing Effect

Following Line 1, it is concluded that the strength of a welded tubular joint specimen is increased by more than 10% by annealing. Following Line 2, it is concluded that the size effect increased by annealing.

Conclusion

Low-cycle fatigue tests were performed for X-type welded tubular joint specimens. An S-N curve was estimated by using the modified values of number of cycles to failure N^s, and after that, the size effect and the annealing effect were considered. They are summarized as follows:

1. Pull-pull tests, conducted for X-type welded tubular joint specimens, were restricted to the low-cycle fatigue whose number of cycles to failure N is less than 600.
2. The tests were performed on a sufficient number of the same size specimens in the case of Case-3 specimens, convenient for the statistical treatments.
3. The static collapse loads S_0 and the cyclic collapse loads S were modified due to chord thickness.

4. The most likely value of N was estimated for the restricted state, in which the static collapse load S_0 of every specimen is equivalent.

5. An S-N curve was estimated by using the modified value of S and N (S''' and N^*), where the S-N curve was assumed to be a straight line on regular scales.

6. Four kinds of specimens of different sizes were prepared in order to examine the size effect. The effect has been evaluated quantitatively based on the index of size effect (r_f/r_a).

7. Annealed and nonannealed specimens were prepared in order to examine the annealing effect. The effect was evaluated quantitatively based on the index of annealing effect r_f''. The tests were also performed on four kinds of specimens of different sizes in order to evaluate the relationship between the size effect and the annealing effect.

The following conclusions have been obtained:

1. The statistical approach developed herein can be applied to the fatigue test data which are strongly influenced by the scatter of welding defects.

2. In case of low-cycle fatigue, ($N < 600$) of welded tubular joint specimens, the S-N curve can be assumed as a straight line on the regular scales.

3. Concerning the size effect in low-cycle fatigue, the relative strength of welded tubular joint specimens shows a downward trend with an increase in the size of specimen.

4. Concerning the annealing effect in low-cycle fatigue, the relative fatigue strength seems to increase as a result of annealing; but no confirmed conclusion can be obtained on the relationship between the size effect and the annealing effect.

Acknowledgments

The tests described herein were sponsored by the Science Research Subsidy of the Japanese Ministry of Education (No. 285097). The tests were executed by S. Shimizu, T. Itoh, J. Inada and T. Sato at the Department of Civil Engineering in Nagoya University. All specimens were manufactured by ARS Bridge & Engineering Co.

The writers wish to make deep acknowledgments to C. Massonnet of Liège University and T. Usami of Nagoya University for their advice.

Appendix I.—References

1. Akiyama, N., Yajima, M., Akiyama, H. and Ohtake, A., "Test Report on the Resistance of Steel Tubular Joint," *Journal*, Society of Steel Construction of Japan, Vol. 10, 1974, pp. 37–68 (in Japanese).
2. Bratt, M. J., Reethof, G. and Weber, G. W., "A Model for Time Varying and Interfering Stress-Strength Probability Density Distributions with Consideration for Failure Incidence and Property Degradation," *Proceedings*, SAE-ASME-AIAA Aerospace Reliability and Maintainability Conference, 1964, p. 566.
3. Gerold, E. and Trachte, K., "Behavior of St37 steel in the Endurance Limit Temporary to Fatigue," *Archiv. Eisenhüttenw.*, Vol. 21, 1950, pp. 175–179 (in French).
4. Kanaya, H., "Experimental Study on the Local Deformation of Steel Tubular Joint: Part I, II, III," *Transactions*, Architectural Institute of Japan, No. 108, 1965, pp. 31–39; No. 109, 1965, pp. 42–51; No. 110, 1965, pp. 8–14 (in Japanese).

5. Kececioglu, D. B., Smith, R. E. and Felsted, E. A., "Distributions of Strength in Simple Fatigue and the Associated Reliabilities," *Ann. Assurance Sci.*, Vol. 9, 1970, pp. 659–672.
6. Maeda, H., Uchino, K., Sakurai, E. and Sugiyama, S., "Study on the Fatigue Strength of Steel Welded Tubular Joint: Part I, II, III," *Ishikawajima-Harima Technical Reports*, Vol. 9, 1969, pp. 589–596; Vol. 10, 1970, pp. 37–42; Vol. 13, 1973, pp. 563–570 (in Japanese).
7. Reber, J. B., "Ultimate Strength Design of Tubular Joints," OTC 1664, 1972.
8. Shiratori, E. and Obataya, Y., "Cyclic Plastic Strain Energy and Low-Cycle Fatigue Strength for Nickel-Chrome Steel," *Proceedings*, Japan Society of Mechanical Engineers, Vol. 35, 1969, pp. 711–717 (in Japanese).
9. Toprac, A. A., "Analysis of In-Plane T, Y and K Welded Tubular Connections," *Welding Research Council Bulletin*, No. 125, 1967.
10. Washio, K. Togo, T. and Mitsui, N., "Experimental Study on the Local Failure of Steel Tubular Truss Chord Joint: Part I, II, III," *Transactions*, Architectural Institute of Japan, No. 138, 1967, pp. 35–43; No. 139, 1967, pp. 45–52; No. 140, 1967, pp. 55–60 (in Japanese).
11. Weisz, M. and Erard, M., "Contribution to the Study of Brittleness caused by Plastic Deformations of Steel for Reactor Vessel," *Memoires Scientifiques, Revue de Métal*, Vol. 63-2, 1966, pp. 180–188 (in French).

Appendix II.—Notation

The following symbols are used in this paper:

a, b, c = parameters;
d_1, d_2 = chord diameter and brace diameter;
f = probability density for S;
g = probability density for N;
k, k' = multipliers;
$l_{1,2}$ = chord length and brace length;
N = number of cycles to failure;
N^a = modified value of N;
r_a = size ratio;
r_f = $1/k$;
r_f/r_a = index of size effect;
r_f'' = index of annealing effect;
S = repeated load;
S^m = repeated load, which is modified due to chord thickness;
S_0 = static tensile collapse load;
S_0^m = collapse load, which is modified due to chord thickness;
s_N = standard deviation of N;
t_1, t_2 = chord thickness and brace thickness; and
$\bar{t}_1$ = chord thickness (average of the data).

JOURNAL OF THE STRUCTURAL DIVISION

BUCKLING OF WEB POSTS IN PERFORATED BEAMS

By Brian K. Dougherty,[1] M. ASCE

INTRODUCTION

Rectangular openings are frequently formed in the webs of steel I-beams to facilitate the passage of services, and have the effect of reducing the plastic and buckling strengths of the members. When two such openings are placed closely together, another potential mode of buckling is introduced, i.e., that of lateral buckling of the web post between the openings (10,13).

This paper proposes a method for determining the critical moment at which buckling of a web post occurs. The validity of the analysis is demonstrated by comparative results of experiments on scale models of web posts; the experimental method is described. The significance of web post buckling for practical beams is illustrated by analyzing three different I-beams containing web posts of varying widths.

FAILURE OF PERFORATED SECTION

Collapse Modes.—There are two basic modes of collapse for perforated sections containing adjacent web openings. In the first of these failure is associated with only one hole, while the other involves the interaction of both holes and the entire perforated section deforms as a single unit. Failure of the web post is a prerequisite for the latter type of collapse, and can occur either by failure of the ends of the web post (Fig. 1), or by lateral buckling of the post. Tests on 8WF17 and 8WF20 beams (2,11) reported failure of the ends of the post, while buckling of the post was reported in a test of a 14WF30 beam (10).

Ultimate Load Analysis.—Fig. 2(*a*) represents a perforated section formed by two adjacent concentric web openings of length a and depth d, separated by a web post of width b. In addition to the primary bending moment, the section is subject to a vertical shear force Q over its total length L, and thus

[1]Sr. Lect., Dept. of Civ. Engrg., Univ. of Natal, King George V Avenue, Durban, Natal 4001, South Africa.

Note.—Discussion open until August 1, 1981. To extend the closing date one month, a written request must be filed with the Manager of Technical and Professional Publications, ASCE. Manuscript was submitted for review for possible publication on October 18, 1979. This paper is part of the Journal of the Structural Division, Proceedings of the American Society of Civil Engineers, ©ASCE, Vol. 107, No. ST3, March, 1981. ISSN 0044-8001/81/0003-0507/$01.00.

has to resist a Vierendeel moment of QL. For analytical purposes the section may be represented by the equivalent line structure of Fig. 2(b), where I_p and I_T are respectively the moments of inertia of the web post and the tee sections above and below the openings. The height H of the line structure is taken as the clear distance between beam flanges; this approximation was used by Redwood (10), and its accuracy had been confirmed by finite element stress analysis (2).

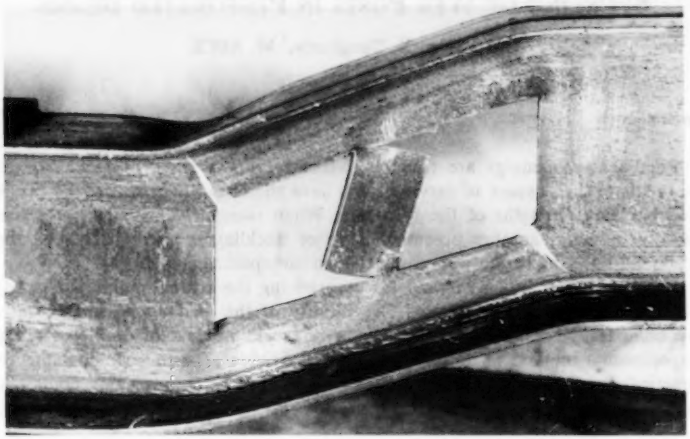

FIG. 1.—Failure of Ends of Web Post

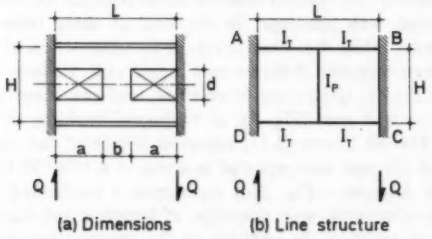

FIG. 2.—Perforated Section

When collapse of the perforated section involves failure of the ends of the web post, the resulting collapse mechanism contains six plastic hinges. This is shown in Fig. 3, where only the upper half of the mechanism is shown—a plastic hinge occurs at each end of the tee section, and in the web post opposite the tops of the openings.

The horizontal shear force F_u in the web post at failure is evaluated by equating the moment $F_u(d/2)$ to the plastic moment of resistance of the post;

the retraining moment exerted by the post on the line structure is thus $F_u(H)$. The ultimate resisting moment M_u of the entire perforated section to Vierendeel bending is therefore given by

$$M_u = M_{PA} + M_{PB} + M_{PC} + M_{PD} + F_u(H) \quad \ldots \ldots \ldots \ldots \ldots \ldots \quad (1)$$

in which M_{PA}, M_{PB}, M_{PC}, and M_{PD} = the plastic moments of resistance of the tees at A, B, C, and D respectively (2).

When collapse of the perforated section involves buckling of the web post, the stresses in the ends of the post depend on its slenderness and can vary from the fully elastic to the fully plastic condition. In the latter case the restraining moment of the post is identical to that of the post in Fig. 3, and the ultimate resisting moment of the perforated section is given by Eq. 1. When, however, these stresses are not fully plastic, the post will develop a smaller restraining moment, and the ultimate resisting moment of the perforated section will be given by

$$M_u = M_{PA} + M_{PB} + M_{PC} + M_{PD} + FH \quad \ldots \ldots \ldots \ldots \ldots \ldots \quad (2)$$

in which F = the horizontal shear force in the web post at buckling. The quantity FH represents the buckling moment of the post, and in general is

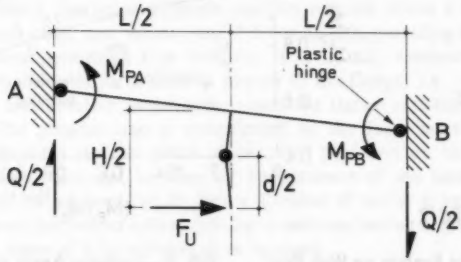

FIG. 3.—Plastic Mechanism

less than the restraining moment $F_u(H)$ developed by the fully plastic post. Therefore, to determine the ultimate moment of resistance of a perforated section such as that of Fig. 2(*a*), a means had to be developed of computing the critical moment at which the web post would buckle.

Buckling Analysis of Web Posts

The collapse mode of a steel beam subject to the force system of Fig. 4 depends on the slenderness of the member. For a short beam the ultimate flexural strength is determined by the full plastic moment of the section, and failure is due to yielding of the beam ends. For a long beam the flexural strength is determined by the critical moment at which the beam buckles elastically, and this depends on the elastic stiffness of the member. For an intermediate span between these two extremes, failure occurs by buckling after the beam has partially yielded. This yielding reduces the stiffness of the affected regions,

and the beam's buckling strength is reduced accordingly.

The analysis of elastic beam buckling presents no difficulty. The solutions to a number of particular cases have been found by solving the governing differential equations (15). Recent research using the finite element technique has provided a more general solution to the problem, and it is now possible (given a suitable computer program) to analyze elastic beam buckling for any arrangement of loads, supports, and restraints (3,7,9,14).

By contrast, the inelastic lateral buckling of beams has not been so extensively investigated. The majority of early investigations had concentrated on simply supported beams under uniform moment, and were directed towards the development of a theoretical model which took proper account of the effects of partial yielding on the various factors controlling lateral stability. The problem of the inelastic buckling of single-span beams under moment gradient has been the subject of recent studies (4,5,6), and these formed the basis of the analysis by Nethercot and Trahair (8) of single-span beams under various load conditions.

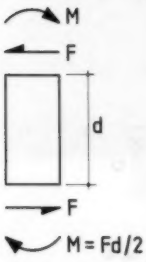

FIG. 4.—Force System on Web Post

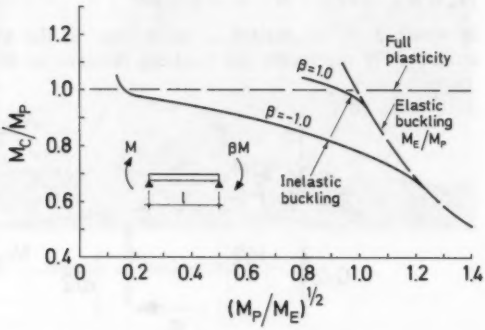

FIG. 5.—Inelastic Beam Buckling under Moment Gradient [Due to Nethercot and Trahair (8)]

The graph which they published for the analysis of beams under moment gradient is of particular relevance to the buckling of web posts, and is reproduced in part in Fig. 5.

Values of the dimensionless inelastic critical moments M_c/M_p were plotted against a modified slenderness $(M_p/M_E)^{1/2}$, in which M_c = inelastic buckling moment; M_p = plastic moment; and M_E = larger end moment at elastic buckling. In the original paper, curves were produced for the β values 1.0, 0.5, 0, −0.5, and −1.0. Only two of these are shown in Fig. 5, i.e., β = 1.0, which corresponds to the web post loading, and β = −1.0, which is the case of uniform moment and is given for purposes of comparison. The difference in the two curves illustrates the importance of the moment gradient in the inelastic range. The critical moments of beams under uniform moment gradient (β = −1) are reduced substantially below the full plastic moment, whereas those for beams under high moment gradient (β = 1) are reduced only slightly up to the point where full plasticity occurs.

Evaluation of M_p, M_E.—By evaluating M_p and M_E, Fig. 5 can be used to determine the buckling moment M_c of a single-span beam. The plastic moment M_p is given by standard plastic theory, and the elastic buckling moment M_E may be found using an equation due to Clark and Hill (1), which is applicable to beams of symmetrical section loaded either at their ends, or by transverse loads applied at the neutral axis. Thus

$$M_E = \frac{\psi\pi}{Kl}(EI_y GJ)^{1/2}\left(1 + \frac{\pi^2 EC_w}{(Kl)^2 GJ}\right)^{1/2} \quad \ldots\ldots\ldots\ldots\ldots\ldots (3)$$

in which C_w = warping constant; E = modulus of elasticity; G = modulus of rigidity; I_y = moment of inertia about minor axis; J = torsion constant; K = coefficient; l = effective buckling length; and ψ = coefficient.

For a rectangular section such as a web post, $C_w = 0$, and Eq. 3 simplifies to

$$M_E = \frac{\psi\pi}{Kl}(EI_y GJ)^{1/2} \quad \ldots\ldots\ldots\ldots\ldots\ldots\ldots\ldots\ldots\ldots (4)$$

Salvadori (12) has established the values of the constants ψ and K for the type of loading acting on a web post (Fig. 4). The value of K depends on the degree to which the beam supports restrain rotation about a vertical axis through the beam ends, and varies from 0.5 for an end providing full restraint to 1.0 for an end permitting free rotation. It is usually assumed for design purposes that the web of an I-beam is pinned to the flange, i.e., $K = 1$. This is a somewhat conservative assumption, since the flange restrains the web to some extent. The present case is complicated by the fact that the degree of restraint also depends on the width of the web post and on the length and height of the web openings; in view of the presence of the latter, the usual value of 1.0 will be adopted for K. For a K-value of unity, ψ varies between 2.56 and 2.74, with the former value applying to sections having negligible warping resistance; the value of 2.56 will therefore be used.

Thus for a web post of width b and thickness t, the elastic buckling moment can be expressed by

$$M_E = \frac{2.56\pi}{1.0\,l}\left[E\frac{bt^3}{12}G\frac{bt^3}{3}\right]^{1/2} \quad \ldots\ldots\ldots\ldots\ldots\ldots\ldots (5)$$

$$M_E = \frac{1.340\,bt^3(EG)^{1/2}}{l} \quad \ldots\ldots\ldots\ldots\ldots\ldots\ldots\ldots (6)$$

Effective Buckling Length of Web Post.—The calculation of the elastic buckling moment of a web post is complicated by the fact that the post is laterally restrained by beam flanges situated a clear distance H apart [Fig. 6(*a*)], while the critical buckling stresses occur at sections a distance d apart [Fig. 6(*c*)]. For the extreme case of d equal to H the critical moment is given directly by Eq. 6, in which H = the effective buckling length; for smaller values of d however, elastic buckling will occur at a larger moment. The problem may be overcome by assuming that this increase in the elastic buckling moment is effectively due to a reduction in the buckling length H of the post. This

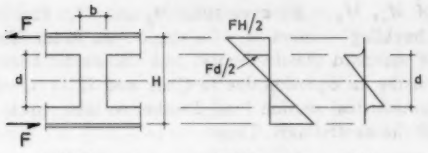

FIG. 6.—Web Post Moments and Bending Stresses

reduced length will be intermediate between d and H, and may be found by comparing the buckling of a typical web post (Fig. 6) with that of a post to which Eq. 6 applies, i.e., a post of uniform section having a length l and loaded as in Fig. 4.

The effective buckling length of the uniform post is l, and the critical stresses at elastic buckling occur at sections a distance l apart, thus

$$M_E = \frac{Fl}{2} \quad \ldots\ldots (7)$$

and substituting M_E from Eq. 6, the horizontal shear force F in the post at elastic buckling is obtained.

$$F = \frac{2.680\, bt^3 (EG)^{1/2}}{l^2} \quad \ldots\ldots (8)$$

For the web post of Fig. 6(a), the buckling length of the post is H, giving

$$M_E = \frac{1.340\, bt^3 (EG)^{1/2}}{H} \quad \ldots\ldots (9)$$

but the critical stresses at buckling occur at sections a distance d apart [Fig. 6(c)]; thus

$$M_E = \frac{Fd}{2} \quad \ldots\ldots (10)$$

$$\text{therefore} \quad F = \frac{2.680\, bt^3 (EG)^{1/2}}{Hd} \quad \ldots\ldots (11)$$

A comparison of Eqs. 8 and 11 gives

$$l^2 = Hd \quad \ldots\ldots (12)$$

$$\text{or} \quad l = (Hd)^{1/2} \quad \ldots\ldots (13)$$

It can be inferred from Eq. 13 that a web post such as that of Fig. 6(a) may be treated as a beam of constant width b and effective buckling length $(Hd)^{1/2}$. The elastic buckling moment is then given by

$$M_E = 1.340\, bt^3 \left(\frac{EG}{Hd}\right)^{1/2} \quad \ldots\ldots (14)$$

Equation 13 is seen to be valid for extreme values of d, e.g.: (1) As $d \to H$, $l \to H$, and M_E is given by Eq. 6; and (2) as $d \to 0$, $l \to 0$, and $M_E \to \infty$, which is true for a post having zero depth and thus infinite width. It was necessary however to verify that Eq. 13 was valid for intermediate values of d, and this was done by testing four scale models having a range of web post heights.

Experimental Investigation

The models of Fig. 7 were manufactured from a single piece of steel sheet and were proportioned to give a wide variation in the height d of the web post; the choice of a 0.787 in. (20 mm) wide post ensured that elastic buckling would occur in each case. Each model was subjected to shearing forces in

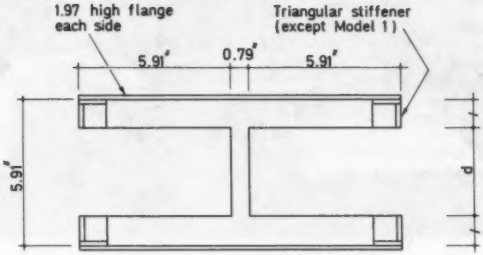

Model 1 : d = 5.91"
Model 2 : d = 4.57"
Model 3 : d = 3.27"
Model 4 : d = 1.97"
Plate thickness = 0.046"
Note : 1 in. = 25.4 mm

FIG. 7.—Model Dimensions

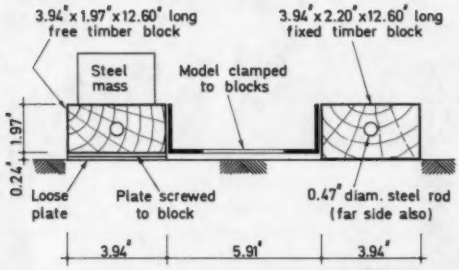

(Clamps and clamping plates are omitted for clarity.)
Note : 1 in. = 25.4 mm

FIG. 8.—Section through Test Arrangement

the plane of the flanges so as to reproduce the force system of Fig. 6(*a*). The method of applying the forces is best described by reference to Figs. 8, 9, and 10.

Each flange of the model was placed in contact with a timber block. A 0.236 in. (6 mm) thick mild steel plate was placed against the flange, and plate and block were clamped together (Fig. 9). One block was clamped to the test table,

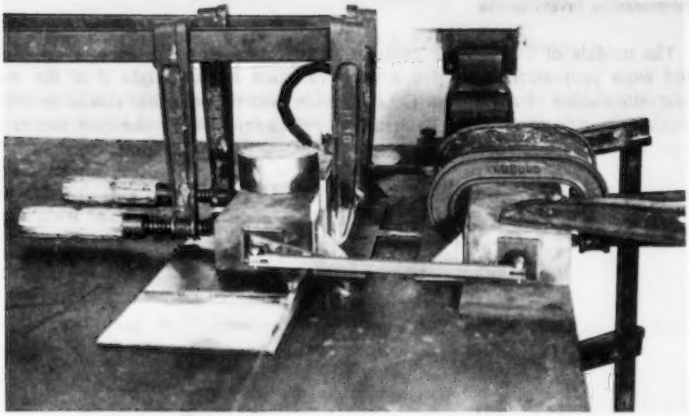

FIG. 9.—General View of Test Arrangement

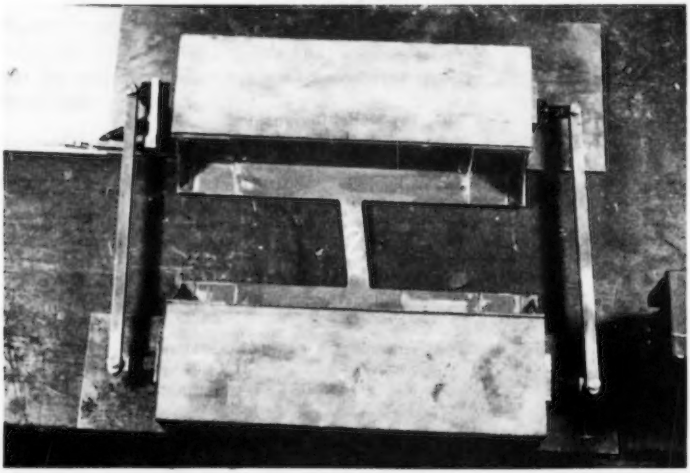

FIG. 10.—View on Connecting Mechanism

and will be referred to as the fixed block. To the underside of the other (the free block) was screwed a 0.118 in. (3 mm) thick precision-ground steel plate, with the screw heads recessed into the plate. This rested on a similar plate placed on the test table, and the contact surfaces were sprayed with a dry lubricant just prior to testing so as to minimize frictional effects. A steel mass was placed on top of the free block to prevent uplift during loading (Fig. 8).

With just this arrangement, the application of a horizontal force to the free block would have caused it to rotate about the distant end of the web post. It was therefore necessary to connect the two blocks in such a way that they remained parallel to one another at all times. A longitudinal hole was drilled through each block, and a 0.472 in. (12 mm) diam mild steel rod was inserted. The projecting ends of the rod were threaded, and it was secured in position by means of square plate washers tightened against the ends of the block. The extreme ends of the rod were tongued, and were drilled to receive a steel pin. The elements linking the blocks comprised two mild steel bars of 0.394 in. (10 mm) square section; the ends of the bars were grooved and drilled, and were pinned to the tongued ends of the rods to form clovis joints. The

TABLE 1.—Buckling Loads of Model Web Posts

Model number (1)	H, in inches (2)	d, in inches (3)	$(HD)^{1/2}$, in inches (4)	Buckling Force, in pounds		Theory/ Test (7)
				Test (5)	Theory (6)	
1	5.91	5.91	5.91	78	105	1.35
2	5.91	4.57	5.19	126	137	1.09
3	5.91	3.27	4.39	179	191	1.07
4	5.91	1.97	3.41	287	318	1.11

Note: 1 in. = 25.40 mm; 1 lbf = 4.45 N.

entire mechanism is shown in Figs. 9 and 10; in the latter figure the steel mass, clamps, and clamping plates have been removed for clarity.

A force was applied to the free block through a steel cable attached to a small welded steel A-frame; this frame was bolted to the block by means of the threaded bar (Fig. 10), and was proportioned so that the line of action of the force passed through the center of the flange. The other end of the cable was led over a pulley clamped to the end of the test table, and was attached to a steel hanger which supported the applied loads.

A preliminary test was conducted to establish the value of the force required to initiate sliding of the free block; with the clamps and steel mass in place, the magnitude of this force was 6.75 lbf (30 N). The models were then clamped in turn to the blocks, and load increments were applied until the web posts buckled; the view on Model 2 in Fig. 10 is typical of the deformed shapes obtained. Model 1 was the only case where the web post received no assistance from adjacent web material, and an examination of the deformed model revealed that despite the presence of the clamping plates, the flanges had buckled locally at their junction with the post. This had the effect of reducing the buckling moment of the web post.

The experimental shear forces causing buckling are given in Table 1 where they are compared with the theoretical values obtained from Eq. 11; the latter values were based on elastic moduli of $E = 29.4 \times 10^6$ psi (203,000 N/mm^2) and $G = 11.3 \times 10^6$ psi (78,070 N/mm^2).

The effect of local buckling of the flanges in Model 1 is clearly shown by the low test load, and this result should be ignored. The use of Eq. 14 overestimated the elastic buckling moments of the remaining models by an average of 9%; Eq. 13 could therefore be regarded as a good approximation for the effective buckling length of a web post.

Practical Application

By using Eq. 14 in conjunction with Fig. 5, it was possible to determine the buckling moment of a web post, and the state of stress at the critical sections. This approach was used to investigate the significance of web post buckling for practical beams. Three beam sizes were considered: (1) An 8WF20 beam, which had the stockiest web of the wide-flange beams available in South Africa; (2) a 16WF26 beam, which had the slenderest web of any wide-flange beam; and (3) a welded plate girder having a 42 in. (1,067 mm) deep by 3/8 in. (9.5 mm) thick web plate. The yield stress of each web was taken as 36,250 psi (250 N/mm^2), and the elastic moduli E and G were taken as 29.4×10^6 psi (203,000 N/mm^2) and 11.3×10^6 psi (78,070 N/mm^2) respectively.

Each beam was considered to be perforated with a pair of concentric holes

TABLE 2.—Values of $(M_p/M_E)^{1/2}$ for Some Typical Beams

Beam (1)	Depth of opening, in inches (2)	Web post width, in inches (3)	$(M_p/M_E)^{1/2}$ (4)
8WF20	5.43	1	0.195
		2	0.276
		3	0.339
		4	0.391
		6	0.479
		8	0.553
16WF26	10.43	2	0.387
		4	0.547
		6	0.670
		8	0.773
		10	0.865
		12	0.947
		14	1.023
		16	1.094
Plate girder	28.00	4	0.602
		8	0.851
		10	0.951
		12	1.042
		16	1.203

Note: 1 in. = 25.40 mm.

of near-optimum depth, i.e., two-thirds of the overall beam depth in the case of the rolled sections, and two-thirds of the web depth in the case of the plate girder. The quantity $(M_p/M_E)^{1/2}$ was calculated for a variety of web post widths (Table 2), and the $\beta = 1$ curve of Fig. 5 was used to determine whether buckling would be elastic or inelastic, and whether in the latter case it would occur before the ends of the post yielded completely.

8WF20 beam.—All values of $(M_p/M_E)^{1/2}$ were distant from the $\beta = 1$ curve. Buckling would not occur before the ends of the post yielded fully, and was in fact unlikely to occur at all.

16WF26 beam.—For a web post width of 12 in. (305 mm), Fig. 5 predicted that buckling would occur just as the ends of the post yielded fully. For narrower widths the ends of the post would be fully yielded before buckling occurred, and buckling was unlikely to occur at all for the smaller widths. It appeared that a 14 in. (356 mm) wide post would come very near to buckling elastically, but when this width was compared with the 15.64 in. (397 mm) beam depth, it was clear that the $(M_p/M_E)^{1/2}$ values for this and larger widths were of academic interest only, since with so strong a post failure would be confined to a single opening.

Plate girder.—For widths of 10 in. (254 mm) and less, the ends of the post would be fully yielded before buckling occurred. For a width of 12 in. (305 mm) or more, the post would buckle elastically. These values illustrate the narrowness of the range between elastic and plastic buckling.

These results show that for rolled sections, web post buckling will be accompanied by complete yielding of the ends of the post. The ultimate flexural strength of the perforated section will therefore be identical to that given by plastic analysis, and it is unnecessary to perform a buckling analysis of the web post. In plate girders, however, the slenderness of the web may be such that the post buckles while its ends are elastic or only partially plastic. This will produce a lower ultimate flexural strength than that given by plastic analysis, and a buckling analysis of the web post is mandatory.

Summary and Conclusions

The provision of adjacent openings in the web of a steel I-beam may cause buckling failure of the post between the openings. If this occurs while the ends of the post are elastic or only partially plastic, the ultimate flexural strength of the perforated section will be lower than that predicted by plastic analysis, and a buckling analysis of the web post must be performed.

A method has been presented for determining the buckling moment of a web post. An expression was derived for the effective buckling length of the post, and its validity was confirmed by means of tests on scale models. The elastic buckling moment of the post could then be found from elastic buckling theory, and was used to obtain the actual buckling moment from an inelastic buckling analysis due to Nethercot and Trahair (8).

Analysis of practical beams showed that web post buckling would not reduce the ultimate flexural strength of perforated rolled sections; this was not the case with plate girders however, and with these structures a buckling analysis of the web post was mandatory.

Acknowledgments

The experimental work described in this paper was carried out in the structural laboratory of the Department of Civil Engineering, University of Natal, Durban, and was financed by a grant from the University of Natal Research Fund.

Appendix I.—References

1. Clark, J. W., and Hill, H. N., "Lateral Buckling of Beams," *Journal of the Structural Division*, ASCE, Vol. 86, No. ST7, Proc. Paper 2559, July, 1960, pp. 175–196.
2. Dougherty, B. K., "The Effects of Rectangular Web Holes on the Behaviour of Steel Beams," thesis presented to the University of Natal, Durban, South Africa, in 1978, in partial fulfillment of the requirements for the degree of Doctor of Philosophy.
3. Johnson, C. P., and Will, K. M., "Beam Buckling by Finite Element Procedure," *Journal of the Structural Division*, ASCE, Vol. 100, No. ST3, Proc. Paper 10432, Mar., 1974, pp. 669–685.
4. Kitipornchai, S., and Trahair, N. S., "Buckling of Inelastic I-Beams under Moment Gradient," *Journal of the Structural Division*, ASCE, Vol. 101, No. ST5, Proc. Paper 11295, May, 1975, pp. 991–1004.
5. Kitipornchai, S., and Trahair, N. S., "Inelastic Buckling of Simply Supported Steel I-Beams," *Journal of the Structural Division*, ASCE, Vol. 101, No. ST7, Proc. Paper 11419, July, 1975, pp. 1333–1347.
6. Nethercot, D. A., "Inelastic Buckling of Steel Beams under Nonuniform Moment," *The Structural Engineer*, Vol. 53, No. 2, Feb., 1975, pp. 73–78.
7. Nethercot, D. A., and Rockey, K. C., "Finite Element Solutions for the Buckling of Columns and Beams," *International Journal of Mechanical Sciences*, Vol. 13, 1971.
8. Nethercot, D. A., and Trahair, N. S., "Inelastic Lateral Buckling of Determinate Beams," *Journal of the Structural Division*, ASCE, Vol. 102, No. ST4, Proc. Paper 12020, Apr., 1976, pp. 701–717.
9. Powell, G., and Klingner, R., "Elastic Lateral Buckling of Steel Beams," *Journal of the Structural Division*, ASCE, Vol. 96, No. ST9, Proc. Paper 7555, Sept., 1970, pp. 1919–1932.
10. Redwood, R. G., "Ultimate Strength Design of Beams with Multiple Openings," presented at the September 30–October 4, 1968, ASCE National Meeting on Structural Engineering, held at Pittsburgh, Pa. (Preprint 757).
11. Redwood, R. G., and McCutcheon, J. O., "Beam Tests with Unreinforced Web Openings," *Journal of the Structural Division*, ASCE, Vol. 94, No. ST1, Proc. Paper 5706, Jan., 1968, pp. 1–17.
12. Salvadori, M. G., "Lateral Buckling of Eccentrically Loaded I-Columns," *Transactions*, ASCE, Vol. 121, Paper No. 2836, 1956, pp. 1163–1178.
13. "Suggested Design Guides for Beams with Web Holes," by the Subcommittee on Beams with Web Openings of the Task Committee on Flexural Members of the Structural Division, *Journal of the Structural Division*, ASCE, Vol. 97, No. ST11, Proc. Paper 8536, Nov., 1971, pp. 2707–2728.
14. Tebedge, N., and Tall, L., "Linear Stability Analysis of Beam Columns," *Journal of the Structural Division*, ASCE, Vol. 99, No. ST12, Proc. Paper 10232, Dec., 1973, pp. 2439–2457.
15. Timoshenko, S. P., and Gere, J. M., *Theory of Elastic Stability*, 2nd ed., McGraw-Hill Book Co., Inc., New York, N.Y., 1961.

Appendix II.—Notation

The following symbols are used in this paper:

a = length of web opening;
b = width of web post;

C_w = warping constant;
d = depth of web opening;
E = modulus of elasticity;
F = horizontal shear force in web post at buckling failure;
F_u = horizontal shear force in web post at plastic failure;
G = modulus of rigidity;
H = effective height of web post;
I_p = moment of inertia of web post about major axis;
I_T = moment of inertia of tee sections above and below openings;
I_y = moment of inertia of web post about minor axis;
J = torsion constant;
K = coefficient;
L = overall length of perforated section;
l = effective buckling length;
M_c = inelastic buckling moment of web post;
M_E = larger end moment at elastic buckling of web post;
M_p = plastic moment of resistance of web post section;
M_{PA}, etc. = plastic moment of resistance of tee sections;
M_u = ultimate resisting moment of perforated section to Vierendeel bending;
Q = vertical shear force acting on perforated section;
t = thickness of web post; and
ψ = coefficient.

JOURNAL OF THE STRUCTURAL DIVISION

BASIC ASPECTS OF BUCKLING OF COOLING-TOWER SHELLS

By Ali Almannai,[1] Yavuz Başar,[2] and Ihsan Mungan[3]

INTRODUCTION

The main loadings of the hyperbolic natural-draft cooling towers are dead load and wind load. The biaxial stress state induced in the axisymmetric shell through these loads is nonaxisymmetric, changing along the height and circumference. Due to this fact, the buckling problem becomes very complicated, even in elastic range.

There is a large number of works on the stability of cooling-tower shells, both theoretical and experimental (4,5,6,7,9,10,11,14). The numerical results are very informative for axisymmetric cases (4,11). Under wind loading, however, the results obtained do not seem to be realistic, due to the nonperiodic buckling configuration in this case (6,12,13). According to the observation made on buckling tests under load control, the buckling is initiated locally as a critical stress state is reached (9). For this reason, in Ref. 9, a critical stress state concept was proposed to check the buckling safety of cooling-tower shells.

The objectives of the present work are to examine the effects of boundary conditions, shape of the meridian, and wall thickness. The parametric studies carried out yield numerical results which define some applicability limits for the buckling stress state concept for different cooling tower geometries.

LINEAR BUCKLING THEORY

A detailed description of the linear bifurcation theory used in the present work is given in Refs. 2 and 3. The equations of equilibrium are derived considering the buckled state, which is supposed to be infinitesimally neighboring. The

[1]Partner and Dir., Mannai Engrg. Co. Ltd., Bahrain, Persian Gulf.
[2]Prof., Devlet Mühendislik ve Mimarlik Akademisi, Istanbul, Turkey.
[3]Wissenschaftlicher Angestellter, Ruhr Universität Bochum, Institut fur Konstruktiven Ingenieurbau, IA-4/152, Universitatsstr, 150, D-4630, Bochum 25, West Germany.

Note.—Discussion open until August 1, 1981. To extend the closing date one month, a written request must be filed with the Manager of Technical and Professional Publications, ASCE. Manuscript was submitted for review for possible publication on July 23, 1979. This paper is part of the Journal of the Structural Division, Proceedings of the American Society of Civil Engineers, ©ASCE, Vol. 107, No. ST3, March, 1981. ISSN 0044-8001/81/0003-0521/$01.00.

terms present in these equations are considered to consist of two parts, one due to the prebuckled state and another due to buckled configuration. After eliminating the part due to the prebuckled state, the following equations are obtained:

$$\overset{+}{n}{}^{\alpha\beta}|_{\alpha} - b_{\alpha}^{\beta}\overset{+}{q}{}^{\alpha} + \dot{n}^{\alpha\lambda}\overset{+}{L}{}_{\alpha\lambda}^{\beta} + \dot{q}^{\alpha}\overset{+}{L}{}_{\alpha}^{\beta} = 0 \quad \ldots\ldots\ldots\ldots (1)$$

$$b_{\alpha\beta}\overset{+}{n}{}^{\alpha\beta} + \overset{+}{q}{}^{\alpha}|_{\alpha} - \dot{n}^{\alpha\beta}\overset{+}{\omega}_{\alpha\beta} = 0 \quad \ldots\ldots\ldots\ldots (2)$$

$$\overset{+}{m}{}^{\alpha\beta}|_{\alpha} - \overset{+}{q}{}^{\beta} + \dot{m}^{\alpha\lambda}\overset{+}{L}{}_{\alpha\lambda}^{\beta} = 0 \quad \ldots\ldots\ldots\ldots (3)$$

homogeneous part of the bending theory | terms of the membrane theory | terms of the bending theory

The coefficients, $\overset{+}{L}{}_{\alpha\lambda}^{\beta}$, $\overset{+}{L}{}_{\alpha}^{\beta}$, and the second strain tensor, $\overset{+}{\omega}_{\alpha\beta}$, allow the transition from the metric of the deformed surface to the metric of the undeformed shell

$$\overset{+}{L}{}_{\beta\gamma}^{\alpha} = \overset{+}{v}{}^{\alpha}|_{\beta\gamma} - (b_{\beta}^{\alpha}\overset{+}{v}_{3})|_{\gamma} + \overset{+}{w}_{\beta}b_{\gamma}^{\alpha} - \overset{+}{w}{}^{\alpha}b_{\beta\gamma} \quad \ldots\ldots\ldots\ldots (4)$$

$$\overset{+}{L}{}_{\alpha}^{\beta} = \overset{+}{w}{}^{\beta}|_{\alpha} + b_{\alpha}^{\lambda}(\overset{+}{v}{}^{\beta}|_{\lambda} - b_{\lambda}^{\beta}\overset{+}{v}_{3}) \quad \ldots\ldots\ldots\ldots (5)$$

$$\overset{+}{\omega}_{\alpha\beta} = \frac{1}{2}(\overset{+}{w}_{\alpha|\beta} + \overset{+}{w}_{\beta|\alpha} - b_{\alpha}^{\lambda}\overset{+}{v}_{\lambda|\beta} - b_{\beta}^{\lambda}\overset{+}{v}_{\lambda|\alpha} + 2\,b_{\alpha}^{\lambda}b_{\lambda\beta}\overset{+}{v}_{3}) \quad \ldots\ldots\ldots\ldots (6)$$

The constitutive equations

$$\overset{+}{\alpha}_{\alpha\beta} = \frac{1}{2}(\overset{+}{v}_{\alpha|\beta}\overset{+}{v}_{\beta|\alpha} - 2b_{\alpha\beta}\overset{+}{v}_{3}) = \frac{H^{*}_{\alpha\beta\rho\lambda}}{Et}\overset{+}{n}{}^{\rho\lambda} \quad \ldots\ldots\ldots\ldots (7)$$

$$\overset{+}{\omega}_{\alpha\beta} = \frac{12H^{*}_{\alpha\beta\rho\lambda}}{Et^{3}}\overset{+}{m}{}^{\rho\lambda} \quad \ldots\ldots\ldots\ldots (8)$$

together with the symmetry condition

$$\epsilon_{\alpha\beta}\overset{+}{n}{}^{\alpha\beta} = \frac{1}{2}\epsilon_{\alpha\beta}(b_{\lambda}^{\alpha}\overset{+}{m}{}^{\lambda\beta} - b_{\lambda}^{\beta}\overset{+}{m}{}^{\lambda\alpha}) \quad \ldots\ldots\ldots\ldots (9)$$

and the Love-Kirchhoff-hypothesis

$$\overset{+}{w}_{\alpha} = -(\overset{+}{v}_{3|\alpha} + b_{\alpha}^{\lambda}\overset{+}{v}_{\lambda}) \quad \ldots\ldots\ldots\ldots (10)$$

complete the system of the differential equations necessary to determine the critical load parameters. In Eqs. 1–10, $\overset{+}{n}{}^{\alpha\beta}$ = the nonsymmetrical stress resultant tensor; $\overset{+}{m}{}^{\alpha\beta}$ stands for the symmetrical tensor of the stress couples; and $\overset{+}{q}{}^{\alpha}$ = the shear force tensor. Superscripts · and + denote the prebuckled or buckled state, respectively. The variable $H^{*}_{\alpha\beta\rho\lambda}$ = the elasticity tensor, E and t being the modulus of elasticity and wall thickness of the shell. If in Eqs. 1 and 3 the last terms are neglected, then the equations of the so-called classical buckling theory are obtained.

Method of Solution

For general shells of revolution, according to Fig. 1, the differential Eqs.

1–10 can be written explicitly using the rules of tensor calculus. If the variables are given as a column vector

$$\overset{+}{\mathbf{Z}} = (\overset{+}{n}^{11}\overset{+}{n}^{12}\overset{+}{n}^{21}\overset{+}{n}^{22}\overset{+}{q}^{1}\overset{+}{q}^{2}\overset{+}{m}^{11}\overset{+}{m}^{12}\overset{+}{m}^{22}\overset{+}{w}_1\overset{+}{w}_2\overset{+}{v}_1\overset{+}{v}_2\overset{+}{v}_3)^T \quad \ldots\ldots\ldots\ldots\ldots\ldots (11)$$

The 14 partial differential equations of the problem can be written in matrix notation as:

$$\underbrace{\mathbf{b}_1\overset{+}{\mathbf{Z}}^{\cdot} + \mathbf{b}_2\overset{+}{\mathbf{Z}}' + \mathbf{b}\overset{+}{\mathbf{Z}}}_{\text{homogeneous part of the bending theory}} \underbrace{+ \mathbf{s}_{11}\overset{+}{\mathbf{Z}}^{\cdot\cdot} + \mathbf{s}_{12}\overset{+}{\mathbf{Z}}^{\cdot\prime} + \mathbf{s}_{22}\overset{+}{\mathbf{Z}}'' + \mathbf{s}_1\overset{+}{\mathbf{Z}}^{\cdot} + \mathbf{s}_2\overset{+}{\mathbf{Z}}' + \mathbf{s}\overset{+}{\mathbf{Z}} = 0}_{\text{stability terms}} \quad \ldots\ldots\ldots\ldots\ldots\ldots (12)$$

$(\,)^{\cdot}$ and $(\,)'$ stand for the partial derivatives with respect to the cylindrical coordinates θ^1 and θ^2, respectively, according to Fig. 1.

For an axisymmetric prebuckling stress state with

$$\dot{n}^{12} = \dot{q}^1 = \dot{m}^{12} = 0 \quad \ldots\ldots\ldots\ldots\ldots\ldots\ldots\ldots\ldots\ldots\ldots\ldots (13)$$

the partial differential equation system can be reduced to a system of ordinary differential equations, if for the symmetric and antisymmetric variables, the

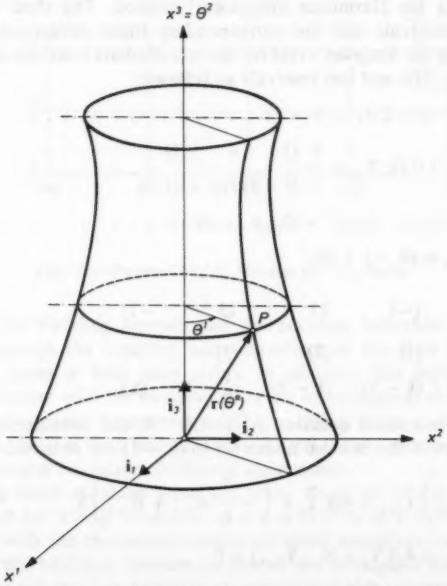

FIG. 1.—Curvilinear Coordinates for Shells of Revolution

following statements are introduced:

$$\overset{+}{\mathbf{Z}}^{(s)} = \overset{+}{\mathbf{Z}}_n^{(s)} \cos n\theta^1; \quad \overset{+}{\mathbf{Z}}^{(a)} = \overset{+}{\mathbf{Z}}_n^{(a)} \sin n\theta^1; \quad n = 0, 1, 2, \ldots \quad (14)$$

$$\overset{+}{\mathbf{Z}}_n^{(s)} = (\overset{+}{n}_n^{11}\, \overset{+}{n}_n^{22}\, \overset{+}{q}_n^{2}\, \overset{+}{m}_n^{11}\, \overset{+}{m}_n^{22}\, \overset{+}{w}_{2n}\, \overset{+}{v}_{2n}\, \overset{+}{v}_{3n})^T \quad (15)$$

$$\overset{+}{\mathbf{Z}}_n^{(a)} = (\overset{+}{n}_n^{12}\, \overset{+}{n}_n^{21}\, \overset{+}{q}_n^{1}\, \overset{+}{m}_n^{12}\, \overset{+}{w}_{1n}\, \overset{+}{v}_{1n})^T \quad (16)$$

The variables $\mathbf{Z}_n^{(s)}$ and $\mathbf{Z}_n^{(a)}$ are now only functions of θ^2. In order to eliminate the derivatives of higher order new variables are introduced:

$$\overset{+}{S}_{\alpha n} = \overset{+}{V}'_{\alpha n}; \quad \overset{+}{V}_{\alpha n} = \overset{+}{v}'_{\alpha n}; \quad \overset{+}{W}_{\alpha n} = \overset{+}{w}'_{\alpha n}; \quad (\alpha = 1, 2) \quad (17)$$

and a new vector $\overset{+}{\mathbf{Y}}$ of the unknowns is obtained:

$$\overset{+}{\mathbf{Y}}{}^T = (\overset{+}{n}_n^{11}\, \overset{+}{n}_n^{12}\, \overset{+}{n}_n^{21}\, \overset{+}{n}_n^{22}\, \overset{+}{q}_n^{1}\, \overset{+}{q}_n^{2}\, \overset{+}{m}_n^{11}\, \overset{+}{m}_n^{12}\, \overset{+}{m}_n^{22}\, \overset{+}{W}_{1n}\, \overset{+}{W}_{2n}$$
$$\overset{+}{w}_{1n}\, \overset{+}{w}_{2n}\, \overset{+}{S}_{1n}\, \overset{+}{S}_{2n}\, \overset{+}{V}_{1n}\, \overset{+}{V}_{2n}\, \overset{+}{v}_{1n}\, \overset{+}{v}_{2n}\, \overset{+}{v}_{3n}) \quad (18)$$

Written in matrix notation, the final system of ordinary differential equations is

$$\mathbf{A}\overset{+}{\mathbf{Y}}' + \mathbf{B}\overset{+}{\mathbf{Y}} + \lambda_{ncr}\mathbf{S}\overset{+}{\mathbf{Y}} = 0 \quad (19)$$

The variables **A**, **B**, and **S** are square matrices of the size 20×20 which depend on (n), the number of waves assumed along the circumference. These matrices are given in Ref. 3. The variable λ_{ncr} = the critical load parameter.

For integration, the differential equations are transformed into finite difference equations using the Hermitian (multilocal) method. The shell is divided into $k - 1$ equal intervals and the corresponding finite difference equations are written applying the Simpson's rule for the intermediate intervals and the Bessel's formula for the first and last intervals as follows:

$$S_{(i)}y' = D_{(i)}y; \quad (i = 2,3, \ldots, k-1) \quad (20)$$

$$\text{with} \quad D_{(i)} = (-1\ 0\ 1); \; S_{(i)} = \frac{h}{3}\frac{(1 \quad 4 \quad 1)}{(i-1)(i)(i+1)} \quad (21)$$

$$\text{and} \quad S_{(1)}y' = D_{(1)}y; \quad S_{(k)}y' = D_{(k)}y \quad (22)$$

$$\text{with} \quad D_{(1)}, D_{(k)} = (0 \ -1 \ 1 \ 0);$$

$$S_{(1)}, S_{(k)} = \frac{h}{24}\begin{matrix}(-1 & 13 & 13 & -1)\\ (1) & (2) & (3) & (4)\\ (k-3) & (k-2) & (k-1) & (k)\end{matrix} \quad (23)$$

Applying the summation operator $S_{(i)}$ to Eq. 19, and considering Eqs. 20 and 21, 20 equations of the internal nodes (2) to $(k - 1)$ are obtained

$$\left(\frac{3}{h}\mathbf{A}_{i+1} + \mathbf{B}_{i+1}\right)\overset{+}{\mathbf{Y}}_{i+1} + 4\mathbf{B}_i\overset{+}{\mathbf{Y}}_i + \left(-\frac{3}{h}\mathbf{A}_{i-1} + \mathbf{B}_{i-1}\right)\overset{+}{\mathbf{Y}}_{i-1}$$
$$+ \lambda_{ncr}(\mathbf{S}_{i+1}\overset{+}{\mathbf{Y}}_{i+1} + 4\,\mathbf{S}_i\overset{+}{\mathbf{Y}}_i + \mathbf{S}_{i-1}\overset{+}{\mathbf{Y}}_{i-1}) = 0 \quad (24)$$

The equations of the first and last nodes (1) and (k) are derived in a similar way using Eqs. 22 and 23. Afterwards, the critical load factor, λ_{ncr}, is calculated

solving the eigenvalue problem of the form

$$\mathbf{K}_B\overset{+}{\mathbf{X}} + \lambda_{ncr}\mathbf{K}_S\overset{+}{\mathbf{X}} = 0 \quad \ldots\ldots\ldots\ldots\ldots\ldots\ldots\ldots\ldots\ldots\ldots\ldots \quad (25)$$

The boundary conditions, four at each boundary, are considered, easily substituting them in the corresponding equations, as explained in Ref. 2.

Correlation of Numerical and Experimental Results

The experimental results considered in this work are those of Ref. 9. In the tests described in detail in Ref. 9, the buckling procedure was always initiated locally, the experimental values for the symmetrical models, SM and for CM being of the same range. In other words, the tests showed that the reduction of the height above the throat from 600 mm (23.65 in.) to 220 mm (8.65 in.)

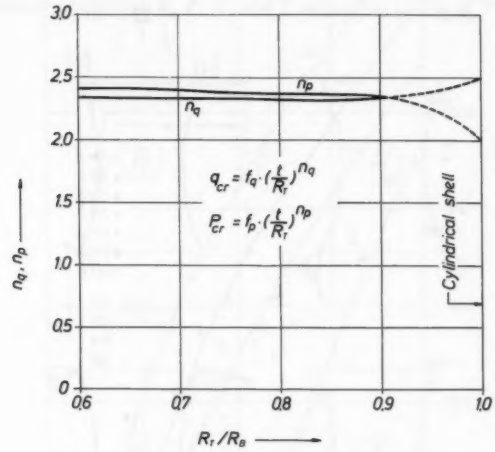

FIG. 2.—Power of t/R_T Versus R_T/R_B Ratio

doesn't affect the buckling stresses and the buckling behavior. This fact can be explained through the buckling initiating effect of the local imperfections, which was the same in both tests series. In addition, this initially surprising result is in agreement with the buckling behavior of cylindrical shells of medium length subjected to axial compression. The buckling stress is independent of the shell length, both in tests and according to the theory, and does not change if clamped or hinged boundary conditions are present.

The buckling loads obtained from the tests, as given in Fig. 5 of Ref. 9, are extrapolated for a wall thickness of 2 mm (0.0785 in.). For that purpose, in accordance with the theoretical results obtained and given in Fig. 2 of the present work, the buckling stresses measured are multiplied by $(2/t_{cr})^{4/3}$ for each model. The results given in Fig. 3 are obtained in this way, and are identical to those given in Fig. 6 of Ref. 9.

The first letter, *S* or *C*, stands for the type of the model as symmetrical or cooling-tower shaped. The second letter denotes the boundary conditions considered. The letter *A* stands for clamped ends at both boundaries. In case *B*, the lower boundary of the model is assumed to be clamped. The upper boundary is also clamped; however a displacement in the vertical direction is allowed, as indicated in Fig. 4. In the tests, the upper head plate of the testing machine was resting free on the model, a vertical displacement or rotation being possible. However, different from case *B*, the upper edge of the model

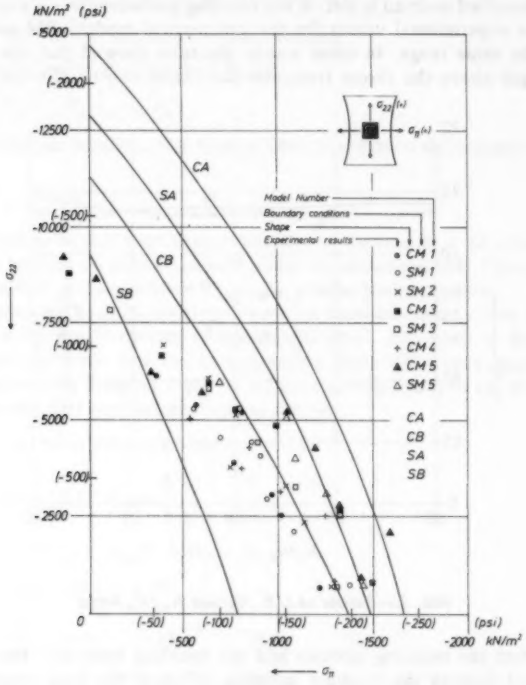

FIG. 3.—Test Results and Theoretical Interaction Diagrams [t = 0.0785 in. (2 mm); E = 500,000 psi (3,450 MN/m^2) and ν = 0.38]

also stuck to the head plate, and only displacements and rotations of the relatively rigid head plate as a plane were possible. Therefore, the real boundary conditions in the tests were between *A* and *B*.

A comparison of the interaction diagrams with the test results provides the following information. The calculation results in different interaction diagrams for the symmetrical and cooling-tower models, a fact in contradiction to the tests. The interaction diagrams *CA* and *SB* can nearly be accepted as the upper

and lower boundaries, respectively. For stress states with nearly zero stress in the circumferential direction, the test results match with the values calculated for symmetrical models having the boundary conditions *B* quite well. For other stress states the interaction diagrams *CB* or *SA* fit better.

The discrepancies of Fig. 3 can be explained mainly by means of the assumption and approximation of the buckling analysis used. For example, the initiation of the buckling procedure is in the tests locally, whereas the theory assumes an instantaneous periodic buckling pattern. Furthermore, as the parametric investigations of the following section shows, the buckling loads calculated are substantially influenced by the boundary conditions.

Other Boundary Conditions

The buckling loads due to lateral pressure and axial compression were obtained for the boundary conditions *B*, *F*, *K*, and *I*, according to Fig. 4. The calculated

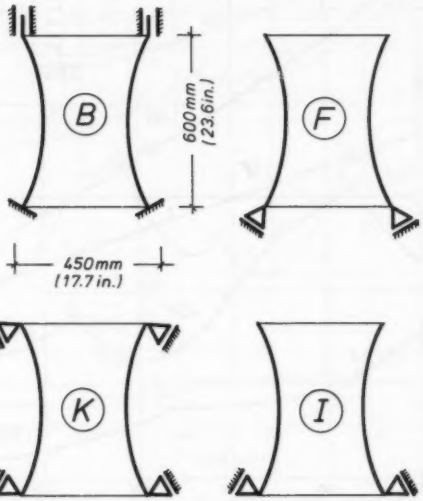

FIG. 4.—Boundary Conditions Considered in Parametric Investigation

shells have a symmetrical shape with respect to the throat, the meridian curve being a circular arch. The height of the shell, H, and the radius at the base, R_B, are 600 mm (23.6 in.) and 225 mm (8.85 in.), respectively. The radius at the throat, R_T, is varied in steps of $(R_T/R_B) = 0.025$, in the range $0.60 \leqq R_T/R_B \leqq = 0.85$. The wall thickness, $t = 1.6$ mm (0.063 in.), and material constants, $E = 3650$ MN/m^2 (530.000 psi), and $\nu = 0.35$ are considered. In applying the finite difference method, the meridian is divided into 12 equidistant intervals.

In Fig. 5, the buckling loads of the symmetrical shells with boundary conditions

B, F, K, and I under lateral radial pressure are given for different ratios of R_T/R_B, with the corresponding number of buckling waves, n, in the circumferential direction. The boundary conditions, F, are nearly the same as those present in natural-draught cooling towers, whereas the type of supporting, K, corresponds to the so-called classical boundary conditions. Boundary conditions I can be considered as representative for a cooling tower on a ground stressed up to the yielding and deforming in the direction of the supporting columns without any resistance, as a hypothetical lower limit.

The curves for the buckling loads change regularly for system SB, SF, and SI, the buckling pressure decreasing with increasing R_T/R_B ratio. Also, the

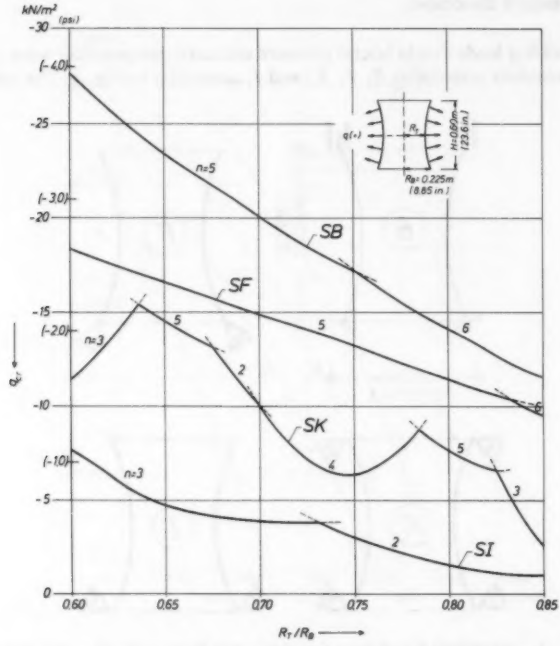

FIG. 5.—Buckling Pressure Versus R_T/R_B Ratio

number of the buckling waves changes regularly and slightly. In contrast to these systems, SK has buckling loads and wave numbers alternating strongly due to slight variations of R_T/R_B. This high geometric dependence can hardly be accepted as realistic. A hyperboloidal shell having classical boundary conditions tends to deform quasi-inextensional, i.e., eliminating the membrane energy. This behavior results in low buckling loads, as shown in Fig. 6 for the cases $R_T/R_B = 0.75$ and 0.85, with $n = 4$ and 3. On the other hand, for $R_T/R_B = 0.65$, the deformation mode with five periodic waves in the circumferential direction

comprises a considerable extensional part. A deformation mode as a combination of modes with different wave numbers, might comprise much lower extensional deformations, and might yield a lower buckling load. However, the present analysis does not include solutions with buckling forms as a combination of different wave numbers. For this reason, as an approximation, the envelope of the buckling curves, which is again a regular curve, can be considered as realistic for shells having classical boundary conditions. The boundary conditions *I* allow in the range $0.60 = R_T/R_B = 0.85$ overall inextensional deformations with $n = 2$ or 3. For this reason, the buckling curve, *SI*, is very low and regular.

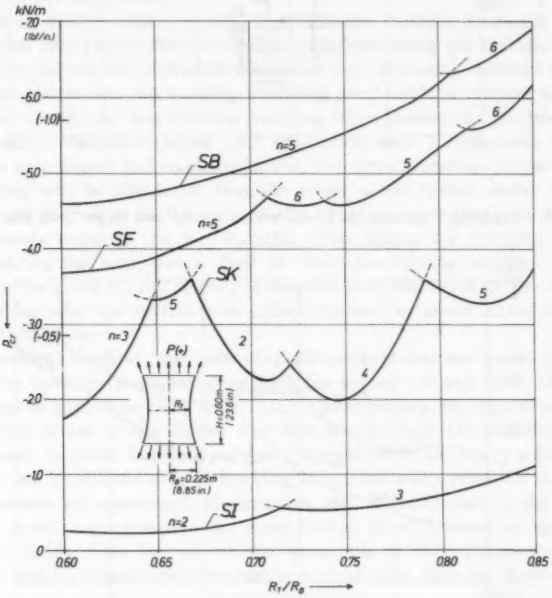

FIG. 6.—Buckling Axial Load Versus R_T/R_B Ratio

The buckling loads under axial compression are given in Fig. 6. Again, for the boundary conditions *B*, *F*, and *I*, the curves are regular, having increasing tendency with increasing R_T/R_B ratio. For the shell having classical boundary conditions, the same interpretation as in the case of external lateral pressure, is valid.

Shape of Meridian

The shape of the meridian is in natural-draught cooling-tower shells mostly a hyperbola. For this reason, the parameter studies were extended also on

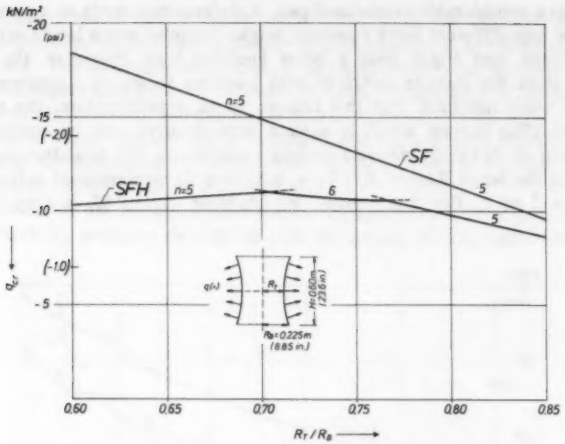

FIG. 7.—Buckling Pressure for Shells with Circular and Hyperbolic Meridian

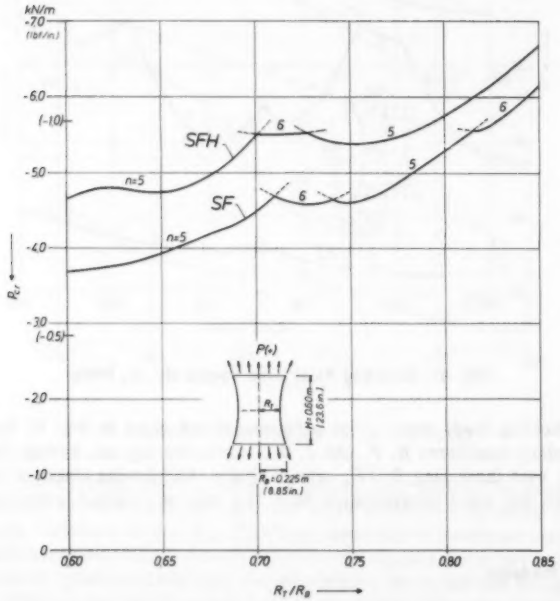

FIG. 8.—Buckling Axial Load for Shells with Circular and Hyperbolic Meridian

such shells with the boundary conditions *F*, which are representative for cooling towers.

Fig. 7 shows the critical lateral pressure as a function of the R_T/R_B ratio for the cases of the circular meridian, *SF*, and of the meridian as a hyperbola, *SFH*. The fact that the critical lateral pressure is, in case *SFH*, almost independent of the R_T/R_B ratio, is very perplexing. In addition, the divergency of the curves *SF* and *SFH* with a decreasing R_T/R_B ratio may be unexpected, due to only a slight difference in the shape of a cooling tower with a circular or hyperbolic meridian, if R_T/R_B is the same for both cases. An interpretation of this initially contradictory behavior is possible if the buckling tests and buckling stresses, as in Ref. 9, are considered.

In tests on models with a circular meridian, the buckling is always initiated at the throat (9). This is due to constant curvature along the meridian. In the case of a hyperbola the curvature decreases with increasing distance from the throat. For this reason the buckling initiating point tends to remove to regions away from the throat, and the first buckling wave forms near the boundaries. This tendency was observed in tests on models with a hyperbolic meridian (11). Due to a bigger radius of curvature, the circumferential stress initiating the buckling will be also larger than the stress at the throat, under the same lateral loading. In Fig. 7, the ratio of the buckling loads for *SFH* and *SF* is approximately equal to the R_T/R_B ratio. That means the buckling initiating stress remains the same for a shell of revolution having negative Gaussian curvature, for given *H*, R_T, and R_B, independent of the shape of the meridian. This explains why we operate with critical stresses or stress states instead of critical loads (9,10).

The buckling loads in the case of axial compression are given in Fig. 8. The curves have the same tendency both for system *SF* and *SFH*, the values for the case of hyperbola being larger. Under axial loading, the biggest meridional stresses are acting at the throat. For this reason, it is obvious that models with circular meridian buckling always at the throat (9) can carry a lower axial load than the hyperbolic models buckling at regions away from the throat (11). If the stresses are concerned, it turns out, that in both cases at the buckling initiating point, approximately the same critical stress interaction relationship of Ref. 9 holds. This fact allows the extension of the equations of Ref. 9 on shells with hyperbolic meridian and to regions other than the throat.

Wall Thickness

In addition to shells with 1.6-mm (0.063-in.) wall thickness shells with 0.8-mm (0.0315-in.) and 0.4-mm (0.016-in.) thicknesses were also calculated. In this way, a range of shell slenderness $1/565 \leqq t/R_T \leqq 1/85$ for $0.60 \leqq R_T/R_B \leqq 1.00$, could be covered. Circular meridian and the boundary conditions of System *F* were considered. The calculations were carried out separately under lateral pressure and axial compression.

The results of this parameter study are given in Fig. 2. In expressions for the critical loads, q_{cr} and P_{cr}, the wall thickness of the shell is separated and considered as the slenderness t/R_T in nondimensional form, with R_T being the radius at the throat. The variables f_q and f_p = functions of the other geometric parameters and material properties. As Fig. 2 shows, both critical lateral and

axial loads are proportional with a nearly constant power of the wall thickness in the range $0.60 \leqq R_T/R_B \leqq 0.90$ which is of interest for hyperboloidal cooling-tower shells. For cylindrical shells, the well-known factors $n_q = 5/2$ and $n_p = 2$ are obtained.

Conclusions

The following conclusions can be made:

1. The agreement between theoretical results and experimental results is for hyperboloidal shells better than in the case of cylindrical shells. For this reason, the results of the bifurcation theory for cooling-tower shells under axisymmetric loading can be accepted as realistic and used for design after a slight correction.
2. An upper cornice ring, reducing the displacements in normal and circumferential directions at the top of the shell, proves to be advantageous, as the comparison of the buckling curves for systems *SB* and *SF* shows.
3. For the boundary conditions *F*, which are in general identical with those of a cooling-tower shell, the relationship between the buckling loads and R_T/R_B is regular, and R_T/R_B is an important geometric parameter of the cooling-tower buckling.
4. In the case of settlement of the supports in the meridional direction, the buckling resistance of the cooling tower shell drops considerably, as the results in the limit case of boundary conditions *I* demonstrate.
5. Although different buckling loads are obtained for a hyperbolic and toroidal cooling-tower shell having the same R_T/R_B ratio, the difference vanishes if the buckling stresses in the points initiating the buckling process are considered. That is an important reason why the buckling design should be based on the stresses and not on the loads.
6. For cooling-tower shells, the buckling loads, as meridional compression or uniform lateral pressure, are proportional to $(t/R_T)^{7/3}$. Therefore $(t/R_T)^{4/3}$ is the parameter taking account of the slenderness of the shell in the expressions of Ref. 9 for the buckling stresses.

Appendix I.—References

1. Almannai, A., Basar, Y., and Mungan, I., "Beuluntersuchungen an Rotationsschalen: Theorie und Versuch," *Der Bauingenieur*, Berlin, West Germany, Vol. 54, No. 6, June, 1979, pp. 205–211.
2. Basar, Y., "Eine Schalentheorie endlicher Verformungen und ihre Anwendung zur Herleitung der linearen Stabilitätstheorie," *Zeitschrift für Angewandte Mathematik und Mechanik*, Berlin, East Germany, Vol. 52, 1972, pp. 197–211.
3. Basar, Y., "Die numerische Behandlung der linearen Stabilitätstheorie allgemeiner Rotationsschalen," *Zeitschrift für Angewandte Mathematik und Mechanik*, Berlin, East Germany, Vol. 56, 1976, pp. 287–298.
4. Cole, P. P., Abel, J. F., and Billington, D. P., "Buckling of Cooling Tower Shells: State of the Art," *Journal of the Structural Division*, ASCE, Vol. 101, No. ST6, Proc. Paper 11364, June, 1975, pp. 1185–1203.
5. Cole, P. P., Abel, J. F., and Billington, D. P., "Buckling of Cooling Tower Shells: Bifurcation Results," *Journal of the Structural Division*, ASCE, Vol. 101, No. ST6, Proc. Paper 11365, June, 1975, pp. 1205–1222.
6. Der, T. J., and Fidler, R., "A Model Study of the Buckling Behaviour of Hyperbolic Shells," *Proceedings*, Institution of Civil Engineers, Vol. 41, Sept., 1968, pp. 105–118.

7. Langhaar, H. L., et al., "Stability of Hyperboloidal Cooling Towers," *Journal of the Engineering Mechanics Division,* ASCE, Vol. 96, No. EM5, Proc. Paper 7635, Oct., 1970, pp. 753–779.
8. Mungan, I., discussion of "Buckling of Cooling-Tower Shells: State-of-the-Art," by Peter P. Cole, John F. Abel, and David P. Billington, *Journal of the Structural Division,* ASCE, Vol. 102, No. ST1, Proc. Paper 11819, Jan., 1976, pp. 302–303.
9. Mungan, I., "Buckling Stress States of Hyperboloidal Shells," *Journal of the Structural Division,* ASCE, Vol. 102, No. ST10, Proc. Paper 12465, Oct., 1976, pp. 2005–2020.
10. Mungan, I., and Lehmkämper, O., "Buckling of Stiffened Hyperboloidal Cooling Towers," *Journal of the Structural Division,* ASCE, Vol. 105, No. ST10, Proc. Paper 14917, Oct., 1979, pp. 1999–2000.
11. Veronda, D. R., and Weingarten, V. I., "Stability of Hyperboloidal Shells," *Journal of the Structural Division,* ASCE, Vol. 101, No. ST7, Proc. Paper 11446, July, 1975, pp. 1585–1602.
12. Yeh, C.-H., and Shieh, Y. J., discussion of "Buckling of Cooling-Tower Shells: State-of-the-Art," by Peter P. Cole, John F. Abel, and David P. Billington, *Journal of the Structural Division,* ASCE, Vol. 102, No. ST1, Proc. Paper 11819, Jan., 1976, pp. 301–302.
13. Yeh, C.-H., and Shieh, Y. J., discussion of "Buckling of Cooling-Tower Shells: Bifurcation Results," by Peter P. Cole, John F. Abel, and David P. Billington, *Journal of the Structural Division,* ASCE, Vol. 103, No. ST3, Proc. Paper 12767, Mar., 1977, p. 733.
14. Zerna, W., Almannai, A., Basar, Y., and Mungan, I., "Randbedingungen und Beulverhalten von Kühlturmschalen," *Beton- und Stahlbetonbau,* Berlin, West Germany, Vol. 75, No. 8, Aug., 1979.

Appendix II.—Notation

The following symbols are used in this paper:

$\mathbf{A}, \mathbf{B}$ = square matrices (20×20);
$\mathbf{b}, \mathbf{b}_1, \mathbf{b}_2$ = square matrices (14×14);
$b_\alpha^\beta, b_{\alpha\beta}$ = curvature tensors;
$D_{(i)}, D_{(k)}, D_{(1)}$ = finite difference operators;
E = modulus of elasticity;
f_p, f_q = functions of geometry and material properties for axial load and external pressure, respectively;
H = height of the shell;
$\mathbf{i}_1, \mathbf{i}_2, \mathbf{i}_3$ = cartesian unit vectors;
$\mathbf{K}_B, \mathbf{K}_S$ = coefficient matrices;
k = number of modes in the finite difference method;
$L_\alpha^\beta, L_{\alpha\beta}^\beta$ = transformation coefficients;
$m^{\alpha\beta}$ = tensor of the stress couples;
n = number of waves around circumference;
$n^{\alpha\beta}$ = tensor of the stress resultants;
n_p, n_q = power of (t/R_T) for axial compression and lateral pressure, respectively;
P_{cr} = critical axial compression;
q_{cr} = critical lateral pressure;
q^α = shear force tensor;
R_B = radius at base;
R_T = radius at throat;
$\mathbf{S}$ = square matrix (20×20);

$S_{\alpha n}$ = new variable;
$S_{(i)}, S_{(k)}, S_{(l)}$ = summation operators;
$\mathbf{s}, \mathbf{s}_1, \mathbf{s}_2, \mathbf{s}_{11}, \mathbf{s}_{12}, \mathbf{s}_{22}$ = square matrices (14×14);
t = wall thickness of shell;
t_{cr} = critical wall thickness of shell;
$V_{\alpha n}, W_{\alpha n}$ = new variable;
V_α, W_α = displacements of the shell middle surface;
$\mathbf{X}$ = solution vector;
X^1, X^2, X^3 = cartesian coordinates;
$\mathbf{Y}, \mathbf{Z}$ = vectors of the unknowns;
$\alpha, \beta, \ldots$ = index 1 or 2;
$\alpha_{\alpha\beta}$ = first strain tensor of the shell middle surface (extensions);
$\epsilon_{\alpha\beta}$ = ϵ-tensor;
$\theta^\alpha, \theta^1, \theta^2$ = curvilinear coordinates;
λ_{ncr} = critical load parameter;
ν = Poisson's ratio;
σ_{11}, σ_{22} = stresses in circumferential and meridional directions, respectively;
$\omega_{\alpha\beta}$ = second strain tensor (change of curvature);
$(\dot{}), (^*)$ = prebuckled and buckled states, respectively;
$(\,)^{\cdot}, (\,)'$ = partial derivatives with respect to θ^1 and θ^2 respectively; and
$(\,)|_\alpha$ = covariant differentiation with respect to θ^α.

JOURNAL OF THE STRUCTURAL DIVISION

SIMPLIFIED ANALYSIS OF EDGE STIFFENED CANTILEVER SLABS

By Baidar Bakht[1]

INTRODUCTION

Some components in bridge and other structures can be designed by treating them as cantilever slabs in isolation without any appreciable loss of accuracy. For the purpose of analysis these components are usually assumed to be composed of homogeneous isotropic material exhibiting linear elastic characteristics. When the cantilever slab is subjected to concentrated loads an accurate assessment of the force effects could often be obtained either by computer based methods (e.g. grillage analogy or finite element methods) or by rigorous methods [e.g., Jarmillo (5) and Silberstein (12)], that are too complex for every day design office applications.

Simplified methods, suitable for design office use, are available for cantilever slabs of linearly varying thickness but having no edge beams (2,3). One possible way of using these simplified methods for the analysis of cantilever slabs with edge beams is to replace the edge beam by slabs of equivalent flexural rigidity and then analyze the resulting slab as a cantilever slab without edge beams. Such an approach produces satisfactory results only if the flexural rigidity of the edge beam is small compared to that of the slab. When the edge beam rigidity is large, the equivalent slab approach does not provide results of acceptable accuracy.

Fig. 1 shows the distribution of longitudinal moments along the cantilever root due to a concentrated load, in a cantilever slab with an edge beam, and in an "equivalent" slab without an edge beam. The moments were obtained by analyzing the two slabs by the grillage analogy method which is examined later in the paper. It can be seen in Fig. 1, that the equivalent slab approach fails to correctly reproduce the behavior of the edge-stiffened slab.

[1]Sr. Research Officer, Research and Development Div., Ontario Ministry of Transportation and Communications, 1201 Wilson Avenue, Central Building, Downsview, Ontario M3M 1J8 Canada.

Note.—Discussion open until August 1, 1981. To extend the closing date one month, a written request must be filed with the Manager of Technical and Professional Publications, ASCE. Manuscript was submitted for review for possible publication on November 20, 1979. This paper is part of the Journal of the Structural Division, Proceedings of the American Society of Civil Engineers, ©ASCE, Vol. 107, No. ST3, March, 1981. ISSN 0044-8001/81/0003-0535/$01.00.

In box-girder bridges those free edges of the cantilever slabs that are parallel to the span of the bridge are often stiffened by beams. These beams are usually provided for functions other than the enhancement of the behavior of the slab, such as providing curbs or barrier walls for the road. Even though their presence may be incidental, the edge beams do enhance the transverse distribution of concentrated loads in cantilever slabs to an extent which makes their consideration in the analysis quite prudent.

A simplified semigraphical method for determining longitudinal moments in edge stiffened cantilever slabs of linearly varying thickness is given in this paper. The paper also contains methods for determining maximum moments

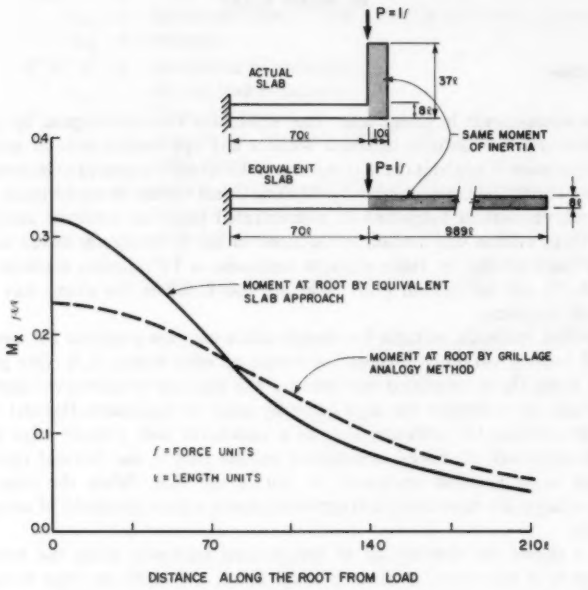

FIG. 1.—Equivalent Slab Method of Analyzing Edge Stiffened Cantilever Slabs

in the edge beam due to concentrated loads anywhere on the slab. Other responses such as deflections and beams cannot be obtained by the proposed methods. The methods given in the paper are based on results obtained by analyses using the grillage analogy method. Therefore, the proposed methods are subject to the same limitations and errors as the grillage analogy method which is briefly examined in the following.

Grillage Analogy Method For Slabs

Lightfoot (6), Yettram and Husain (13), and Sawko (8) are among many who have suggested that the behavior of an isotropic slab can be predicted by an

equivalent assembly of orthogonally connected beams, which can be solved by any one of the (by now) many commercially available grillage programs. The writer (1) has shown that for slabs with zero Poisson's ratio all the proposed idealizations converge to a common approach in which the flexural rigidity, *EI*, of a beam in the equivalent grillage is equal to the flexural rigidity of

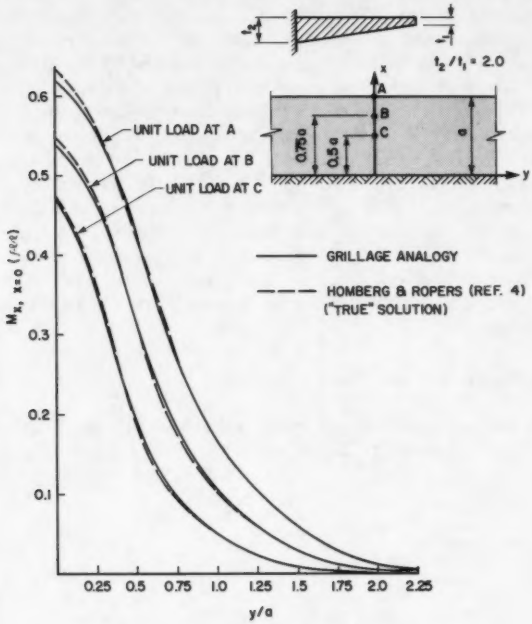

FIG. 2.—Grillage Analogy Versus Plate Solution

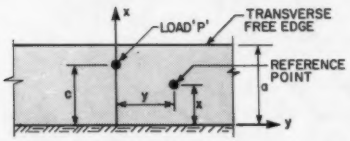

FIG. 3.—Plan of an Infinitely Wide Cantilever Slab

the strip of slab that it represents. The torsional rigidity, GJ, of the beam is taken to be numerically equal to its flexural rigidity. This concept of idealization, which was proposed for slabs of uniform thickness, could also be extended to slabs of linearly varying thickness in which case the idealized grillage consists of beams of varying rigidity in one direction and those of constant rigidity

in the other. At all points the torsional rigidities of beams should be equal to their corresponding flexural rigidities. The grillage programs for analyzing the resulting grillage should be capable of dealing with beams of varying properties, such as the program described in Ref. 11. The aforementioned program is based on techniques described by Sawko and Wilcock (10).

The validity of the grillage analogy for cantilever slabs of linearly varying thickness is demonstrated in Fig. 2, which shows the distribution of longitudinal moments for various load cases along the cantilever root in a very wide cantilever slab of linearly varying thickness. The results obtained by the grillage analogy method are compared with those given by Homberg and Ropers (4). The latter results were obtained by using classical plate theory assuming small deflections and no shear deformations. Both analyses assumed the Poisson's ratio to be equal to zero. From the results plotted in Fig. 2, it can be seen that the grillage analogy gives results identical to those predicted by the plate theory.

The assumption of zero Poisson's ratio is necessary to be able to idealize the slab by orthogonally connected beams. Consideration of a finite value of Poisson's ratio necessitates the introduction of disposal members to the grillage (13). Neglect of Poisson's ratio results in an underestimation of the longitudinal moments. The underestimation, however, is usually small being less than about 5% in concrete slabs.

Moments in Cantilever Slabs of Infinite Width

The simplified solution proposed by the writer and Holland (3) for cantilever slabs with linearly varying thickness but without edge beams is given in the form

$$M_x = \frac{PA'}{\pi}\left[\frac{1}{\cosh\left(\frac{A'y}{c-x}\right)}\right] \quad \ldots\ldots\ldots\ldots\ldots\ldots\ldots\ldots\ldots\ldots\ldots\ldots (1)$$

in which M_x = the longitudinal moment; and A' = a constant given in graphical form for various slab thickness ratios, distances of the load, and reference points from the cantilever root. The notation for other variables is shown in Fig. 3. The solution, which is modelled on a previous solution by Sawko and Mills (9), provides results comparable to those obtained by rigorous methods; it satisfies the following essential conditions:

1. For a given load position M_x has a peak value at $y = 0$.
2. The area under the longitudinal moment curve plotted for a given value of x is equal to $P(c - x)$.
3. M_x tends to zero as y tends to infinity.

The introduction of an edge beam in a cantilever slab does not change any of the foregoing conditions. Therefore it seemed probable that the solution of the writer and Holland (3) with different values of A' could also be applicable to edge stiffened cantilever slabs of infinite width. The main problem with such a proposition remained that of characterizing the edge beam parameters in a nondimensional form. A literature search revealed a rigorous solution by

Reissmann and Cheng (7) for edge stiffened cantilever slabs of constant thickness and infinite width. The series solution is given in terms of two nondimensional parameters, k_1, and k_2, given by

$$k_1 = \frac{EI_B}{Da} \quad \text{(2)}$$

$$k_2 = \frac{GJ_B}{Da} \quad \text{(3)}$$

in which EI_B and GJ_B = the flexural and torsional rigidities of the edge beam;

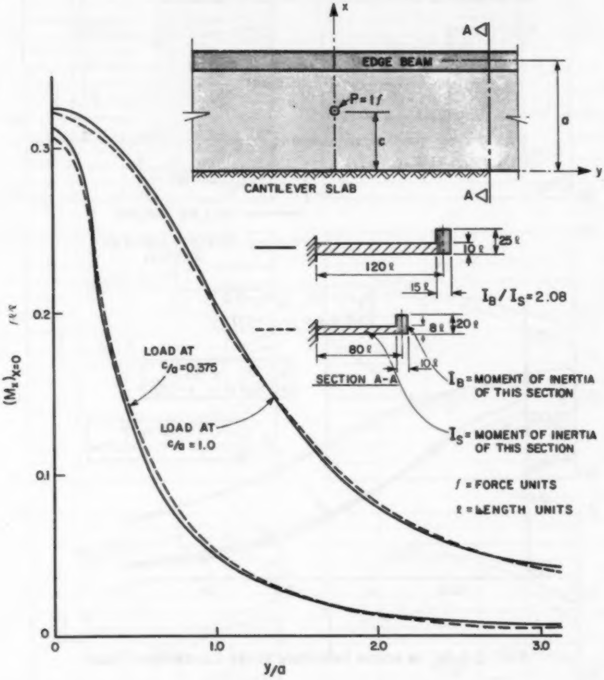

FIG. 4.—M_x in Edge Stiffened Cantilever Slabs

respectively; and D = the flexural rigidity of the slab per unit length. Denoting Da by EI_s Eqs. 2 and 3 can be written as

$$k_1 = \frac{I_B}{I_S} \quad \text{(4)}$$

$$k_2 = \frac{G}{E}\frac{J_S}{I_S} \qquad (5)$$

in which I_S = the moment of inertia of the longitudinal section of the slab about its middle surface.

Reismann and Cheng (7) show that the behavior of an edge reinforced slab is affected mainly by k_1 and that changes in k_2 have relatively little effect on the manner in which deflections and longitudinal moments are distributed. For example, they show that in a very wide cantilever slab of uniform thickness

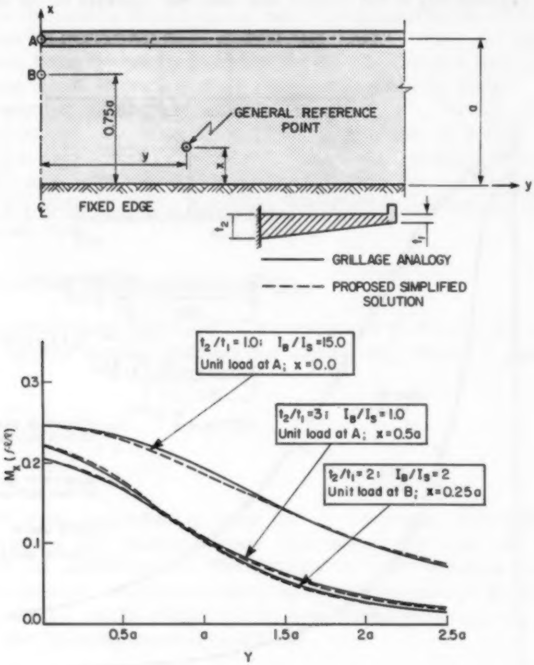

FIG. 5.—M_x in some Infinitely Wide Cantilever Slabs

the maximum longitudinal moment at the cantilever root due to a concentrated load on the free edge increase by only 0.34% due to a 400% increase in k_2. It seemed reasonable to delete k_2 from consideration and assume that the load distribution behavior of a very wide cantilever slab can be characterized by only k_1. Later calculations, which are not reported in this paper, justified this assumption.

Fig. 4 demonstrates that k_1 is one of the parameters characterizing the distribution of longitudinal moments in edge stiffened cantilever slabs; it shows

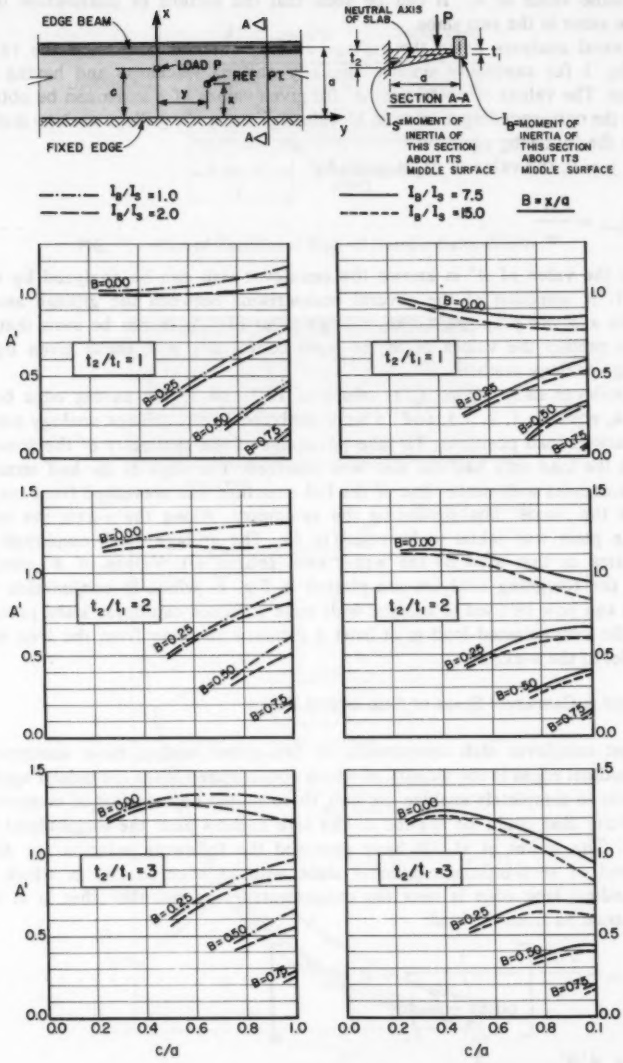

FIG. 6.—Values of Coefficient *A'*

the distribution of M_x in cantilever slabs of different dimensions but having the same value of k_1. It can be seen that the pattern of distribution of M_x is the same in the two slabs.

Several analyses using the grillage analogy method confirmed the validity of Eq. 1 for cantilever slabs of linearly varying thickness and having edge beams. The values of coefficient A' for given values of c and x can be obtained from the corresponding maximum M_x values given by the grillage analogy method, from the following equation:

At $y = 0$, the value of M_x is given by

$$(M_x)_{y=0} = \frac{PA'}{\pi} \quad \ldots\ldots\ldots\ldots\ldots\ldots\ldots\ldots\ldots\ldots\ldots\ldots\ldots\ldots\ldots\ldots (6)$$

Once the value of A' is known the cantilever slab can be analyzed by using Eq. 1. A selection of the several comparisons between the grillage analogy results and the proposed solution is given in Fig. 5. It can be seen that Eq. 1 can predict the values of M_x in close conformity with those given by the grillage analogy method.

Cantilever slabs having t_2/t_1 values of 1, 2 and 3, and having edge beams with k_1 equal to 1, 2, 7.5, and 15 were analyzed by the grillage analogy method for various load positions. To take advantage of the symmetry of the structure about the load only half the slab was analyzed. The edge of the half structure that coincides with center line of the full structure was prevented from rotating about the x-axis thus simulating the symmetry. Along the y-axis the length of the plate was taken to be equal to $4a$. The grillage mesh employed was the same as that used by the writer and Holland (3). Values of A' obtained from the foregoing analyses are plotted in Fig. 6, which in conjunction with Eq. 1 can now be used to analyze wide edge stiffened cantilever slabs provided that the concentrated load is at least a distance $3a$ away from the free edges parallel to the x-axis.

Moment in Cantilever Slabs of Semi-Infinite Width

Most cantilever slab components of box-girder bridges have unsupported longitudinal edges in the vicinity of which concentrated loads are indeed applied. In order to completely analyze the slab, there should be a method of comparable simplicity that could be applied to the slab regions near the longitudinal free edges. The writer et al. (2) have provided the following solution for M_x at the root of semi-infinite cantilever slabs without edge beams, in which one longitudinal free edge is near the concentrated load but the other is at least a distance $3a$ from the load:

$$(M_x)_{x=0} = \frac{PA'}{\pi}\left[\frac{1}{\cosh\left(\frac{A'y}{c}\right)} + B'e^{(-K\bar{y}/a)}\right] \quad \ldots\ldots\ldots\ldots\ldots\ldots (7)$$

$$K = \frac{a}{c}\,\frac{A'B'}{2}\,\frac{1}{\tan^{-1}\left[e^{(-A'd/c)}\right]} \quad \ldots\ldots\ldots\ldots\ldots\ldots\ldots\ldots\ldots\ldots\ldots\ldots (8)$$

in which A' = the same coefficient as that for infinitely wide cantilever slabs,

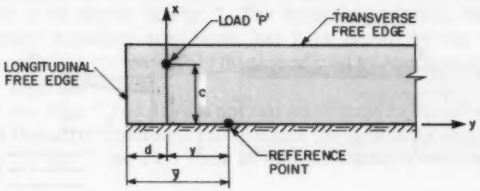

FIG. 7.—Plan of Cantilever Slab of Semi-Infinite Width

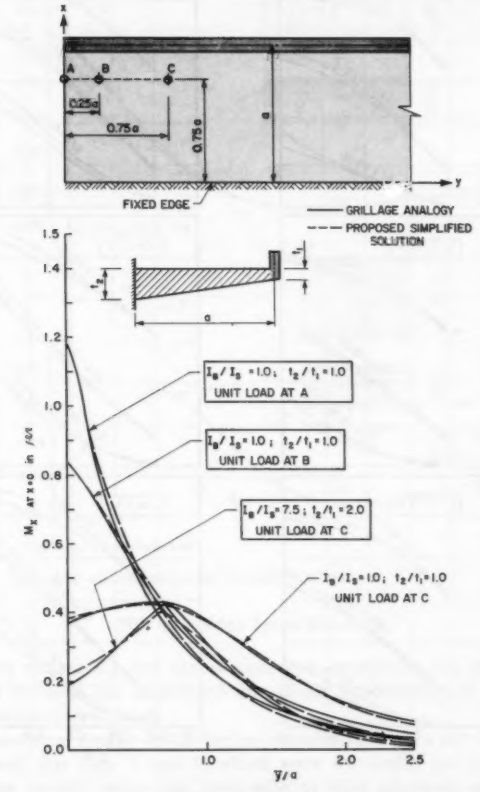

FIG. 8.—M_x in some Semi-Infinite Cantilever Slabs

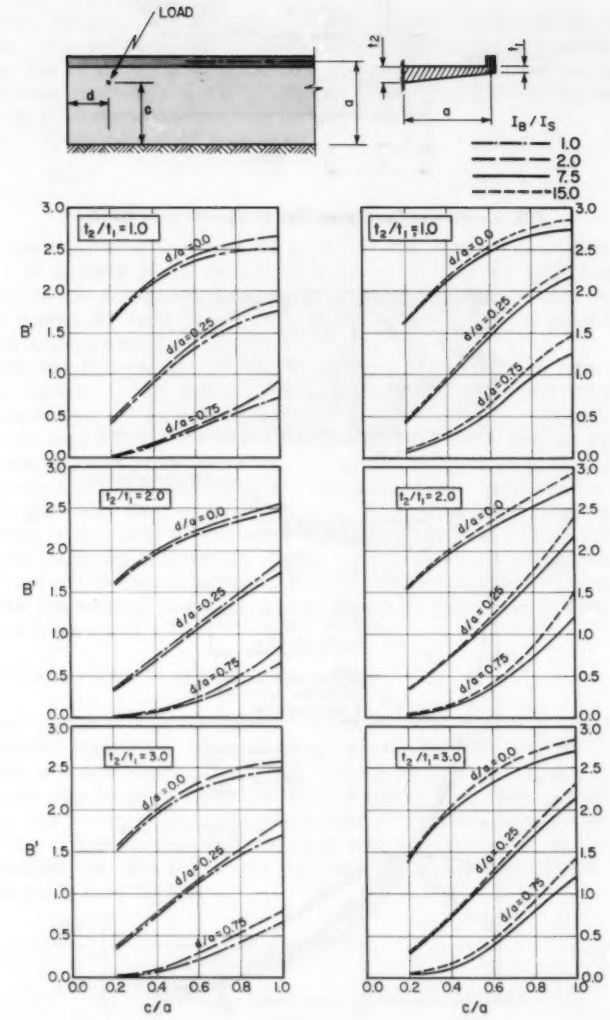

FIG. 9.—Values of Coefficient B'

examined earlier; B' = a coefficient which depends upon t_2/t_1 and the load position with respect to a longitudinal free edge and the transverse free edge; other notation is as shown in Fig. 7. The foregoing solution, which satisfies all the necessary boundary conditions, has been shown by the writer, et al. (2) to provide solutions comparable to those predicted by computer based rigorous linear elastic methods.

It is noted that Eqs. 7 and 8 were not rationally derived but chosen to satisfy the necessary boundary conditions and to match the rigorously obtained solutions most closely. In Eq. 7 the first term in the parenthesis provides solution for

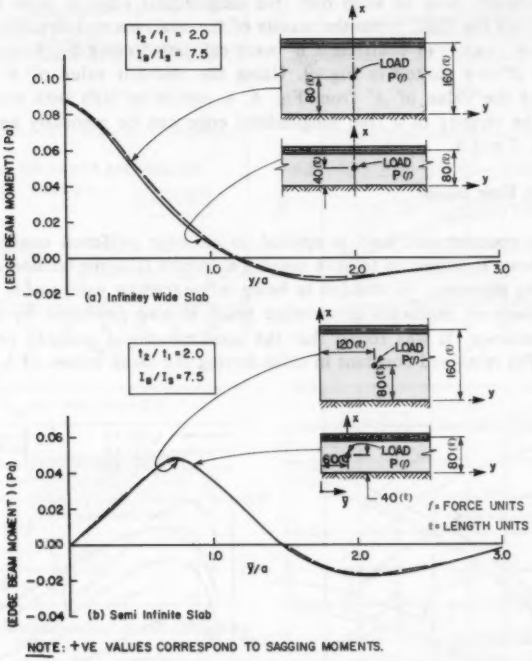

FIG. 10.—Edge Beam Moments

the infinitely wide plate and the second term represents the increase in the longitudinal moment that is induced due to the introduction of a longitudinal cut in the infinitely wide slab.

Several analyses, similar to the earlier examined analyses for wide cantilever slabs, showed that Eqs. 7 and 8, which were developed for cantilever slabs without edge beams, were also applicable to edge stiffened cantilever slabs with a good degree of accuracy. A selection of comparisons between the grillage analogy results and those obtained by Eqs. 7 and 8 is given in Fig. 8. For $\bar{y} = 0$, rearranging Eq. 7

$$B' = \frac{(\pi M_x)_{x=0;\,y=d}}{PA'} - \frac{1}{\cosh\left(\frac{A'd}{c}\right)} \quad \ldots\ldots\ldots\ldots\ldots\ldots\ldots\ldots\ldots\ldots (9)$$

Thus from known values of M_x at the cantilever root at the longitudinal free edge and A', the value of B' can be obtained from Eq. 9.

A large number of edge stiffened cantilever slabs, having various values of k_1 and t_2/t_1, were analyzed for different load positions in the vicinity of one of the longitudinal free edges. The length of the slabs along the y-axis was kept sufficiently long to keep one free longitudinal edge at least a distance $3a$ away from the load. From the results of the analyses and already developed values of A', values of coefficient B' were calculated using Eq. 9; the resulting values of B' are plotted in Fig. 9. Using the relevant value of B' from the graphs and the value of A' from Fig. 6, a cantilever slab with concentrated loads in the vicinity of a free longitudinal edge can be manually analyzed by using Eqs. 7 and 8.

Moments in Edge Beams

When a concentrated load is applied to an edge stiffened cantilever slab, the edge beam is subjected to both sagging moments (causing tension at bottom) and hogging moments. In addition to being influenced by values of k_1 and t_2/t_1, the magnitude of moments in an edge beam is also governed by the length of the cantilever. It was found that the nondimensional quantity (edge beam moment/Pa) remained constant in slabs having the same values of k_1 and t_2/t_1

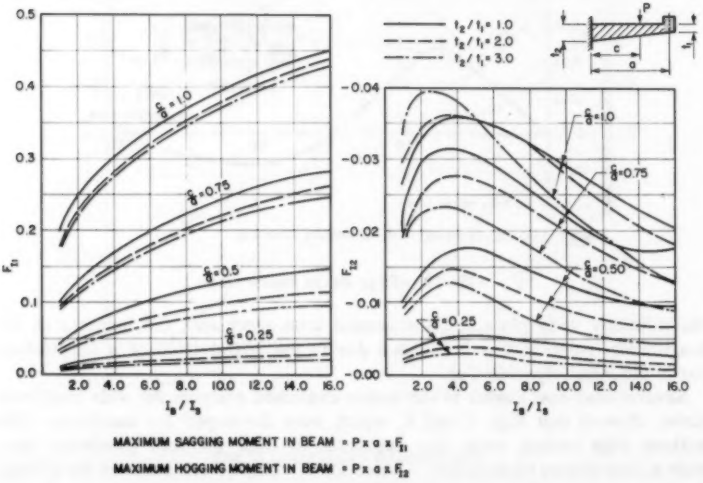

FIG. 11.—Values of Coefficients F_{f1} and F_{f2}

but different lengths. Fig. 10(*a*) shows the distribution of (edge beam moment/*Pa*) in two cantilever slabs of infinite extent. Both slabs have $t_2/t_1 = 2.0$ and $k_1 = 7.5$, but one slab has a cantilever length of 80 units and the other of 160 units.

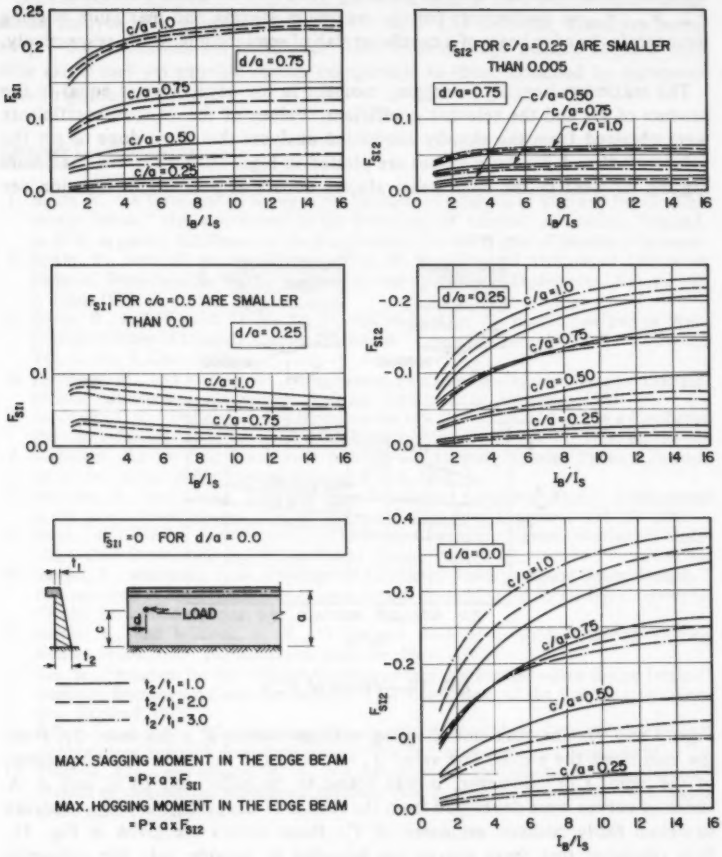

FIG. 12.—Values of Coefficients F_{SI1} and F_{SI2}

It can be seen that inspite of the large difference in the cantilever length the manner of distribution of edge beam moments is very nearly the same in the two cases. The foregoing exercise was repeated for cantilever slabs of semi-infinite extent. Again it was found, as shown in Fig. 10(*b*), that the nondimensional quantity (edge beam moment/*Pa*) was the same in the two

cases. It was concluded that the maximum edge beam moments could be obtained using the following nondimensional coefficients:

1. F_{I1}, F_{I2} = coefficients for the maximum sagging and maximum hogging moments in the edge beam of an infinitely wide cantilever slab, respectively.
2. F_{SI1}, F_{SI2} = coefficients for the maximum sagging and maximum hogging moments in the edge beam of a cantilever slab of semi-infinite width, respectively.

The maximum hogging or sagging moment in the edge beam is equal to the product of Pa and the relevant coefficient. Values of the various coefficients were obtained from the already conducted analyses that were done to get the values of A' and B'; these values are plotted in Figs. 11 and 12. The maximum sagging moment in the edge beam always occurs at $y = 0$ (for notation see

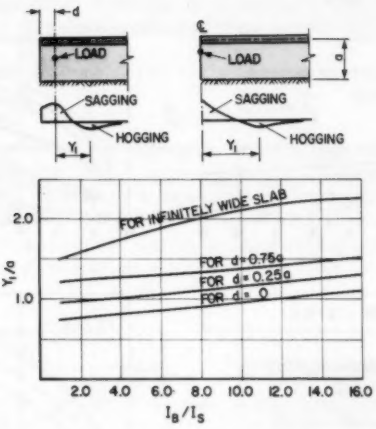

FIG. 13.—Values of Y_1/a

Figs. 3 and 7). The maximum hogging moment occurs at a distance, Y_1, from the load along the y-axis. The value Y_1 was found to be relatively independent of the ratio, t_2/t_1; however, it was found to be influenced by k_1 and d. A series of curves were developed from the results of the grillage analogy analyses to obtain fairly realistic estimates of Y_1; these curves are given in Fig. 13. It is reminded that these curves are intended to provide only fair estimates with an accuracy of about $\pm 10\%$, and not exact values of Y_1.

Conclusions

In edge stiffened cantilever slabs the longitudinal moments anywhere in the slab can be obtained by Eq. 1 in conjunction with Fig. 6, if the concentrated load is at least a distance $3a$ away from both the longitudinal free edges. When the concentrated load is in the vicinity of a longitudinal free edge the longitudinal

moments along the cantilever root can be obtained by Eqs. 7 and 8 in conjunction with Figs. 6 and 9. Locations and values of maximum moments in edge stiffened cantilever slabs of infinite and semi-infinite width can be obtained with the help of Figs. 11, 12 and 13.

Simplified semigraphical method for manual application are presented for linear elastic analysis of edge stiffened cantilever slabs. The methods, which are based on previous solutions for cantilever slabs without edge beams, require very little effort and yet provide results comparable to those obtained by computer based rigorous methods.

Appendix I.—References

1. Bakht, B., "A Comparative Study of the Methods of Analysis of Slab and Pseudo-Slab Bridge Decks," thesis presented to the University of London, at London, England, in 1972, in partial fullfillment of the requirements for the degree of Master of Science.
2. Bakht, B., Aziz, T. A., and Bartusevicius, K. F., "Manual Analysis of Cantilever Slabs of Semi-Infinite Width," *Canadian Journal of Civil Engineering,* Vol. 6, No. 2, June, 1979.
3. Bakht, B., and Holland, D. A., "A Manual Method for the Elastic Analysis of Wide Cantilever Slabs of Linearly Varying Thickness," *Canadian Journal of Civil Engineering,* Vol. 3, No. 4, Dec., 1976.
4. Homberg, H., and Ropers, W., *Kragplatten. Beidseitiz Einzepannte Platten Dreifeld-platten Verschiedener Stutzweiten,* Springer Verlag, Berlin, Germany, 1965.
5. Jaramillo, T. J., "Deflections and Moments due to a Concentrated Load on a Cantilever Plate of Infinite Length," *Journal of the Applied Mechanics,* Vol. 77, 1950, pp. 69–72.
6. Lightfoot, E., "A Grid Framework Analogy for Laterally Loaded Plates," *Journal of the Institution of Mechanical Science,* Vol. 6, 1964.
7. Reisman, H., and Cheng, S., "The Edge Reinforced Cantilever Strip," *Publications of the International Association for Bridge and Structural Engineers,* Vol. 30, 1970.
8. Sawko, F., "Bridge Deck Analysis—Electronic Computers Versus Distribution Methods," *Civil Engineering and Public Works Review,* Apr., 1965.
9. Sawko, F., and Mills, J. H., "Design of Cantilever Slabs for Spine Beam Bridges," *Developments in Bridge Design and Construction, Proceedings of the Cardiff Conference,* Crosby Lockwood and Son Ltd., London, England.
10. Sawko, F., and Wilcock, B. K., "Computer Analysis of Bridges having Varying Section Properties," *The Structural Engineer,* Nov., 1967.
11. Sen, R., "Program for the Grillage Analysis of Slab and Pseudo—Slab Bridge Decks," *Highway Engineering Computer Branch/B/9,* Department of the Environment, London, England, 1975.
12. Silberstein, J. P. O., "The Infinitely Wide Cantilever Plate Under Concentrated Load," *Aeronautical Research Laboratory Report SM.257,* Melbourne, Australia, 1959.
13. Yettram, A. L., and Husain, M. H., "Grid-Framework Method for Plates in Flexure," *Journal of Engineering Mechanics Division,* ASCE, Vol. 91, No. EM3, Proc. Paper 4361, June, 1965, pp. 53–64.

Appendix II.—Notation

The following symbols are used in this paper:

A' = dimensionless constant defined by Eq. 1 and obtained from Fig. 6;
a = length of cantilever slab measured perpendicular to supported edge;
B' = dimensionless constant defined by Eq. 7 and obtained from Fig. 9;
C = distance of concentrated load from supported edge measured along x-axis;

D = flexural rigidity of slab per unit length;
d = distance of concentrated load from longitudinal free edge, measured along y-axis as shown in Fig. 7;
E = modulus of elasticity;
F_{I1}, F_{I2} = coefficient for maximum sagging and maximum hogging moments in edge beam of an infinitely wide cantilever slab, respectively;
F_{SI}, F_{SI2} = coefficients for maximum sagging and maximum hogging moment in edge beam of cantilever slab of semi-infinite width, respectively;
G = shear modulus;
I = moment of inertia of grillage beam;
I_B = moment of inertia of edge beam;
I_S = moment of inertia of longitudinal section of slab about its middle surface;
J = torsional inertia of grillage beam;
J_B = torsional inertia of edge beam;
J_S = torsional inertia of longitudinal section of slab;
K = coefficient defined by Eq. 8;
k_1 = ratio of flexural rigidities of edge beam and cantilever slab;
k_2 = ratio of torsional rigidities of edge beam and cantilever slab;
M_x = longitudinal moment per unit width;
P = intensity of concentrated load;
t_1 = slab thickness at free edge;
t_2 = slab thickness at supported edge;
x = distance measured perpendicular to and from supported edge;
Y_1 = distance of maximum hogging moment from concentrated load, measured along y-axis;
y = distance measured along supported edge from concentrated load; and
$\bar{y}$ = distance measured along supported edge from longitudinal free edge, as shown in Fig. 7.

JOURNAL OF THE STRUCTURAL DIVISION

EXPERIMENTAL EVALUATION OF COMPOSITE ACTION

By Rafik Y. Itani,[1] M. ASCE, Houssain M. Morshed,[2] and Robert J. Hoyle,[3] M. ASCE

INTRODUCTION

Diaphragms are common and economical structural systems for resisting lateral forces that develop from wind and earthquake. A typical diaphragm consists of several layers of beam elements that are bonded together by shear connectors. Loadings act in the plane of the diaphragm. The system is highly indeterminate and its analysis is complex (Fig. 1).

The layers in a diaphragm are connected together by shear connectors. The "shear connector system" may be nails, glue, bolts, screws, welded spots, or shear clips. Regardless of the shear connector used, the connector deforms when the diaphragm is loaded and allows the layers to slip. Thus a partial composite action between the layers is developed.

The design of diaphragms is a complex problem and, at present, employs empirical methods which are based on experience and testing.

The first writer and Hiremath (8) presented a theoretical method for the analysis of diaphragms. The method develops a set of differential equations for the analysis of a multilayer diaphragm. The solution to these equations was obtained using a finite difference method. The study, however, did not present experimental verification of results.

Almost all the lumber diaphragms will have courses containing members of different lengths to make up the full length of the diaphragm. This causes discontinuities in the courses. In addition, diaphragms may have boundary members, with effects not included in the theory that has been presented by the first writer and Hiremath (8).

The purpose of this paper is to present an experimental comparison with

[1]Assoc. Prof., Dept. of Civ. and Environmental Engrg., Washington State Univ., Pullman, Wash. 99164.

[2]Grad. Student, Dept. of Civ. and Environmental Engrg., Washington State Univ., Pullman, Wash. 99164.

[3]Prof., Wood Tech. Section, Washington State Univ., Pullman, Wash. 99164.

Note.—Discussion open until August 1, 1981. To extend the closing date one month, a written request must be filed with the Manager of Technical and Professional Publications, ASCE. Manuscript was submitted for review for possible publication on July 24, 1980. This paper is part of the Journal of the Structural Division, Proceedings of the American Society of Civil Engineers, ©ASCE, Vol. 107, No. ST3, March, 1981. ISSN 0044-8001/81/0003-0551/$01.00.

the theoretical procedure in Ref. 8. This is accomplished by constructing a lumber diaphragm without any discontinuities or boundary members and subjecting it to a uniform loading. Axial strains in the different layers and deflection at the midspan are measured.

A second objective of this study is to observe the effects of discontinuities and boundary members on diaphragm behavior. It is evident that the discontinuities in the layers will permit increased deflection and strain, while the boundary members will reduce these effects. Magnitudes of these effects are evaluated from this experimental study.

The third objective is to evaluate the effect of connecting joists to the diaphragm with glue. This will develop resisting couples that will add to the stiffness and strength of the diaphragm.

Literature Review

A brief review of the major previous development leading to the study of diaphragms is presented here. The study of diaphragms with layers can be

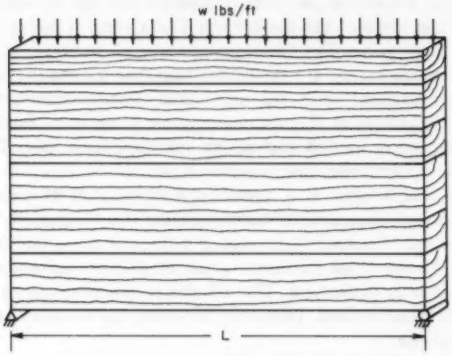

FIG. 1.—Typical Diaphragm System

classified broadly in the area of partial composite action or incomplete interaction between structural components.

The basis of theoretical study in the area of incomplete interaction is the pioneering work of Newmark (13) in 1951, who studied the incomplete interaction of a composite T-beam having a concrete deck connected to a steel I-beam by shear connectors. He formulated a second-order differential equation to express the relationship between the interlayer slip and the longitudinal force in each element of the T-beam. A few years later, Clark (2) reported his study on laminated beams where he employed the moment-area method to compute the deflection of a beam with two or more laminations. Goodman (4) extensively studied the interlayer slip problem involving layered systems.

The third writer and McGee (7), using the same type of differential equation as Newmark, analyzed wooden T-beams consisting of wood joist and deck connected with elastomeric adhesives. They considered a concentrated load

at any point on the beam and a distributed load. For these loading conditions they obtained the closed form solution of this system. Using the superposition method, solutions for other types of load are possible. Similar solutions were also reported by Vanderbilt (15). Expansion of the foregoing approach to a three-layer system subjected to a uniformly distributed load was done by Anderson (1). The first writer and Brito (9) developed a closed form solution for a two-layer system with gaps in one layer. The interlayer slip in this study is applicable to both adhesive bonds and mechanical connector links if the compliance relationships can be determined. The only difference is that in the case of adhesives the width and thickness of the glueline must be accounted for while the mechanical connectors the spacing must be considered.

As the number of layers becomes greater than three, it becomes very difficult to use a closed-form solution. Finite difference and finite element techniques may be used. Ko (12) applied a finite difference technique to solve the governing equations for composite beams having an axis of symmetry and arbitrary number of layers fastened together with mechanical connectors. Foschi (3) developed a computer program to analyze a plywood diaphragm using finite element techniques. His study accounted for the orthotropic plate action and nonlinear connection behavior. The analysis gives good estimates for the deformation of diaphragms and ultimate loads related to connection yielding. The first writer and Hiremath (8) extended the three-layer system solution developed by Anderson (1) to a system with an arbitrary number of layers using a finite difference to solve the equations.

Diaphragms for floor and roof construction have been tested by the Forest Research Laboratory at Oregon State University, the American Plywood Association, and the United States Forest Products Laboratory to develop data for the design of buildings. Wood diaphragms are usually sheathed with either plywood or lumber. Johnson (10) tested two diaphragms 20 in. × 60 in. in the year 1968. One used nailed connections only and the other employed nails and elastomeric adhesive to provide additional strength. He found that the roof section with adhesive was several times as stiff as a similar roof section without adhesive. The diaphragm with adhesive sustained three times the maximum load of the nailed system. He also made some openings in the diaphragms and studied the effect on performance. He found deflection increased due to the openings in the glued diaphragms and the recovery of the diaphragm after the release of this load was retarded. Later Johnson tested four more diaphragms of the same size (11). One of these was 100% glued, the second one was 50% glued, the third one was 100% mechanically fastened, and the fourth one was 50% mechanically fastened. The fasteners were shear clips. It was found that maximum loads for roof sections with 100% shear clips or adhesive were about 1.6 times greater than maximum loads for corresponding roofs with 50% shear clips or adhesive. Diaphragms with shear clips were about 15% stronger than those with the elastomeric adhesive used in this study. All four roof sections were two or three times as strong as a simple nailed diaphragm with neither shear clips nor adhesive (this result would be greatly affected by frequency of nailing and nail size). He also found that shrinkage of wood due to change of moisture content caused about 2% of the total length of glue line to be cracked. This directs attention to a problem in glue systems which merits some consideration.

THEORY

A brief review of the theory presented by the first writer and Hiremath (8) is examined next.

The partial composite action at an interface of connected layers develops a shear force. This shear force can be represented (refer to Fig. 2) by a couple acting at the centroids of the two layers. The sum of the moments acting on the two layers is given by:

$$M_j + M_k = M - F_{jk}(C_j + C_k) \quad \ldots\ldots\ldots\ldots\ldots\ldots\ldots\ldots\ldots\ldots (1)$$

in which M_j and M_k = moments in layers, j and k, respectively; M = the external moment at a section in the beam; F_{jk} = the shearing force acting

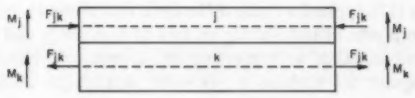

FIG. 2.—Analysis Model for Two Layer Diaphragm System

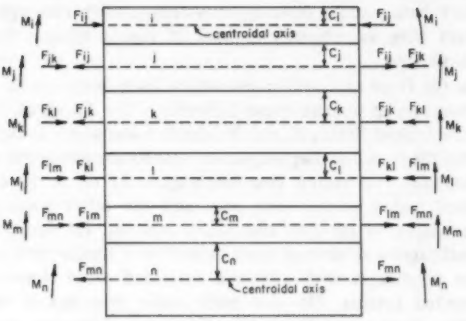

FIG. 3.—Analysis Model for Multilayer Diaphragm System

between layers, j and k; and C_j and C_k = the extreme fiber distances from the centroids of layers, j and k, respectively.

The preceding approach to two-layer systems can be extended to include multilayer systems. Referring to Fig. 3, the slip between connected layers gives rise to the forces shown. The strain at the bottom of layer, j, ϵ_{jb}, is given by:

$$\epsilon_{jb} = \frac{-(F_{jk} - F_{ij})}{E_j A_j} + \frac{M_j C_j}{E_j I_j} \quad \ldots\ldots\ldots\ldots\ldots\ldots\ldots\ldots\ldots\ldots (2)$$

in which E_j, = the elastic modulus; A_j, = cross-sectional area; and I_j = moment of inertia of layer, j.

Similarly the strain in the top fibers of layer, k, can be written as:

$$\epsilon_{kt} = \frac{-(F_{kl} - F_{jk})}{E_k A_k} - \frac{M_k C_k}{E_k I_k} \quad \ldots\ldots\ldots\ldots\ldots\ldots\ldots\ldots\ldots\ldots\ldots\ldots (3)$$

The rate of change of slip between layers, j and k, along the length of the diaphragm is given by the difference of strains in Eqs. 2 and 3. Thus:

$$\frac{1}{S}\frac{d^2F_{jk}}{dx^2} = \epsilon_{kt} - \epsilon_{jb} \quad \ldots\ldots\ldots\ldots\ldots\ldots\ldots\ldots\ldots\ldots\ldots\ldots (4)$$

in which S = the stiffness of glue line which is a function of the modulus of rigidity, thickness, and width of glue.

Upon substituting Eqs. 2 and 3 into Eq. 4 the following is obtained:

$$\frac{1}{S}\frac{d^2F_{jk}}{dx^2} = F_{ij}\left(\frac{-1}{E_jA_j}\right) + F_{jk}\left(\frac{1}{E_jA_j} + \frac{1}{E_kA_k}\right)$$

$$+ F_{kl}\left(\frac{-1}{E_kA_k}\right) - \left(\frac{M_jC_j}{E_jI_j} + \frac{M_kC_k}{E_kI_k}\right) \quad \ldots\ldots\ldots\ldots\ldots\ldots\ldots\ldots (5)$$

Assuming that each layer is bent to the same curvature and upon substituting the values of M_j and M_k in terms of all couples into Eq. 5, an expression is obtained relating the rate of change of slip along the length of the diaphragm and the shear forces. This procedure is repeated for each glue line to obtain the following:

$$\begin{Bmatrix} \frac{1}{S}\frac{d^2F_{ij}}{dx^2} \\ \frac{1}{S}\frac{d^2F_{jk}}{dx^2} \\ \vdots \\ \vdots \\ \frac{1}{S}\frac{d^2F_{mn}}{dx^2} \end{Bmatrix} = [K]_{n-1,n-1} \begin{Bmatrix} F_{ij} \\ F_{jk} \\ \vdots \\ \vdots \\ F_{mn} \end{Bmatrix} - \frac{M}{\sum_{i=1}^{n} E_iI_i} \begin{bmatrix} C_i + C_j \\ C_j + C_k \\ \vdots \\ \vdots \\ C_m + C_n \end{bmatrix} \quad \ldots\ldots\ldots\ldots (6)$$

in which $\mathbf{K}$ = the symmetric coefficient matrix which is a function of E, I, A, and C of each layer; and n = the number of layers in the diaphragm.

Eq. 6 contains systems of second-order linear differential equations that must be solved simultaneously at any given point in the beam to determine shear forces between adjacent layers. Once shear forces are determined, the moments and stresses in each of the layers are obtained.

Experimental Setup and Procedure

Because of the expense associated with the construction and instrumentation of a lumber diaphragm, only one was tested. The test was carefully conducted

and measurements of various component properties were obtained.

The test diaphragm (Fig. 4) was 15 ft (4.57 m) long and 5 ft (1.52 m) wide. It consisted of 31 layers that were glued with Scotch-Grip Wood Adhesive No. 5230. The size of each layer was 1/2 in. × 1.5 in. (12.7 mm × 38.3 mm).

Eleven 7/8-in. × 3-1/4-in. (22.2-mm × 82.5-mm) joists were used at spacings of 1.5 ft (0.46 m) on center. These joists provided the overall lateral stability of the diaphragm. Each joist was approx 5 ft (1.52 m) long.

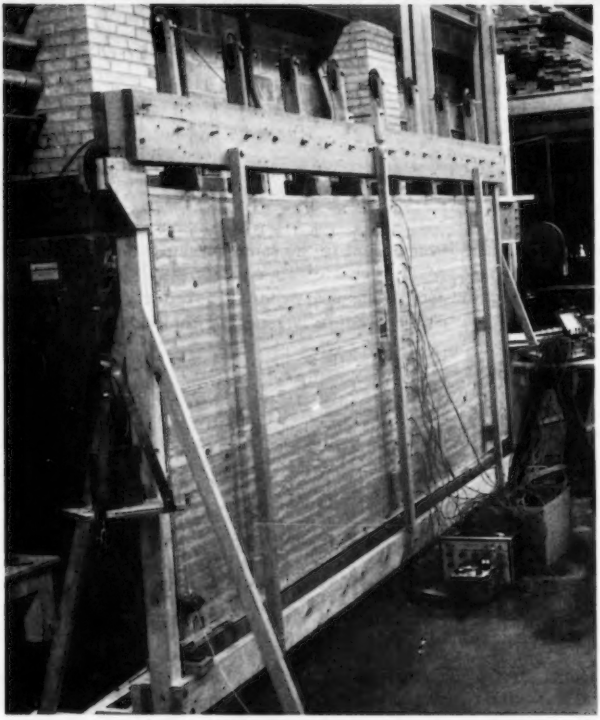

FIG. 4.—Quarter Scale Model of 60 ft × 20 ft Diaphragm

The 15-ft long lumber layers were installed starting from one end of the joists. Each layer was nailed at its center to each joist. Before placing the next layer, nails of approx 0.09-in. (2.3-mm) diam were placed to act as glue line spacing shims to keep the glue line thickness constant (Fig. 5). Glue was then applied using a cartridge applicator and the next layer was placed and nailed to the joists. All the layers were placed in the same manner. After the glue was cured, any excess glue outside the plane of the diaphragm was taken

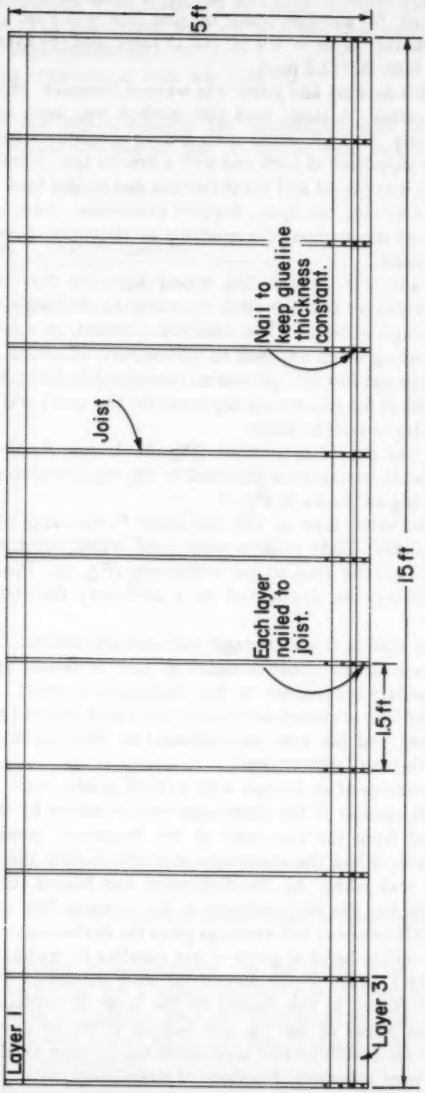

FIG. 5.—Construction of Model Diaphragm

off by using a chisel. The final dimensions of the diaphragm are: (1) Length = 15 ft (4.5 m); (2) width = 5 ft (1.5 m); (3) average thickness of glue line = 0.09 in. (2.3 mm); (4) average width of glue line = 0.5 in. (12.7 mm); (5) average width of lumber layer = 1.9 in. (48.25 mm); and (6) average thickness of lumber layer = 0.48 in. (12.2 mm).

The wood used for decking and joists was western hemlock. Moisture content was about 12% average. A static load test method was used to measure the modulus of elasticity of each wood strip before diaphragm assembly. Each piece of wood was supported at each end with a known span length. At midspan a small known load was placed and the deflection due to that load was measured with a dial gage. Knowing the span, support conditions, load, deflection and moment of inertia of the section, the modulus of elasticity, E, was calculated for each piece of wood.

An elastomeric adhesive, Scotch-Grip Wood Adhesive No. 5230, was used for bonding the diaphragm to resist shear between the decking boards and thus increase the diaphragm stiffness. The adhesive contains no solvent and cures without much shrinking when exposed to atmospheric moisture. The resulting seal is water resistant and flexible, yet retains considerable strength and stiffness.

The shear modulus of the adhesive is important for this study and was measured by testing 30 samples in double shear.

The diaphragm was placed in a frame (Fig. 4). It was simply supported at both ends. Some guide beams were provided in the test frame to prevent lateral deflection or buckling as shown in Fig. 4.

A uniformly distributed load of 200 lbs/linear ft was applied by a system of weights and pulleys. Eight pulleys were used which were equally spaced and transferred the gravity load to the diaphragm (Fig. 4). These small equal concentrated loads may be considered as a uniformly distributed load with negligible error.

Before taking any reading, the diaphragm was loaded to 200 lbs/ft and unloaded 10 times. The reason is that shear modulus of glue decreases up to 10 cycles of loading (6). Loads were applied to the diaphragm in steps. Increments of load of 50 lbs/linear ft were chosen arbitrarily. After each increment was reached, readings were taken and the load was released to zero again. The load was then increased to the next greater load.

Deflection was measured by a scale with 1/32-in graduations. The scale was fixed at the middle section of the diaphragm with a mirror by its side. A taut cord was stretched from the two ends of the diaphragm passing across the scale and the mirror. When the diaphragm was not loaded, the reading of the cord on the scale was taken. As the diaphragm was loaded, the scale moves with the diaphragm but the cord remains in its position. The scale is read at each load and the difference of two readings gives the deflection of the diaphragm for that load. The mirror helps to prevent any parallax in reading.

Strains at different layers of the diaphragm were measured by strain gages. Strain gages were placed at the middle of the layer to measure the average strain. Because the strain at the top and bottom fibers of any layer are not the same, strain at the middle of that layer gives the average axial strain. Strains at alternate layers were measured. Positions of strain gages across the diaphragms are shown in Fig. 6.

To analyze the diaphragm analytically, the slip modulus, S, defined by S

$= Gb/t$, is needed. Here, G is the shear modulus of glue, b and t are the width and thickness of glue line, respectively. The actual slip modulus of glue lines of the diaphragm were measured by taking double shear specimens from the diaphragm. The diaphragm was cut and the specimens were taken after all other tests were completed.

The following sequence of tests was conducted:

1. The first test was conducted for comparison with the results obtained from the theoretical analysis of Ref. 8. In the first test, the diaphragm had

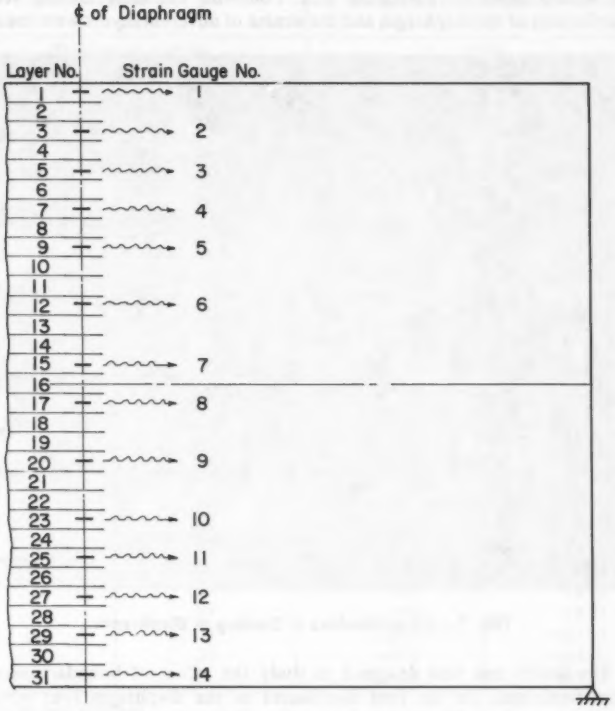

FIG. 6.—Positions of Strain Gages in Diaphragm

no boundary members or discontinuities in the layers. Each decking layer was connected to each joist by a single nail so that no resisting moment could develop. This is in accordance with the theoretical method presented in Ref. 8. The diaphragm was loaded up to 200 lbs/ft and the readings of deflection and axial strain were recorded.

2. The second test measured the realistic effect of discontinuous layers. The same diaphragm was used for the second test. The layers of the diaphragm

were cut transversely with a sabre saw, to produce an end joint pattern typical of real diaphragms (Fig. 7). The lengths of different pieces in the courses of lumber decking were selected using the limitations of selecting random lengths described in the American Institute of Timber Construction (AITC) Standard 112-65 found in Ref. 14. The diaphragm was loaded and readings of deflection and strains were made.

3. The third test was done to study the effect of gluing the joists to the deck courses on the deflection and strains of the diaphragm. The same diaphragm was used for the third test. The joists were glued with the same glue. Thirty days were allowed for curing the glue. Following the same loading sequence the deflection of the diaphragm and the strains of different layers were measured.

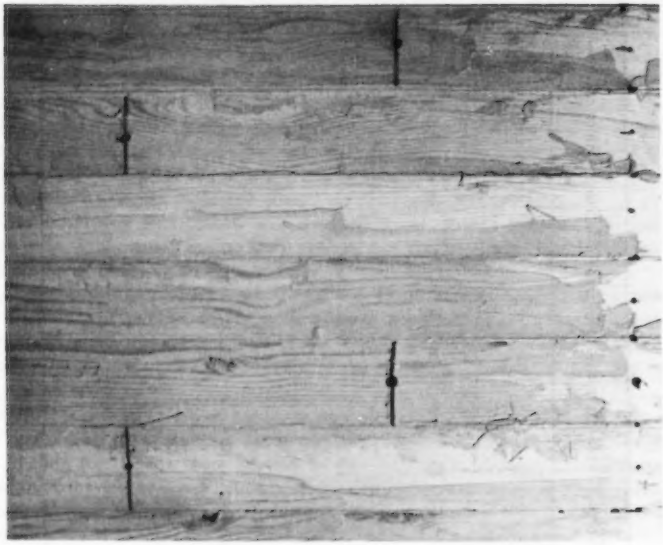

FIG. 7.—Discontinuities in Decking of Diaphragm

4. The fourth test was designed to study the effect of boundary members on the diaphragm. At the four boundaries of the diaphragm four boundary members were glued. Thirty days were allowed for glue cure before testing.

Results

In addition to the analytical results, four different sets of experimental results were obtained from this study. All of these results consist of strains at different layers of the diaphragm and deflection at midspan.

The first set consists of results obtained from the theoretical analysis of the diaphragm, using the computer program DAD—Difference Analysis of Diaphragms (5). The computer program does not account for any discontinuity

in the decking of the diaphragm and does not account for any effect from the joists or boundary members.

The second set of results was obtained from the test of the diaphragm model. The diaphragm for this test had no discontinuity in its decking and no boundary members. The joists in the diaphragm were not structurally connected to the

TABLE 1.—Deflection Obtained from Theoretical Analysis and Model Test

Variable (1)	Deflection at mid-span in inches (2)
Theoretical analysis	0.815
Model test	0.735

Note: Loading is 200 lb/ft uniformly distributed; 1 lb = 4.448 N; 1 in. = 25.4 mm.

TABLE 2.—Strains at Different Layers Obtained from Theoretical Analysis and Model Test

Gage number (1)	Layer number in diaphragm starting from top (total number of layers in 31) (2)	Theoretical analysis strain, in micro inch per inch (3)	Model test strain, in micro inch per inch (4)
1	1	−330.7	−288.23
2	3	−66.4	−73.67
3	5	−13.9	−9.50
4	7	−2.7	[a]
5	9	−0.5	−7.83
6	12	0	+2.50
7	15	+0.1	+0.0
8	17	+0.1	+7.33
9	20	+0.1	+21.17
10	23	+0.6	+8.50
11	25	+3.0	+5.67
12	27	+14.5	+27.17
13	29	+67.9	+64.50
14	31	+334.8	293.33

[a]No reading obtained.

Note: Positive strain indicates tension; Loading is 200 lb/ft length; 1 lb = 4.448 N; 1 in. = 25.4 mm.

diaphragm (one nail was driven at the intersection of each joist and deck course). This model had identical properties to the diaphragm analyzed theoretically.

The third set of results was obtained by testing the model with discontinuities in its layers. The comparison between the second and third set of results shows the effect of discontinuities in the layers of a diaphragm.

The fourth set of results was obtained by testing the model with discontinuities

in its layers and with the joists glued to the decking, thus developing resisting couples.

The fifth set of results was obtained by testing the diaphragm with boundary members on all of its four sides. Boundary members were 0.5 in. × 1.9 in. in cross section.

The comparison of the fourth and fifth sets with the third set shows the effects of joists and boundary members on the diaphragm behavior.

Tables 1 and 2 show the first and second result sets. These tables indicate that theoretical and experiment results are in reasonable agreement. The theoreti-

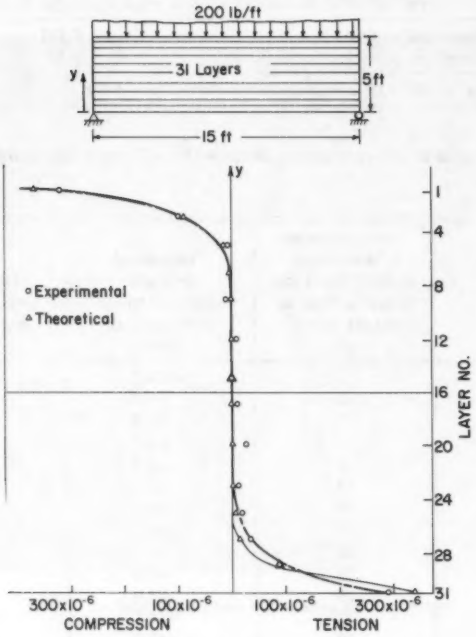

FIG. 8.—Strain Distribution in Diaphragm

cal analysis overestimates deflections and axial strains in the critical outer layers. The deflection obtained by the theoretical analysis is about 10% more than the experimental value. Outer layer strains obtained by theoretical analysis are 14% greater than experimental strains. Strain distribution pattern was almost identical in both cases (Fig. 8).

The reason for this discrepancy is that the theory, in its development, does not account for the effect of joists. The joists were nailed to the decking. It was assumed that the joists act like stiffeners in a plate girder and distribute load to the layers as well as prevent buckling. However, for a lumber diaphragm

where the courses of decking slip with respect to each other, the joists develop some resisting moment. In other words, the joists oppose the interlayer slip of the decking and make it stiffer than the theory assumes. As a result the

TABLE 3.—Deflections Obtained from Model Tests for Various Conditions

Type of diaphragm (1)	Deflection at midspan, in inches (2)
Diaphragm without any discontinuity in its layers	0.73
Diaphragm having discontinuous layers	0.78
Diaphragm having joists glued	0.64
Diaphragm having glued joists and boundary members	0.63

Note: Loading is 200 lb/ft; 1 lb = 4.448 N; 1 in. = 25.4 mm.

TABLE 4.—Strains at Different Layers, Obtained from Model Tests for Various Conditions

Gage number (1)	Layer number from top (2)	Diaphgram with continuous layers strain, in micro inch per inch (3)	Diaphgram with discontinuous layers strain, in micro inch per inch (4)	Diaphgram with glued joists strain, in micro inch per inch (5)	Diaphgram with boundary members glued strain, in micro inch per inch (6)
1	1 (top)	−288.23	−322.14	−320.03	−180.73
2	3	−73.67	−21.33	−13.67	−2.25
3	5	−9.50	−2.50	−0.83	[a]
4	7	[a]	−6.0	−2.17	[a]
5	9	−7.83	−17.17	−16.83	0
6	12	+2.50	+5.0	0	0
7	15	+0.0	−8.0	0	0
8	17	+7.33	+6.83	0	0
9	20	+21.17	+18.33	0	0
10	23	+8.50	[a]	[a]	[a]
11	25	+5.67	+13.33	+11.33	+4.5
12	27	+27.17	+31.83	+26.5	+14.25
13	28	+64.5	+65.83	+59.0	+20.0
14	31 (bottom)	+293.33	+350.17	+339.67	+163.0

[a]No reading obtained.

Note: Positive strain indicated tension; Loading is 200 lb/ft length; 1 lb = 4.448 N; 1 in. = 25.4 mm.

joists reduce the deflection of the diaphragm. They also affect the strain distribution, reducing the outer layer strains and increasing the inner layer strains.

The average modulus of elasticity of a layer was measured. In actuality the modulus of elasticity of a wood layer varies along its length. The experimental

strains are local strains while theoretical strains are average values. This is another source of error which can be further evaluated with additional tests.

Tables 3 and 4 show the second, third, fourth and fifth set of results. These tables compare the effect of discontinuities in the layers and the effect of joists and boundary members. They also show the deflection of the diaphragm increases about 6% and the outer layer stresses increase about 15% due to the discontinuity in its layers.

The effect of discontinuities is not very significant. When the joists were glued to the decking, the deflection of the diaphragm was reduced about 18% (Table 3). The change in strain was insignificant (Table 4). These are important observations for the designer, and were less than expected.

The effects of boundary members on the deflection of the diaphragm was insignificant but it reduced the outer layer strain by about 50% (Tables 3, 4).

The reduction of the outer layer strains is due to the fact that boundary members become the outer layers of the diaphragm and change the outer layers to inner layers.

There is no significant stiffness gain from the addition of boundary layers and it should be possible to compute their effect on deflections by incorporating them into the analysis as additional layers. The small effect of the boundary members may seem unusual since they are usually considered very important in conventional plywood sheathed diaphragm design. Their small effect is due to the fact that the boundary members were not large, especially when compared to the size of the lumber deck members. This is a special feature of thick lumber diaphragms. In plywood sheathed diaphragms, the relatively large boundary members contribute more to the overall performance.

Conclusions

The experiment verified the theoretical analysis of a diaphragm in a satisfactory manner. The study also defined the effects of different structural features of the diaphragm. From this study the following conclusions may be drawn:

1. The theoretical analysis of the diaphragm over estimates strains and deflections because it does not account for the effects of joists in the diaphragm.
2. Presence of discontinuities in layers of a glued lumber diaphragm does not have a considerable significance.
3. Gluing the joists to the decking of a lumber diaphragm reduces deflections, but has little effect on strains in each layer.
4. Addition of boundary members does not have significant effect on the deflection of a parallel course lumber diaphragm for members of the size used in this study. Larger boundary members might have a greater effect, but probably boundary members contribute less to diaphragm performance for glued lumber diaphragms than would be the case for nailed plywood diaphragms.
5. Additional testing of diaphragms is needed to reach more conclusive results.

Appendix I.—References

1. Anderson, M., "Behavior of Wood Beams Bonded with an Elastomeric Adhesive," thesis presented to Washington State University, at Pullman, Wash., in 1976, in partial

fulfillment of the requirements for the degree of Master of Science.
2. Clark, L. G., "Deflection of Laminated Beams," *Transactions*, ASCE, Vol. 119, Proc. Paper 2694, 1954, pp. 721–736.
3. Foschi, R. O., "Analysis of Wood Diaphragms and Trusses—Part I: Diaphragms," *Canadian Journal of Civil Engineering*, Vol. 4, No. 3, 1977.
4. Goodman, J. R., and Popov, E. R., "Layered Beam Systems with Interlayer Slip," *Journal of the Structural Division*, ASCE, Vol. 94 No. ST11, Proc. Paper 6214, Nov., 1968, pp. 2535–2547.
5. Hiremath, G. S., "Analysis of Composite Action in Lumber Diaphragms," thesis presented to Washington State University, at Pullman, Wash., in 1979, in partial fullfillment of the requirements for the degree of Master of Science.
6. Hoyle, R. J., and Hsu, J. K., "Shear Strength and Shear Modulus of an Elastomeric Adhesive Subjected to Repeated Stress," *Wood Science*, Vol. 11, No. 2, 1978.
7. Hoyle, R. J., and McGee, D. W., "Design Methods for Elastomeric Adhesive Bonded Joist-Deck System," *Wood Fiber*, Vol. 6, No. 2, 1974.
8. Itani, R. Y., and Hiremath, G. S., "Partial Composite Action in Diaphragms," *Journal of the Engineering Mechanics Division*, ASCE, Vol. 106, No. EM4, Proc. Paper 15624, Aug., 1980, pp. 739–752.
9. Itani, R. Y., and Brito, F. A., "Elastomeric Bonded Wood Beams with Transverse Gaps," *Journal of Structural Division*, ASCE, Vol. 104, No. ST10, Proc. Paper 14095, Oct., 1978, pp. 1595–1609.
10. Johnson, J. W., "Roof Diaphragms with 3-in Decking, Effect of Adhesive and Openings," *Report T-25*, Forest Research Laboratory, School of Forestry, Oregon State University, Corvallis, Oreg., July, 1968.
11. Johnson, J. W., "Lateral Tests of Wood Roof Sections Sheathed with Lodgepole Pine Decking," *Forest Products Journal*, Vol. 29, No. 1, 1979.
12. Ko, M. F., "Layered Beam System with Interlayer Slip," thesis presented to Colorado State University, at Fort Collins, Colo., in 1972, in partial fullfillment of the requirements for the degree of Master of Science.
13. Newmark, N. M., Siess, D. P., and Viest, I. M., "Tests and Analysis of Composite Beams with Incomplete Interaction," *Proceedings, Society for Experimental Stress Analysis*, Vol. 19, No. 1, 1951.
14. *Timber Construction Manual*, American Institute of Timber Construction, John Wiley and Sons, Inc., New York, N.Y., 1974.
15. Vanderbilt, M. D., Goodman, J. R., and Criswell, M. E., "Service and Overload Behavior of Wood Joist Floor System," *Journal of the Structural Division*, ASCE, Vol. 100, No. ST1, Proc. Paper 10274, Jan., 1974, pp. 11–29.

Appendix II.—Notation

The following symbols are used in this paper:

A_i = cross section area of layer i;
C_i = distance from centroidal axis of layer i to extreme fibers of that layer ($i = 1, 2 \ldots n$);
E_i = modulus of elasticity of layer i ($i = 1, 2 \ldots n$);
F_{ij} = force between layers i and j;
I_i = moment of inertia of layer i ($i = 1, 2 \ldots n$);
k = coefficient matrix;
M = external moment;
M_i = internal moment of layer i ($i = 1, 2 \ldots n$);
n = total number of layers;
S_{ij} = shear connected stiffness between layer i and j;
y = deflection;
ϵ = strain; and
σ = stress.

JOURNAL OF THE
STRUCTURAL DIVISION

TECHNICAL NOTES

Note.—Discussion open until August 1, 1981. To extend the closing date one month, a written request must be filed with the Manager of Technical and Professional Publications, ASCE. This paper is part of the Journal of the Structural Division, Proceedings of the American Society of Civil Engineers, ©ASCE, Vol. 107, No. ST3, March, 1981.

Technical Notes

To provide a place within ASCE for publication of technical ideas that have not advanced, as yet, to the point where they warrant publication as a Proceedings paper in a *Journal*, the publication of Technical Notes was authorized by the Board of Direction on October 16–18, 1967, under the following guidelines:

1. An original manuscript and two copies are to be submitted to the Manager of Technical and Professional Publications, ASCE, 345 East 47th Street, New York, N.Y., 10017, along with a request by the author that it be considered as a Technical Note.
2. The two copies will be sent to an appropriate Technical Division or Council for review.
3. If the Division or Council approves the contribution for publication, it shall be returned to Society Headquarters with appropriate comments.
4. The technical publications staff will prepare the material for use in the earliest possible issue of the *Journal*, after proper coordination with the author.
5. Each Technical Note is not to exceed 4 pages in the *Journal*. As an approximation, each full manuscript page of text, tables, or figures is the equivalent of one-half a *Journal* page.
6. The Technical Notes will be grouped in a special section of each *Journal*.
7. Information retrieval abstracts and key words will be unnecessary for Technical Notes.
8. The final date on which a Discussion should reach the Society is given as a footnote with each Technical Note.
9. Technical Notes will not be included in *Transactions*.
10. Technical Notes will be included in ASCE's annual and cumulative subject and author indexes.

The manuscripts for Technical Notes must meet the following requirements:

1. Titles must have a length not exceeding 50 characters and spaces.
2. The author's full name, Society membership grade, and a footnote reference stating present employment must appear on the first page of the manuscript. Authors need not be Society members.
3. The manuscript is to be submitted as an original copy (with two duplicates) that is typed double-spaced on one side of 8-1/2-in. (220-mm) by 11-in. (280-mm) white bond paper.
4. All mathematics must be typewritten and special symbols must be properly identified. The letter symbols used must be defined where they first appear, in figures or text, and arranged alphabetically in an Appendix.—Notation.
5. Standard definitions and symbols must be used. Reference must be made to the lists published by the American National Standards Institute and to the *Authors' Guide to the Publications of ASCE*.
6. Tables must be typed double-spaced (an original ribbon copy and two duplicate copies) on one side of 8-1/2-in. (220-mm) by 11-in. (280-mm) paper. An explanation of each table must appear in the text.
7. Figures must be drawn in black ink on one side of 8-1/2-in. (220-mm) by 11-in. (280-mm) paper. Because figures will be reproduced with a width of between 3 in. (76 mm) to 4-1/2 in. (110 mm), the lettering must be large enough to be legible at this width. Photographs must be submitted as glossy prints. Explanations and descriptions must be made within the text for each figure.
8. References cited in text must be typed at the end of the Technical Note in alphabetical order in an Appendix.—References.
9. Dual units, i.e., U.S. Customary followed by SI (International System) units in parentheses, should be used throughout the paper.

Effect of Bowing on Rectangular Plane Frames

By Alfred Korn,[1] M. ASCE

Introduction

When a member is subjected to bending, there is a shortening of the chord length, as shown in Fig. 1. This change in length has been called bowing deformation or curvature shortening. Researchers in the area of inelastic frame analysis continue to debate the merits of including bowing in second-order analyses (1). There are structural configurations for which a thorough nonlinear analysis, including bowing effects, is necessary to describe structural response. But, is bowing so small in comparison to axial deformation that the effect is negligible in changing rectangular frame response?

The purpose of this paper is to present results of frame analyses that allow the reader to compare the magnitude of bowing and axial deformation, and to examine the influence of bowing in altering structural response at service and collapse load level (4). The analyses are based on second-order elastic-plastic analysis (beam-column rotational and translational stiffness with allowance for the formation of plastic hinges). In addition, axial deformation and bowing are included (4,5).

Bowing

The change in chord length, δ_b, caused by bending is shown in Fig. 1. Bowing deformation is evaluated by the following formula (3,7):

$$\delta_b = \frac{1}{2}\int_0^L \left(\frac{dy}{dx}\right)^2 dx \quad \ldots\ldots\ldots\ldots\ldots\ldots\ldots\ldots\ldots\ldots\ldots\ldots\ldots\ldots (1)$$

The mathematical expressions for δ_b have been presented by several authors (e.g., see Ref. 6). The expressions used herein are shown in Appendix I as a function of end moments, M_1 and M_2, axial load, P, original member length, L, and bending stiffness, EI.

For the case of a central lateral load, F, bowing is evaluated by parts (see Fig. 2). The reduced chord lengths, $K_1L/2$ and $K_2L/2$, are computed by separate

[1]Prof. of Civ. Engrg., School of Sci. and Tech., Dept. of Engrg. and Tech., Sci. Building, Southern Illinois Univ. at Edwardsville, Edwardsville, Ill. 62026.

Note.—Discussion open until August 1, 1981. To extend the closing date one month, a written request must be filed with the Manager of Technical and Professional Publications, ASCE. Manuscript was submitted for review for possible publication on July 8, 1980. This paper is part of the Journal of the Structural Division, Proceedings of the American Society of Civil Engineers, ©ASCE, Vol. 107, No. ST3, March, 1981. ISSN 0044-8001/81/0003-0569/$01.00.

bowing analyses. Denoting the angle of inclination of the subchords to the main chord as ψ, the overall bowing deformation is given by

$$\frac{\delta_b}{L} = 1 - \left(\frac{K_1 + K_2}{2}\right)\cos\psi \quad \ldots\ldots\ldots\ldots\ldots\ldots\ldots\ldots\ldots\ldots\ldots\ldots\ldots\ldots (2a)$$

$$\approx 1 - \left(\frac{K_1 + K_2}{2}\right)\left(1 - \frac{\psi^2}{2}\right) \quad \ldots\ldots\ldots\ldots\ldots\ldots\ldots\ldots\ldots\ldots\ldots\ldots\ldots\ldots (2b)$$

The aforementioned formulation is also valid for the case of a plastic hinge at either end or at the load point.

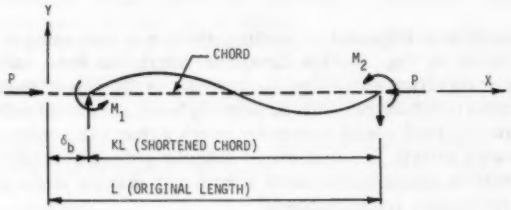

FIG. 1.—Bowing

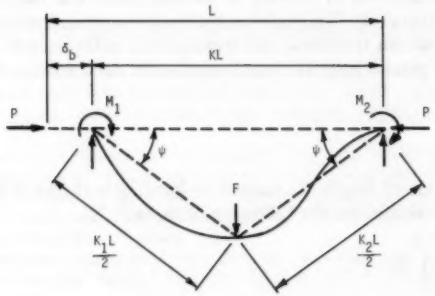

FIG. 2.—Bowing by Parts

Note that bowing deformation is dependent on the squares of member slopes. Accordingly, the use of small deflection assumptions for ψ seem inappropriate in an analysis considering bowing. However, when bowing deformation, δ_b, is compared to deformation caused by axial load, δ_a, the relative magnitude of terms can only be judged by examining typical frame analyses.

Frame Analysis Results

Several single-bay, multistory frames have been analyzed up to collapse (both with and without the consideration of bowing) (4). Thus, it is possible to compare

the magnitude of bowing deformations with axial deformations at service and collapse load level. Also, it is possible to examine how much the collapse capacity and overall frame deformations are influenced by bowing.

The results of all of the analyses are well represented by the behavior of the four-story frame shown in Fig. 3. The frame is a "weak-beam, strong-column" design suggested by Horne and Majid (2). The frame was proportionally loaded up to collapse. Thus, any load level is represented by a load factor, λ, ranging from unity at service loads up to the collapse load factor. The complete history of load, deformation, and plastic hinging was recorded (4). The summary of member shortenings (δ_a, axial, and δ_b bowing) are shown in nondimensional form in Table 1.

Behavior at Service Loads, $\lambda = 1$.—For the imposed loading, the columns tend to be bent into double curvature, while transversely loaded girders have a much higher contribution of single curvature. With reference to Eq. 4, Appendix

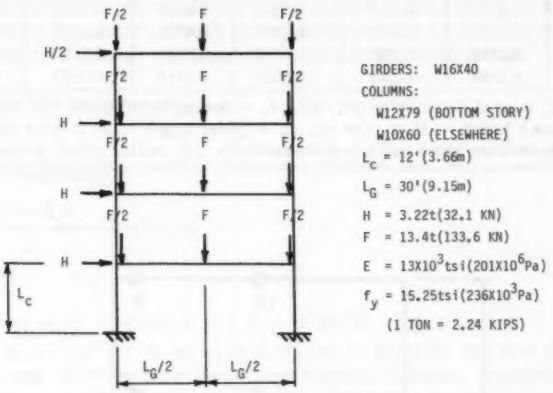

FIG. 3.—Frame, Properties, Service Loads

I, it can be shown that for equal forces the ratio of bowing deformation for double curvature is never more than a fifteenth of the bowing for single curvature. Thus, δ_b/L_g for the girders should be higher than δ_b/L_c for the columns. Also, it is known that the columns have the larger axial strains. Both observations were verified by the results: (1) The axial deformations in the columns was generally two orders of magnitude higher than the bowing in the columns; and (2) the bowing and axial deformations in the girders were of the same order of magnitude. Even when both bowing and axial deformations are considered, the total nondimensional shortening of any girder was less than that for the least compressed column. Realizing that axial deformation is secondary to bending, the bowing effects at service load are clearly negligible.

Behavior at Collapse Loads, $\lambda = 1.499$.—The order of plastic hinge formation is shown in Fig. 4. Failure occurred by instability prior to the formation of a complete collapse mechanism. Each girder had developed plastic hinges at

TABLE 1.—Member Shortenings

Story (1)	Left-Side Column		Girder		Right-Side Column	
	$\frac{\delta_a}{L_c} \times 10^3$ (2)	$\frac{\delta_b}{L_c} \times 10^3$ (3)	$\frac{\delta_a}{L_g} \times 10^3$ (4)	$\frac{\delta_b}{L_g} \times 10^3$ (5)	$\frac{\delta_a}{L_c} \times 10^3$ (6)	$\frac{\delta_b}{L_c} \times 10^3$ (7)
(*a*) Service Loads, $\lambda = 1$						
Top	0.0559	0.0004	0.0420	0.0100	0.0608	0.0012
3	0.1081	0.0002	−0.0036	0.0065	0.1252	0.0006
2	0.1557	0.0000	0.0119	0.0083	0.1942	0.0010
Bottom	0.1541	0.0013	0.0066	0.0080	0.2006	0.0007
(*b*) Collapse Loads, $\lambda = 1.499$						
Top	0.0777	0.0017	0.0592	0.0236	0.0972	0.0100
3	0.1553	0.0051	−0.0070	0.0746	0.1945	0.0040
2	0.2330	0.0015	0.0164	0.2685	0.2917	0.0032
Bottom	0.2360	0.0163	0.0027	0.1517	0.2957	0.0075

Note: δ_a = axial deformation (PL/EA); δ_b = bowing deformation (see Appendix I); L_c = column length = 12 ft (3.66 m); L_g = girder length = 30 ft (9.15 m); and δ_a, δ_b are positive when chord length is shortened.

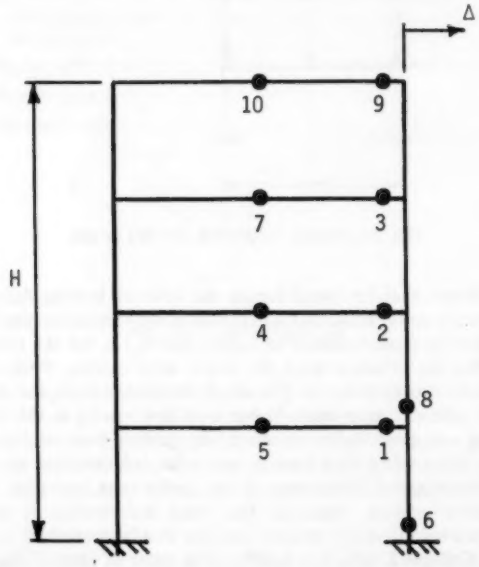

FIG. 4.—Frame at Collapse Load Level (Numbers Indicate Order of Hinge Formation)

the center and right end, and earlier formed hinges in the bottom two stories had time to develop appreciable rotations. Now, bowing terms predominate for the girder, and are of the same order of magnitude as the larger axial shortenings in the columns. Bowing deformations of the columns were negligible.

The only time that bowing deformation was appreciable was when plastic hinges developed at midspan, and had undergone rotation. Yet, the result of such deformation on the overall frame behavior was negligible at collapse! The collapse load factor, λ, changed by only 0.001 (from 1.498–1.499) when bowing was considered. The top sway to height ratio, Δ/h, was 0.0160. When bowing deformations were also included, the ratio changed by 0.0001.

Conclusions

The results obtained for the four-story frame were typical for all frames analyzed. The state of deformation at collapse is still sufficiently small, so that the basic mode of frame behavior predicted by simplified models is adequate. This computer experiment, though limited in scope, does support the contention that bowing deformations are negligible in rectangular planar frames.

Appendix I.—Bowing Formulas

The bowing deformation, δ_b, shown in Fig. 1, has been evaluated by the following formulas (4):

$$\frac{\delta_b}{L} = \frac{\dfrac{(m_1^2 + m_2^2)c_1}{2} + (m_1 m_2)c_2}{2c_3} \quad \ldots\ldots\ldots\ldots\ldots\ldots\ldots\ldots\ldots\ldots (3)$$

in which $c_1 = \phi^2 + \phi \sin \phi \cos \phi - 2 \sin^2 \phi$; $c_2 = \phi^2 \cos \phi + \phi \sin \phi - 2 \sin^2 \phi$; $c_3 = \phi^4 \sin^2 \phi$; $m_1 = M_1 L/EI$; $m_2 = M_2 L/EI$; and $\phi = L\sqrt{P/EI}$ where L and EI = member length and bending stiffness, respectively. The bending moments, M_1 and M_2, are positive if they are counterclockwise. The stability factor, ϕ, is a function of axial load, and is always positive. The aforementioned expressions are for compressive axial load. In the case of tension, hyperbolic functions replace the trigonometric functions.

For small axial load ($0 \leq \phi \leq 0.5$), the following series expressions are accurate to about 1/50th of a percent:

$$\frac{\delta_b}{L} = (m_1^2 + m_2^2)c_4 + (m_1 m_2)c_5 \quad \ldots\ldots\ldots\ldots\ldots\ldots\ldots\ldots\ldots\ldots (4a)$$

$$\text{in which} \quad c_4 = \frac{1}{90}\left(\frac{1 \pm \phi^2/7 + \phi^4/105}{1 \pm \phi^2/3 + 2\phi^4/45}\right) \quad \ldots\ldots\ldots\ldots\ldots\ldots (4b)$$

$$\text{and} \quad c_5 = -\frac{7}{360}\left(\frac{1 \pm 6\phi^2/49 + 11\phi^4/1{,}680}{1 \pm \phi^2/3 + 2\phi^4/45}\right) \quad \ldots\ldots\ldots\ldots\ldots\ldots (4c)$$

Where dual signs are shown, the positive sign applies for tensile axial load and the negative sign for compressive axial load.

Appendix II.—References

1. Birnstiel, C., and Iffland, J. S. B., "Factors Influencing Frame Stability," *Journal of the Structural Division*, ASCE, Vol. 106, No. ST2, Proc. Paper 15196, Feb., 1980, pp. 491–504.
2. Horne, M. R., and Majid, K. I., "Elastic-Plastic Design of Rigid Jointed Sway Frames by Computer," 1st Report, Study of Analytical and Design Procedures for Elastic and Elastic-Plastic Structures, University of Manchester, Manchester, England, Mar., 1966.
3. Horne, M. R., and Merchant, W., "The Stability of Frames," Pergamon Press, Inc., New York, N.Y., 1965, p. 12.
4. Korn, A., "The Elastic-Plastic Behavior of Multi-Story, Unbraced Planar Frames," thesis presented to Washington University, at St. Louis, Mo., in 1967, in partial fulfillment of the requirements for the degree of Doctor of Science.
5. Korn, A., and Galambos, T. V., "Behavior of Elastic-Plastic Frames," *Journal of the Structural Division*, ASCE, Vol. 94, No. ST5, Proc. Paper 5942, May, 1968, pp. 1119–1142.
6. Massonnet, C. E., "European Approaches to P-Δ Method of Design," *Journal of the Structural Division*, ASCE, Vol. 104, No. ST1, Proc. Paper 13454, Jan., 1978, pp. 193–198.
7. Timoshenko, S. P., and Gere, J. M., "Theory of Elastic Stability," 2nd ed., McGraw Hill Book Co., Inc., New York, N.Y., 1961, p. 28.

JOURNAL OF THE
STRUCTURAL DIVISION

DISCUSSION

Note.—This paper is part of the Journal of the Structural Division, Proceedings of the American Society of Civil Engineers. ©ASCE, Vol. 107, No. ST3, March, 1981. ISSN 0044-8001/81/0003-0577/$01.00.

Discussions

Discussions may be submitted on any Proceedings paper or technical note published in any *Journal* or on any paper presented at any Specialty Conference or other meeting, the *Proceedings* of which have been published by ASCE. Discussion of a paper/technical note is open to anyone who has significant comments or questions regarding the content of the paper/technical note. Discussions are accepted for a period of 4 months following the date of publication of a paper/technical note and they should be sent to the Manager of Technical and Professional Publications, ASCE, 345 East 47th Street, New York, N.Y. 10017. The discussion period may be extended by a written request from a discusser.

The original and three copies of the Discussion should be submitted on 8-1/2-in. (220-mm) by 11-in. (280-mm) white bond paper, typed double-spaced with wide margins. The length of a Discussion is restricted to two *Journal* pages (about four typewritten double-spaced pages of manuscript including figures and tables); the editors will delete matter extraneous to the subject under discussion. If a Discussion is over two pages long it will be returned for shortening. All Discussions will be reviewed by the editors and the Division's or Council's Publications Committees. In some cases, Discussions will be returned to discussers for rewriting, or they may be encouraged to submit a paper or technical note rather than a Discussion.

Standards for Discussions are the same as those for Proceedings Papers. A Discussion is subject to rejection if it contains matter readily found elsewhere, advocates special interests, is carelessly prepared, controverts established fact, is purely speculative, introduces personalities, or is foreign to the purposes of the Society. All Discussions should be written in the third person, and the discusser should use the term "the writer" when referring to himself. The author of the original paper/technical note is referred to as "the author."

Discussions have a specific format. The title of the original paper/technical note appears at the top of the first page with a superscript that corresponds to a footnote indicating the month, year, author(s), and number of the original paper/technical note. The discusser's full name should be indicated below the title (see Discussions herein as an example) together with his ASCE membership grade (if applicable).

The discusser's title, company affiliation, and business address should appear on the first page of the manuscript, along with the *Proceedings* paper number of the original paper/technical note, the date and name of the *Journal* in which it appeared, and the original author's name.

Note that the discusser's identification footnote should follow consecutively from the original paper/technical note. If the paper/technical note under discussion contained footnote numbers 1 and 2, the first Discussion would begin with footnote 3, and subsequent Discussions would continue in sequence.

Figures supplied by the discusser should be designated by letters, starting with A. This also applies separately to tables and references. In referring to a figure, table, or reference that appeared in the original paper/technical note use the same number used in the original.

It is suggested that potential discussers request a copy of the *ASCE Authors' Guide to the Publications of ASCE* for more detailed information on preparation and submission of manuscripts.

Model for Mild Steel in Inelastic Frame Analysis[a]

Closure by T. K. Santhanam[4]

The writer thanks Jain and Hays for their enlightening discussion. Jain's observations are answered here first. The subject matter of the paper forms only a part of the writer's more general work (17), and the strut inelastic behavior is one of the examples chosen for presentation. Thus not all the literature on strut modeling has been included. A few of the papers mentioned by Jain are quoted in Ref. 17. A few others are of almost contemporary period.

The convergence difficulty mentioned in the paper was specific to the type of discrete element (6,17), and not due to formation of plastic hinge at midspan. At the interior of each discrete element plastification is monitored at two cross sections. Thus when the kink is positioned exactly at midspan, two plastic hinges are formed, due to symmetry, close to the midspan, one in each of the two discrete elements on either side.

This can be overcome by defining a "rigid" or "linear" behavior for one of these two discrete elements. Such a procedure has been used by Harung and Millar (42) to overcome a mathematical singularity resulting from the simultaneous formation of two plastic hinges at a structural node where two members with equal plastic properties meet. This will, to some extent, affect the accuracy of the predicted deformations and therefore was not adopted. Adoption of the noncentral kink was used as a better contrivance. There are the other class of discrete elements where plastification occurs at the junction of two elements. In such models, the kink can be positioned at midspan. The writer wishes to add that considerable number of days were spent in trying to debug, before the aforementioned phenomenon of two simultaneous hinges was spotted as the cause of convergence failure. Refs. 7 and 38 contain the remedial measures that can be adopted to overcome convergence difficulties due to inelastic material behavior. Ref. 17 contains an example of convergence failure of a strut inelastic analysis due to the combined effect of geometric nonlinearity and the method of discretization. The problem here is the kink originally input to simulate imperfection is removed due to inelastic reversals. The subsequent analyses are thus made closer to the difficult problem of buckling of perfect structures.

Jain quotes Kaldjian and Fan (30) on the closeness of the results obtained by Ramberg-Osgood and elasto-plastic moment-curvature models. This is not surprising. The Ramberg-Osgood moment-curvature relation for a cross section was derived from a Ramberg-Osgood representation of the stress-strain relation. This accounts only for the gradual plastification across the depth of the section, as against the abrupt transition inherent in the ideally elastic-perfectly plastic

[a]January, 1979, by T. K. Santhanam (Proc. Paper 14333).

[4]Scientist, Structural Engrg. Research (Regional) Centre, CSIR Campus, Adyar, Madras-600020, India.

moment-curvature relation. The more important effect of the strain-hardening of mild steel is not accounted in such a procedure unless the Ramberg-Osgood algorithm is modified and enhanced, for example, as done by Eisenberg (41). The normal Ramberg-Osgood model and the multilinear representation of the Masing model (7,38) may be said to be equivalent. The advantage of the latter is that other types of stress-strain, or in general, force-deformation behaviors, such as shown in Table 1 for example, can be easily incorporated. The improved model of Eisenberg encompasses a wider area including multi-axial states of stress.

The writer does not wholly agree with Jain's conclusion on the proposed stress-strain model. Inelastic modeling techniques are necessarily computationally expensive, and thus, are not to be directly adopted for analysing large structural systems. Some of the alternatives adopted in dealing with such structures are to restrict the material model sophistications to a small region and use finer mesh size, or adopt condensation techniques to separate regions requiring more rigorous treatment. In either of these a good apriori knowledge of the location of the probable influential zone in the structure is needed. In dynamic analyses, if not in static analyses, such guesses are difficult to make, and a wrong judgement can lead to a significant wasted effort. The writer proposes a third approach wherein a lower-order macro-analysis of the entire structure is performed first, and a subsequent more sophisticated micro analysis of one or two selected smaller segments are carried out for further detailed study, e.g., on ductility requirements, etc. The boundary conditions, including their history, at the cutoff nodes defining the smaller segment can be obtained from the historical displacements, accelerations etc. of the macro-analysis stored on a tape. This treatment differs from the usually understood substructure analysis in that it is based on hindsight and not dependent on foresight.

A program such as FRAME 63 can be successfully used to analyze moderately sized structural segments of about 20–25 joints and 15–20 inelastic members, though the total number of members can be more (43). Noting the organization of the computations wherein the member inelastic analyses are isolated from the global analysis of the structural nodes (6,17), a structural segment of about a total of 3,000 degrees of freedom–4,000 degrees of freedom can be realistically solved. The band width is greatly reduced compared to that of a frontal solution of a similar structure. Schrem (44) considers such a structure to be of decent size for an inelastic analysis though not for a linear elastic analysis. The writer has found that the simpler elasto-plastic model predicts very large ductility demands at the local regions for which it might be difficult to design the structural connections. The writer agrees with the general spirit behind Jain's conclusion that attempts must be made to simplify material models in the light of more experimental data, consistent with cost-accuracy considerations.

The writer thanks Hays for comparing the present model with a Masing type treatment (7,38) of the virgin stress-strain curve of mild steel. This Masing representation was one of the early models tried by the writer towards his research (17) but was discarded because it had no correlation with experimentally observed behavior in the reversed range. Such a model was used by Chen and Atsuta (40) for stress-strain representation wherein a gross under estimation could be seen on the negative side of the stress axis. The same behavior has been reported by Hays whose model bridged up about 18% gap between the

experiment and the model in the final cycle of Fig. 5, but undershot by as much as 36% on the negative side of stress (39). Thus the adoption of Masing decomposition for the special shape of the virgin stress-strain curve of mild steel yields a good fit for monotomic loading, despite one of the three basic components being of negative stiffness (39), which is difficult to give a reasonable physical meaning to. However this deficiency persists under reversed conditions quite contrary to experimentally observed behavior (14). This explains the 36% deviation from the test results and the inaccuracies of the locally predicted moment-curvature responses (39).

Accepting these inaccuracies and deviations, it is computationally more cheap to adopt a two-component Masing curve of the shape shown in Fig. 8 and analyze the structure of Fig. 10 than to use Hays' three-component Masing curve. This avoids the convergence failure represented in Fig. 11, but overshoots the experimental curve on the positive side of the load axis, as can be easily expected. The writer is grateful to Hays for his observation that the proposed α-β model would give more precise results for other load histories. Hays has also identified a probable increase in the base rotational stiffness of the frame of Fig. 10 as one of the reasons for the increased stiffness and load of Fig. 11 in the reversed direction (39).

APPENDIX.—REFERENCES

40. Chen, W. F., and Atsuta, T., "Inelastic Response of Column Segments under Biaxial Loads," *Journal of the Engineering Mechanics Division*, ASCE, Vol. 99, No. EM4, Proc. Paper 9957, Aug., 1973, pp. 685–701.
41. Eisenberg, M. A., "A Generalization of Plastic Flow Theory with Application to Cyclic Hardening and Softening Phenomena," *Journal of Engineering Materials and Technology*, Vol. 98, July, 1976, pp. 221–228.
42. Harung, H. S., and Millar, M. A., "General Failure Analysis of Skeletal Plane Frames," *Journal of the Structural Division*, ASCE, Vol. 99, No. ST6, Proc. Paper 9776, June, 1973, pp. 1051–1074.
43. Santhanam, T. K., *Dissertation Abstracts International*, Vol. XXXIX, No. 4, 1978.
44. Schrem, E., "Structural Aspects of Software Systems for Nonlinear Finite Element Analysis," *Finite Elements in Nonlinear Mechanics*, Vol. 2, TAPIR, Norwegian Institute of Technology, Trondheim, Norway, 1978.

Errata.—The following corrections should be made to the original paper:

Page 199, paragraph 3, line 7: Should read "material as mild steel (11–13)." instead of "material as mild steel (10–12)."

Page 202, paragraph 1, line 1: Should read "The spotted line represents the virgin" instead of "The dashed line represents the virgin"

Page 202, Fig. 3: Line segments JK and AB must be shown to be of equal slope E_{sm} and not as printed.

Page 217, Appendix I, central block of the flow chart: Should read $\sigma_{yst} = \sigma_{yg}$ instead of $\sigma_{yst} = \sigma_t$

Parametric Investigation of Vibrating Cable Networks[a]

Discussion by Hassan I. A. Hegab[3]

The authors presented a theoretical investigation of vibrating cable networks.

A scale factor is needed in comparing a model with the real structure. If the material of the model is the same as that of the real structure, the cross-sectional areas of the cables of the model must be such that the stresses in the cables of both the model and the prototype are identical. Thus, the statement ". . . while leaving the cable areas unchanged," mentioned by the authors on p. 471, is unrealistic. For a real suspension structure, it is not logical to build a laboratory model using the same cable areas of the real structure. Also, the use of the same cable areas (and, of course, the same sag-span ratios) will mean that the load intensity on the model must be greater than that on its prototype in order to obtain same cable stresses (assuming same cable material). But, again, this is not logical. If the load intensity (per unit area of the surface) is kept unchanged, the cable areas must be altered according to the relation

$$A_n = (SF)^2 A_b \quad (39)$$

in which A_n = cross-sectional area of the new system (model); and A_b = cross-sectional area of the base system (prototype).

Also, Eq. 21 is incorrect and it should have the form

$$[M]_n = (SF)^2 \cdot [M]_b \quad (40)$$

This is true, again, provided that the intensity of the total (dead + live) loads per unit area of the surface is identical in both the model and the real structure.

Eq. 21 may be correct for only a single cable (not a network), if the load intensity per unit length is the same in both the model and its prototype. However, for a network, Eq. 21 may be correct if

$$p_n = \frac{p_b}{SF} \quad (41a)$$

in which p_n = load intensity per unit area of the model; and p_b = load intensity per unit area of the prototype. This is not logical. A more reasonable choice may be

$$p_n = (SF)\, p_b \quad (41b)$$

This gives as a network

$$[M]_n = (SF)^3 \cdot [M]_b \quad (42)$$

The use of Eqs. 18, 20, and 40 gives

---

[a]March, 1979, by Louis F. Geschwindner, Jr. and Harry H. West, (Proc. Paper 14436).

[3]Lect., Faculty of Engrg., Ain Shams Univ., Abbassia, Cairo, Egypt.

$$\omega_n = \frac{\omega_b}{(SF)^{3/2}} \quad \ldots \quad (43a)$$

while the use of Eqs. 18, 20, and 42 yields

$$\omega_n = \frac{\omega_b}{(SF)^2} \quad \ldots \quad (43b)$$

Both Eqs. 43*a* and 43*b* are obviously different from Eq. 23. However, the authors did not offer any applications that can prove the correctness of Eqs. 21 and 23, and Figs. 4 and 5 represent the effect of the corresponding parameters on the dynamic response of a cable network rather than single cables.

On p. 472, the authors said:

> To complete the investigation of the influence of an applied load on the natural frequencies and mode shapes of the network, an equal variation in force is applied at each joint of the network without the corresponding change being made in the mass of the system.

On this statement, the writer has the following comments:

1. The natural frequencies and mode shapes are obtained for free vibrations. Thus, no exciting forces are needed.
2. The application of any dead or live loads at joints result only in a change in the masses at these joints, but not in the forces (which are zero for free vibrations).
3. The fourth conclusion given by the authors on p. 476, as well as the work of Krishna, et al. (8) support the point of view of the writer mentioned in his second comment.

It should be noticed that, due to the nonlinearity of cable structures, the stiffness (or flexibility) matrix is different for any individual loading condition than for any other loading condition. A secant stiffness (or flexibility) matrix for the working loads condition gives usually reasonable results (20).

In his work, the writer (20) uses the flexibility matrix instead of the stiffness matrix, by premultiplying Eq. 18 by $[K]^{-1}$ to have

$$[X] = \omega^2 [K]^{-1} \cdot [M] \cdot [X] \quad \ldots \quad (44)$$

in which the flexibility matrix $[K]^{-1}$ is obtained directly and not by finding the inverse of the stiffness matrix $[K]$.

Finally, for Fig. 4(*a*) and the corresponding section on pp. 472–473, the word "load" must replace the word "force." The change of loading yields a corresponding change in both the stiffness and mass matrices of the cable network. It seems to the writer that the authors were confused between the exciting forces and live loads. Exciting forces produce forced vibrations, while live loads are added to the dead loads in the mass matrix.

Appendix.—Reference

20. Hegab, H. I. A., "Statics and Dynamics of Suspension Bridges with Notes on Suspension Cables and Nets," thesis presented to the University of Tasmania, at Hobart, Australia, in 1977, in partial fulfillment of the requirements for the degree of Doctor of Philosophy.

CONTINUOUS COMPOSITE-BRIDGE MODEL TESTS[a]

Closure by Paul W. Botzler,[7] A. M. ASCE and James Colville,[8] M. ASCE

The writers would like to thank Starkey and Rabb for their comments regarding the role they feel that limit analysis should have in the design of bridge structures. The writers agree that by designing each section with an equal overload capacity, the importance of longitudinal redistribution of moment in continuous span structures will be diminished. However, the ultimate capacity of each section depends on the post-elastic effective width of the slab section. Also, a main conclusion of the paper—namely, that even prior to yielding, the distribution factors in the positive and negative moment regions differ—will have an effect on the ability to design so as to create simultaneous yielding at each section for the same overload. Despite these questions, the writers concur that, at present, the design approach outlined by Starkey and Rabb is proper.

With respect to the comments and questions raised by Kostem and Hall, the writers have reviewed the experimental data for the three-span model in order to clarify the effect of support movement on the reported displacements.

The support movements recorded during testing are given in Table 5.

In the paper the reported displacements of the specimen at the center line of the loaded span, Δ, were computed as follows:

$$\Delta = \Delta_m - \Delta_s \quad \ldots \quad (2)$$

in which Δ_m = measured midspan displacement; and Δ_s = average measured displacement of interior supports. The use of Eq. 2 does not account for the uplift of the exterior supports. A moment distribution analysis indicates that the following relation more accurately reflects this influence:

$$\Delta = \Delta_m - [1.15(\Delta_a + \Delta_s) - \Delta_a] \quad \ldots \quad (3)$$

in which Δ_a = average measured uplift at exterior supports.

Using Eqs. 2 and 3 and the data given in Table 5 yields the corrected displacements presented in Table 6, which indicates that consideration of the exterior support uplift reduces the estimated bending displacements.

The main purpose of the paper was to interpret the test results as they relate to the distribution of load and the effective widths of the slab. These factors were investigated using strain data and revealed that the effective widths were 9 in. (0.2 m) and 6 in. (0.15 m) for the center girder at loads of 20 kips (90 kN) and 40 kips (180 kN), respectively. Corresponding values for the edge girders were 19.4 in. (0.5 m) and 16.5 in. (0.4 m), respectively. The load carried by the center girder was 0.55 P (P = 20 kips), and 0.58 P (P = 40 kips).

[a]September, 1979, by Paul W. Botzler and James Colville (Proc. Paper 14824).

[7]Struct. Engr., Tamarack Corp., Glen Arm, Md.; formerly Grad. Research Asst., Dept. of Civ. Engrg., Univ. of Maryland, College Park, Md. 20742.

[8]Prof., Dept. of Civ. Engrg., Univ. of Maryland, College Park, Md. 20742.

Using these results, simple elastic theory gives the values given in Col. 5 of Table 6. These latter values compare well with the adjusted displacements computed using Eq. 3.

Results reported by the discussers for $P = 20$ kips (90 kN) are:

1. BOVA—center girder: $\Delta = 0.0343$ in. (0.87 mm); edge girders: $\Delta = 0.0132$ in. (0.34 mm).
2. SAP4—center girder: $\Delta = 0.0304$ in. (0.77 mm); edge girders: $\Delta = 0.0126$ in. (0.32 mm).

These results suggest that the load carried by the center girder is around $0.547P$–$0.565P$. This compares favorably with the value of $0.55P$ given previously by the writers. Furthermore, using an effective width of slab of 21 in. (0.53 m), and a load of $0.55P$ on the center girder, simple theory indicates that at a load of 20 kips (90 kN), the center girder would displace 0.0314 in. (0.80

TABLE 5.—Three-Span Model: Support Movements, in inches

Support location (1)	Load, in kips 20 (2)	40 (3)
(*a*) Exterior supports (average)		
Center girder	−0.007	−0.011
Edge girders	−0.004	−0.075
(*b*) Interior supports		
Center girder (left)	+0.013	+0.023
Center girder (right)	+0.008	+0.015
Edge girder 1 (left)	+0.012	+0.019
Edge girder 1 (right)	+0.014	+0.022
Edge girder 2 (left)	+0.009	+0.012
Edge girder 2 (right)	+0.011	+0.025

Note: 1 kip = 4.45 kN; 1 in. = 25.4 mm. A negative displacement indicates upward movement; a positive displacement indicates downward movement.

TABLE 6.—Three-Span Model Bending Displacements, in inches

Location (1)	Load, in kips (2)	Eq. 2 (3)	Eq. 3 (4)	Simple elastic theory values[a] (5)
Center girder	20	0.059	0.050	0.051
Edge girder	20	0.019	0.017	0.015
Center girder	40	0.125	0.120	0.124
Edge girder	40	0.027	0.023	0.030

[a]Displacements computed using simple elastic beam theory and effective widths and distribution factors from experimental strain data.

Note: 1 kip = 4.45 kN; 1 in. = 25.4 mm.

mm) and the edge girder displacements would be 0.013 in. (0.33 mm). These values are in close agreement with the numerical results reported by Kostem and Hall. It is, therefore, suggested that the major difference between the numerical results obtained by the discussers and the experimental data presented by the writers is not due to the effect of the support movements, but rather is due to the reduced effective width of slab acting compositely with the steel beam.

A literature survey by Fan (28) related to effective width indicates the complexity of the problem, producing a corresponding wide variety of equations and procedures for predicting effective widths for use with simple beam theory. A brief review of these procedures indicates that predictions of the effective width of slab in the three-span tests reported by the writers could range from 6 in. (0.15 m)–18 in. (0.46 m), and that stress concentrations due to concentrated loads will result in smaller effective widths than those induced by uniform loads. These indications are compatible with the findings of the writers.

In summary, since it has not been possible for the writers to perform a review of the numerous assumptions made by Kostem and Hall in their numerical analysis procedures, the writers are unable to explain satisfactorily the reasons for the reported discrepancies between test and theory. However, the writers believe that it is unlikely that these differences are due solely to the effect of support movements during testing. A more thorough consideration of these effects reduces but does not eliminate the noted differences. It is suggested that the relatively small width of concrete acting compositely with the steel beam may in fact be the primary reason why the experimental displacements are noticeably larger than those predicted by the numerical procedures.

The writers would be pleased to discuss this possibility further with Kostem and Hall.

Appendix.—Reference

28. Fan, H. M., "Effective Width of Composite Bridges at Ultimate Load," thesis presented to the University of Maryland, at College Park, Md., in 1974, in partial fulfillment of the requirements for the degree of Doctor of Philosophy.

Cyclic Inelastic Buckling of Thin Tubular Columns[a]

Closure by Egor P. Popov,[5] F. ASCE, Victor A. Zayas,[6] and Stephen A. Mahin,[7] A. M. ASCE

The writers would like to thank Hays for his interest in the paper and for raising an important question regarding material properties of the model tubes as they relate to actual structures. This question has been carefully considered, and as can be seen from Fig. 3 of the paper, experimental results with unannealed tubes are totally misleading. On the other hand, the stress-strain diagrams for annealed specimens closely resemble those for steels used in real structures.

The writers believe that fully annealed specimens provide reasonably accurate models for simulating the inelastic cyclic behavior of tubular members used in the field. It would be impractical and prohibitively expensive to fabricate 4-in. OD tubing using the same techniques as are used to manufacture 24-in. OD rolled pipes to obtain a reasonable simulation of residual stresses. It is recognized that initial residual stresses will affect the first buckling load of a column. These effects, however, can be accounted for if the initial buckling load is predicted using the stress-strain curve from a column stub test of a full size member (16). The effects of the initial residual stresses on the buckling load in the second and subsequent cycles usually is greatly reduced because of compressive and tensile axial yielding during the first inelastic cycle. The writers recommend that for the inelastic analysis of braced frames, data for both monotonic and cyclic material properties of the members in the frame be used to predict the initial and cyclic buckling loads (17).

Appendix.—References

16. *Guide to Stability Design Criteria for Metal Structures*, B. G. Johnston, ed., 3rd ed., John Wiley and Sons, Inc., New York, N.Y., 1975.
17. Zayas, V. A., Popov, E. P., and Mahin, S. A., "Cyclic Inelastic Buckling of Tubular Steel Braces," *Report UCB/EERC 80/16*, University of California, Berkeley, Calif., June, 1980.

[a]November, 1979, by Egor P. Popov, Victor A. Zayas, and Stephen A. Mahin (Proc. Paper 14982).

[5]Prof. of Civ. Engrg., Coll. of Engrg., Div. of Struct. Engrg. and Struct. Mechanics, Univ. of California, Berkeley, Calif. 94720.
[6]Grad. Student in Civ. Engrg., Univ. of California, Berkeley, Calif. 94720.
[7]Asst. Prof. of Civ. Engrg., Univ. of California, Berkeley, Calif. 94720.

Practical Bridge Code Calibration[a]

Closure by Andrzej S. Nowak,[5] A. M. ASCE and Niels C. Lind,[6] M. ASCE

The writers would like to thank Carskaddan and Haaijer for their discussion on one of the aspects of the OHBD Code calibration.

In the OHBD Code, kinking is defined as a permanent deflection, and the tolerance is set at 0.001 of the span length. The code allows a load causing permanent deformation to occur on average once in 10 yrs. Load factors were derived accordingly.

Several steel girder bridges, recently built in Ontario, were considered. The allowable permanent deflection (kinking) never governed the design. It seems that the differences between Carskadden and Haaijer's results and the writer's findings are due to different definitions of kinking and tolerancies.

Natural Frequency of Curved Box Girder Bridges[b]

Closure by Conrad P. Heins,[4] M. ASCE and M. A. Sahin[5]

The writers would like to thank Tabba for his discussion and contribution.

In response to the particular questions Tabba has noted, we offer the following:

1. A thorough study (12) of typical bridges, constructed in the United States, indicates that the central angle between supports is always less than 40°. Thus the condition of $\alpha \geq 45°$ is not a *practical* situation and thus not relevant.
2. The definition of low torsional stiffness has not been defined by Tabba; however the bridges under study have significant torsional stiffness, K_T, as indicated in Table 1.
3. The bridges under study have symmetrical cross sections, thus coupling between flexural vertical and torsional vibrations is valid.

---

[a]December, 1979, by Andrzej S. Nowak and Niels C. Lind (Proc. Paper 15061).

[5]Asst. Prof., Coll. of Engrg., Dept. of Civ. Engrg., Univ. of Michigan, Ann Arbor, Mich. 48109.

[6]Prof., Dept. of Civ. Engrg., Univ. of Waterloo, Waterloo, Ontario, Canada.

[b]December, 1979, by Conrad P. Heins and M. A. Sahin (Proc. Paper 15064).

[4]Prof., Dept. of Civ. Engrg., Inst. for Physical Science and Tech., Univ. of Maryland, College Park, Md. 20742.

[5]Grad. Student, Dept. of Civ. Engrg., Univ. of Maryland, College Park, Md. 20742.

4. The example relating the computed frequencies for a two-span bridge relative to a single-span bridge were not computed correctly.

The results should be $f_2 = 1.006\, f_1$, $0.62\, f_1$, and $0.43\, f_1$, which conforms to the general trend. The discusser *should* have used the referenced maximum span length (NL) in Eq. 21. In all cases the maximum span length should be used in applying Eq. 21.

Appendix.—Reference

12. Heins, C. P., "Box Girder Bridge Design—State of Art," *AISC Engineering Journal*, American Institute of Steel Construction, Vol. 15, No. 4, Dec., 1978.

Current Structural Engineering Reference Sources[a]

Closure by Sam Chan[3]

The writer would like to thank J. M. Saul for having pointed out the discrepancies in the reference sources listed in the paper and submitted corrections on them. He especially appreciates the efforts of the reviewers of his paper because they have done a tremendous job in the process. Had not been for their kind of efficiency, the writer would have still been revising the manuscript instead of writing up a closure like this. Last, but not least, is the writer's sincere gratitude toward the ASCE for having offered the opportunity and the spot in its journal for the publication of his paper.

---

[a]February, 1980, by Sam Chan (Proc. Paper 15211).

[3]Coordinator of Engrg., Div. of Sci., Louisiana State Univ., P.O. Box 1129, Eunice, La. 70535.

Cooling Towers Using Measured Wind Data[a]

Closure by Prodyot K. Basu,[4] M. ASCE and Phillip L. Gould,[5] F. ASCE

The writers thank A. K. Gupta for his contributions to their study.

The discusser's comments on the maximum frequency content of wind records essentially agree qualitatively with the writers' study although it is somewhat severe, in the writers' opinion.

The use of longer rise times as suggested by the discussion would be ideal but would add inordinately to the computational expense. The discusser's dynamic load factor computations may not recognize the initiation of the time history analysis from the *mean* pressure at $t = 0$, which partially compensates for the short rise times.

Finally, the use of 2% initial damping seems to be sufficiently conservative.

End Effects of Pressure-Resistant Concrete Shells[b]

Errata

The following correction should be made to the original paper:

Page 754, paragraph 1, line 4: Should read "ϵ_t is 0.0008." instead of "ϵ_t is 0.008."

---

[a]March, 1980, by Prodyot K. Basu and Phillip L. Gould (Proc. Paper 15259).

[4]Asst. Prof., Dept. of Civ. Engrg., Washington Univ., St. Louis, Mo. 63130.

[5]Prof. and Chmn. of Civ. Engrg., Washington Univ., Campus Box 1130, St. Louis, Mo. 63130.

[b]April, 1980, by Wai-Fah Chen, Hiroyuki Suzuki, and Tse-Yung P. Chang (Proc. Paper 15316).

Quinnipiac River Bridge Cracking

Closure by John W. Fisher,[6] F. ASCE, Alan W. Pense,[7] Hans Hausammann,[8] and George R. Irwin[9]

The writers have reviewed the comments provided by M. O. Elkow and have the following observations.

We are in agreement with the discusser that the high tensile residual stress from welding and the joint geometry are major contributors to crack extension, particularly when a large lack of fusion region from partially made weld exists. However, we are not able to ascertain the reasons for his concluding that a "fully" made groove weld would experience cracking, had it been erected without a flaw and then been subjected to a service temperature drop to 0° F.

The intersection of sound groove welds by continuous fillet welds as were used to attach the longitudinal stiffener to the girder web is common practice and also occurred elsewhere on the structure in question. No adverse behavior has been experienced at such locations when sound groove welds have been produced.

A sound groove weld without a flaw will not crack as a result of shrinkage from a longitudinal fillet or groove welded connection crossing it, unless poor welding practice is utilized, e.g., introducing hydrogen in the weld.

The writers are not sure of the analytical basis of the statements made. It would appear that the discusser is suggesting an alternate method of analysis. However, a lack of information prevents a more detailed discussion and evaluation.

It should be also noted that the thickness of the longitudinal stiffener and web plate results in residual tensile stresses through the web thickness at the stiffener-web connection. The longitudinal welds were made by the submerged arc process and the penetration of the weld into the stiffener and web plates is sufficient to cause tensile yield stress through the web thickness at the longitudinal stiffener connection.

This condition is not as severe at the web-to-flange connection, because the flange plate is much thicker than the web plate. This results in a different residual stress distribution as was shown in Fig. 16. The residual stress distributions have an impact on the fracture behavior of the two welded connections that were examined in the paper. The residual stress gradient in the flange was a factor in arresting the running crack that developed in the girder web.

---

[a]April, 1980, by John W. Fisher, Alan W. Pense, Hans Hausammann, and George R. Irwin (Proc. Paper 15343).

[6]Prof. of Civ. Engrg. and Assoc. Dir., Fritz Engrg. Lab., Building 13, Lehigh Univ., Bethlehem, Pa. 18015.

[7]Prof. and Chmn., Metallurgy and Materials Engrg., Lehigh Univ., Bethlehem, Pa. 18015.

[8]Research Asst., Fritz Engrg. Lab., Lehigh Univ., Bethlehem, Pa. 18015.

[9]Adjunct Prof. of Mechanics, Fritz Engrg. Lab., Lehigh University, Bethlehem, Pa. 18015.

Dynamic Seismic Analysis: Economic Considerations[a]

Discussion by Robert F. Martin[2] and Robert F. Farrell[3]

The author addresses a very practical consideration, namely, the cost of conducting dynamic seismic analyses which frequently are conducted in conjunction with other stress calculations. The computer models illustrated, however, appear to be restricted to beam elements. Where components cannot be modeled as beams, the author acknowledges that detailed finite element analysis may be required to obtain equivalent beam properties. No mention is made of the cost of these subsidiary calculations, although the author claims that in general this is an economic approach. In other instances, the adequacy of the models illustrated seems to rest heavily on the fact that the frequency predicted by analysis is conservative with respect to some known value (perhaps established by test?) for the physical article. In many instances, the analyst does not have the advantage of such prior knowledge for assessing the adequacy of his computer model and, therefore, must resort to a more detailed model, while at the same time living within the constraints of the inevitable budgetary limitations.

The writers have considerable experience in modeling equipment of varying complexity (some for nuclear applications) requiring dynamic seismic/stress analysis. A general purpose structural analysis program, e.g., NASTRAN, ANSYS, having a fairly extensive library of finite elements (beam, quad plate, spring, concentrated mass, etc.) has not only proven to be useful, but with experience, rather economical. As a consequence, it has been possible to synthesize, in much the same way as the author's paper suggests, a basic library of computer models for various types of fans, cabinets, etc. which can be used repeatedly, thus resulting in cost effectiveness. Moreover, a single model is adequate for both dynamic and static analysis since a condensation technique, Guyan reduction, is available facilitating the resonant frequency computations, while a re-expansion of the modes is available for the dynamic seismic stress portion of the analysis. Thus, one model suffices for the entire problem, in distinction to two models in the author's approach. Certain post-processing features make it possible and economical to combine dynamic stress results with static stresses arising from dead weight and operating loads.

[a]July, 1980, By C. K. McDonald (Proc. Paper 15571).

[2]Mgr., Computer Operations, McMahon Engrg. Co., 2322 Bowen Rd., P.O. Box C, Elma, N.Y. 14059.

[3]Dynamics Analyst, McMahon Engrg. Co., 2322 Bowen Rd., P.O. Box C, Elma, N.Y. 14059.

Technical Papers

Original papers should be submitted in triplicate to the Manager of Technical and Professional Publications, ASCE, 345 East 47th Street, New York, N.Y. 10017. Authors must indicate the Technical Division or Council, Technical Committee, Subcommittee, and Task Committee (if any) to which the paper should be referred. Those who are planning to submit material will expedite the review and publication procedures by complying with the following basic requirements:

1. Titles must have a length not exceeding 50 characters and spaces.

2. The manuscript (an original ribbon copy and two duplicate copies) should be double-spaced on one side of 8-1/2-in. (220-mm) by 11-in. (280-mm) paper. Three copies of all figures and tables must be included.

3. Generally, the maximum length of a paper is 10,000 word-equivalents. As an *approximation*, each full manuscript page of text, tables or figures is the equivalent of 300 words. If a particular subject cannot be adequately presented within the 10,000-word limit, the paper should be accompanied by a rationale for the overlength. This will permit rapid review and approval by the Division or Council Publications and Executive Committees and the Society's Committee on Publications. Valuable contributions to the Society's publications are not intended to be discouraged by this procedure.

4. The author's full name, Society membership grade, and a footnote stating present employment must appear on the first page of the paper. Authors need not be Society members.

5. All mathematics must be typewritten and special symbols must be identified properly. The letter symbols used should be defined where they first appear, in figures, tables, or text, and arranged alphabetically in an appendix at the end of the paper titled Appendix.—Notation.

6. Standard definitions and symbols should be used. Reference should be made to the lists published by the American National Standards Institute and to the *Authors' Guide to the Publications of ASCE*.

7. Figures should be drawn in black ink, at a size that, with a 50% reduction, would have a published width in the *Journals* of from 3 in. (76 mm) to 4-1/2 in. (110 mm). The lettering must be legible at the reduced size. Photographs should be submitted as glossy prints. Explanations and descriptions must be placed in text rather than within the figure.

8. Tables should be typed (an original ribbon copy and two duplicates) on one side of 8-1/2-in. (220-mm) by 11-in. (280-mm) paper. An explanation of each table must appear in the text.

9. References cited in text should be arranged in alphabetical order in an appendix at the end of the paper, or preceding the Appendix.—Notation, as an Appendix.—References.

10. A list of key words and an information retrieval abstract of 175 words should be provided with each paper.

11. A summary of approximately 40 words must accompany the paper.

12. A set of conclusions must end the paper.

13. Dual units, i.e., U.S. Customary followed by SI (International System) units in parentheses, should be used throughout the paper.

14. A practical applications section should be included also, if appropriate.